DURABILITY OF REPAIR TECHNIQUES
OF FINE CRACKS IN CONCRETE

DURABILITY OF

REPAIR TECHNIQUES OF FINE CRACKS

IN CONCRETE

By

ANNA-KRYSTYNA RZEZNICZAK, B.ENG.

A Thesis

Submitted to the School of Graduate Studies

in Partial Fulfillment of the Requirements

for the Degree

Master of Applied Science

McMaster University

MASTER OF APPLIED SCIENCE (2013)   McMaster University

(Civil Engineering)   Hamilton, Ontario

TITLE: Durability of Repair Techniques of Fine Cracks in Concrete

AUTHOR: Anna-Krystyna Rzezniczak, B.Eng. (McMaster University, 2010)

SUPERVISOR: Professor Samir E. Chidiac, Ph.D., P.Eng

NUMBER OF PAGES: x, 127.

ABSTRACT

Aging public infrastructure in North America continues to challenge engineers and scientists to develop repair and rehabilitation strategies that are practical, durable and cost effective. Of specific interest is the state of concrete and concrete repair in buildings and civil engineering infrastructures that are in deteriorating condition. In particular, cracks pose a threat to the durability and ultimately the structural integrity of concrete. Cracks in concrete may form for several reasons, e.g. plastic shrinkage, thermal contraction, mechanical loading or as a result of overloading. Once formed, cracks present a combination of problems to the service life and performance of the structure. Therefore cracks must be repaired for the following reasons: to prevent the ingress of deleterious agents such as water, other liquids, vapour, gas, chemicals and biological agents; to either restore or increase the structural load-bearing capacity of the cracked concrete member; to restore the aesthetic condition of the structure.

The effectiveness of two different repair methods, crack injections and cementitious overlays, were examined. Two repair materials, a low viscosity epoxy and polyurethane were injected into the cracks, and a thin polymer-modified cementious overlay was applied on the cracked surface. Two types of cement were used, an ordinary Portland cement and a blended cement with 8% silica fume. The specimen properties were evaluated using non-destructive testing, prior to being subjected to a series of freeze-thaw conditioning regimes. From the experimental program, it was determined that the epoxy injection repair was more effective in restoring the air tightness than the thin overlay. The polyurethane material was unsuccessful. Following the freeze-thaw regimes, an overall improvement of conditions for all three repairs was observed, with the cementitious overlay seeing the greatest improvement in air tightness. These results indicate that the on-going cement hydration mechanism had a greater effect on the performance in comparison to the deleterious effects of the environmental loads.

ACKNOWLEDGEMENTS

TABLE OF CONTENTS

LIST OF TABLES

LIST OF FIGURES

CHAPTER 1 INTRODUCTION

1.1 Objective of Thesis

In recent years, the state of degradation of concrete infrastructure has become a critical issue in North America. A yearly cost of $18 billion has been estimated for concrete repair, protection and strengthening in the United States alone (Emmons & Sordyl, 2006). Concrete durability problems have left buildings and infrastructure in deteriorating conditions. Rehabilitation techniques and materials are becoming increasingly important in the construction industry. Cracking in particular poses a threat both to the structural integrity as well as the durability of concrete. The ingress of water and harmful agents lead to damaging mechanisms, such as the corrosion of steel reinforcement. Accordingly, cracks are repaired as a preventative maintenance measure to prolong the service life of the structure.

Cracking is a common occurrence in concrete bridge decks and barrier or parapet walls. In certain regions of North America where harsh winters are experienced, it is common practice to use de-icing chemicals. The effects of freeze-thaw alongside chloride ingress in the presence of cracks present ideal circumstances to promote the premature deterioration of the concrete material. The presence of cracks leads to poor durability and a shorter service life of the structure. The successful repair of cracks would reduce the deterioration effects resulting in a longer service life. Prolonging the service life defers the rehabilitation or replacement of the bridge and the government sectors responsible for the management of multiple bridges would experience economic benefits. The result of a longer service life is also indicative of a sustainable practice.

The objective of this study is to develop an experimental program to study the durability and longevity of repair methods of hairline cracks in concrete. The influence of these cracks on the concrete's transport properties is measured using non-destructive testing. The long term effectiveness of the repairs is examined through the use of environmental cycling regimes.

1.2 Outline of Thesis

This thesis is broken into five chapters, including the introduction. Chapter 2 presents a literature review on the different cracking mechanisms in concrete which occur in the early ages of concrete. It also presents the influences of cracks in concrete on the transport properties as well as the different repair techniques. It examines the effects of various environmental stressors on concrete and repaired concrete.

Chapter 3 outlines the experimental procedures and evaluation techniques used to examine the effectiveness of the different repair methods and the influence of the freeze-thaw regimes. Provided are the details of the concrete specimen fabrication method used as well at the repair application procedures. The freeze-thaw regimes implemented were derived from the Ontario's Ministry of Transportation (MTO-LS412, 1997) specifications for the resistance of concrete to scaling.

In Chapter 4 the data is summarized, analyzed, and discussed. A series of statistical tests were performed to interpret the data and determine the effectiveness of the

repair methods and the effects of the freeze-thaw regimes. The results are then compared to existing literature. The effects of the freeze-thaw regimes are modelled using mechanics and compared to the results. Furthermore, based on the results, the durability of the repaired specimens is predicted using service life models.

The final chapter summarizes the results of the experimental program and the analysis of the data. Suggestions and recommendations for future research in concrete crack repairs and its long term performance are presented.

CHAPTER 2 LITERATURE REVIEW

2.1   Introduction

Concrete is one of the most widely used construction materials. A proportioned mixture of cement, water and fine and coarse aggregates, it is mouldable into various shapes and forms making it favourable in large construction projects. Within the infrastructure sector, in particular, many bridges are constructed with cast-in-place concrete bridge decks and barriers. Over the past few years, with the addition of supplementary cementing and admixture materials concrete has achieved a high compressive strength, also referred to as High Performance Concrete. Despite this, the issues with concrete durability remain unchanged and cracking in concrete is one of the primary reasons.

Cracking in concrete can be caused by one of many different factors which includes loading conditions, corrosion of reinforcement, alkali aggregate reaction, and the restraint of concrete in shrinkage. Shrinkage in concrete appears in several different forms: plastic shrinkage, drying shrinkage, autogenous shrinkage, and thermal shrinkage. All of these processes are caused by a mechanism that occurs while the concrete is curing at an early age. Concrete shrinkage is an inherent property of concrete that can be minimized with a proper concrete mix and ideal environmental conditions, but cannot be completely avoided.

There exists a variety of traditional crack repair methods that are implemented in concrete structures in order to preserve both durability and strength. Some of these repair methods include: mechanical stitching, routing and sealing, overlays, epoxy injection, and cementitious grouting. Apart from traditional methods, research has been directed towards the development of self-healing cementitious materials. The advantages of self-healing materials include the elimination of a maintenance-repair program and human intervention to apply the repairs (Joseph, Gardner, Jefferson, Isaacs, & Lark, 2011).

To produce long-lasting effective concrete crack repairs it is necessary to study their performance under various environmental conditions. This includes such conditions that will occur over the lifetime of the repaired system: freeze-thaw cycles, temperature fluctuations, and the presence of salt solutions. These factors on concrete have deteriorating effects leading to scaling and delamination, and in the case of reinforced concrete, ultimately leading to corrosion of the reinforcement. In the case of repaired concrete, these factors may have additional effects on the adhesion and interfacial bonding of the repair to the substrate.

This chapter provides a review of the available literature on the causes, implication, and remedies to fine concrete cracks. The focus of this thesis is to examine the durability of crack repairs, therefore, the literature avoids putting emphasis on the structural aspects of the repairs.

2.2 Causes of Early-Age Cracking In Concrete

2.2.1 Plastic Shrinkage

Concrete is susceptible to cracking when it is still in its plastic state. Segregation occurs in concrete as the suspended aggregates tend to move downward under the force of gravity. The result is the appearance of a thin layer of water on the surface of the concrete, also known as bleeding. Plastic shrinkage occurs when the rate of evaporation exceeds that of bleed water. Associated with plastic shrinkage is the formation of thin patterned cracks on the surface of the concrete. Two separate mechanisms have been acknowledged as the driving forces: the development of capillary pressure and differential settlement. These two mechanisms will be discussed in detail.

Powers (1968) originally related the development of capillary pressure within plastic concrete to the formation of curved surfaces (meniscuses) between particles caused by the evaporation of water. Due to the internal pressure differential with the atmosphere, attractive forces are created between the cement particles, reducing the mean distance between the particles and initiating shrinkage. This plastic shrinkage mechanism however fails to fully explain the occurrence of cracks. With the continuous evaporation of water from the surface, the capillary pressure increases until a "break-through pressure" is reached (Whittman, 1976). At this moment the air rushes into the system and rearranges the capillary water which causes an immediate decrease in the capillary pressure as depicted in Figure 2.1. Drained pores in the microstructure act as weak points and cause localized strains which may result in cracking. The break-through pressure may thus serve as an indicator for cracking potential within plastic concrete.
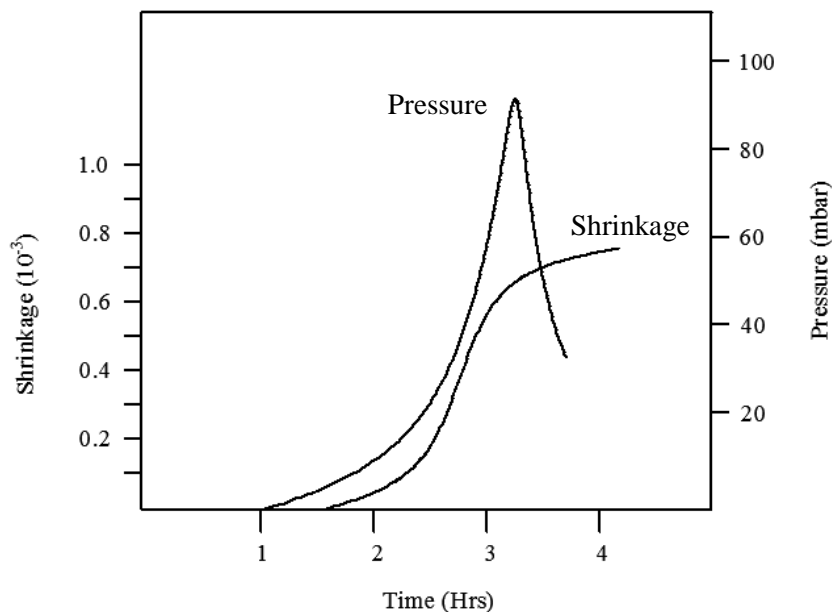
Figure 2.1 Capillary pressure and shrinkage (Whittman, 1976)

Cracking may also be caused by plastic settlement. A sudden cross sectional change or the placement of reinforcement will result in differential settlement within the concrete. Using photoelastic analysis Weyers et al. (1982) were able to capture the effects and stresses caused by the reinforcement inclusions in concrete. It was found that the maximum tensile stresses occurred directly above the reinforcement. These tensile stresses create a tearing effect which lead to the formation of cracks. The experimental design employed gelatine rather than concrete which raises suspicions about the validity of the results. Although the numerical values are not synonymous with true stresses experienced in concrete, Weyers et al. were successful in confirming the cracking mechanism caused by settlement.

2.2.2 Drying Shrinkage

Once the concrete has set, it is no longer susceptible to plastic shrinkage cracking. The loss of water from the system to the environment continues in its quasi hardened state. This process is known as drying shrinkage. If large stresses are induced which exceed the tensile strength cracking will occur. There exist several theories which attempt to explain the physical mechanisms of drying shrinkage. To this day, it is uncertain which one is truly representative of the processes occurring in concrete. The four mechanisms that have been postulated and will be discussed include: capillary tension, surface energy, movement of interlayer water and disjoining pressure.

Capillary tension is one of the most commonly documented mechanisms in literature. It has already been mentioned when discussing plastic shrinkage however it also forms in hardening concrete as moisture is lost to the surroundings. The concrete develops a skeleton and thus the meniscuses are formed within the capillary pores. Tensile stresses are formed in the water which are equalised by compressive forces in the solid skeleton. The capillary forces can be related to the surface energy (γ) and the radii of the meniscuses (r_1, r_2) using the Gauss-Laplace equation (Slowik, Hubner, Schmidt, & Villmann, 2009):

$$\sigma = \gamma \left(\frac{1}{r_1} + \frac{1}{r_2} \right) \qquad 2.1$$

The second mechanism that describes drying shrinkage is the surface tension. Molecules that are on the surface of a material experience additional forces caused by the lack of symmetry and the absence of equating repulsive and attractive forces caused by interacting particles. This mechanism is deemed to be valid for a relative humidity (RH) greater than 50% at which point capillary condensation takes place (Whittmann, 1982). Consequently, the only water considered with surface tension is the physically adsorbed water.

The third and fourth mechanisms are best portrayed using Munich`s model. With the discovery that the Calcium Silicate Hydrate (CSH) paste is in fact composed of thin sheets and foils, Feldman and Sereda (1970) proposed that at a low RH the shrinkage and

expansion is caused by the existence and movement of interlayer water. Swelling occurs when CSH sheets attract highly polarized waster molecules up to several monolayers represented by Δl_o in Figure 2.2 from an RH of 0% to 40%.

0% RH   40% RH   80% RH
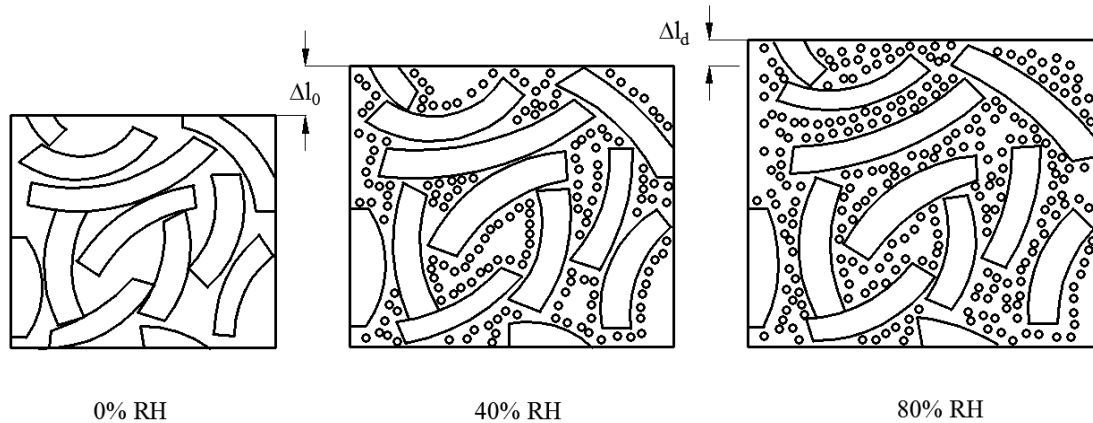
Figure 2.2 Munich Model of CSH (Whittmann, 1982)

The last mechanism is the disjoining or swelling pressure that is experienced in the CSH at a RH greater than 50% (Whittmann, 1982). With the addition of extra water into the system, the attractive forces of the monolayers of water to the CSH sheets decrease due to the increasing distance. This causes additional swelling or shrinkage that cannot be captured by the surface energy mechanism.

The different models and mechanisms that have been developed to describe drying shrinkage have all led to an increased knowledge about the physical processes that occur within hardened concrete. No one mechanism can be proved incorrect. Rather it is beneficial to assume that drying shrinkage is a result of the interaction of all the mechanisms. Some models may better describe particular observations and results than others. When the pressure created by any one of the mechanisms exceeds the tensile strength of the concrete, cracking will occur. With evaporation on the exposed concrete surface, the RH will be much lower on the outside of the concrete. The RH increases with the depth into the concrete as seen in Figure 2.3. The varying humidity creates a strain gradient with tensile stresses forming on the surface of the concrete. This leads to cracking of the surface.
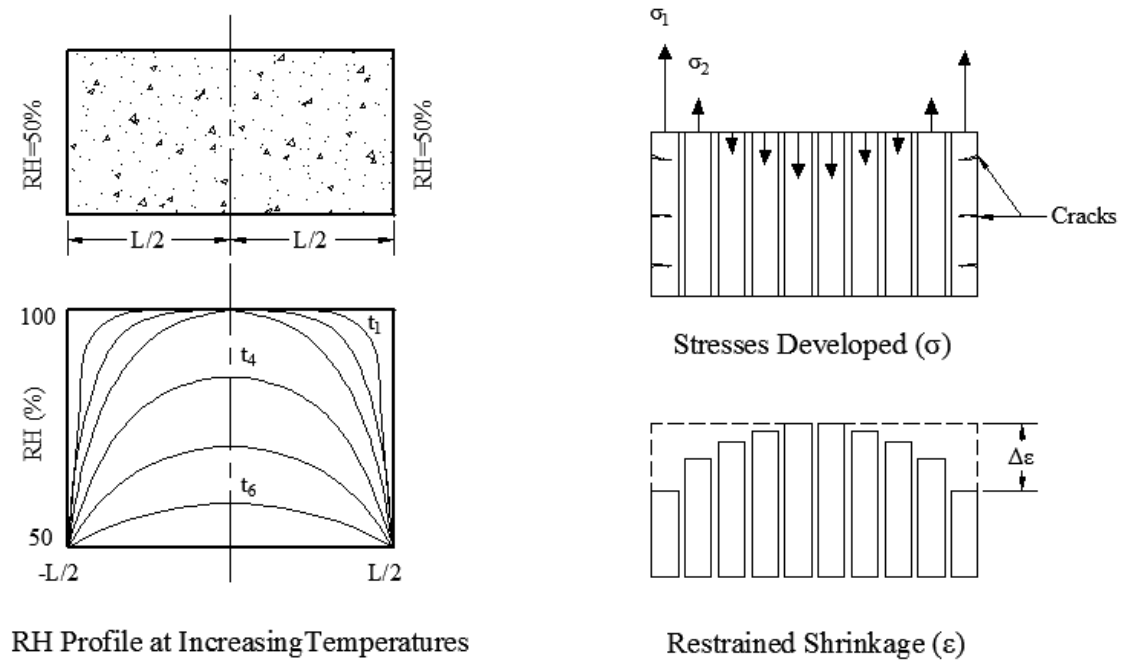
Figure 2.3 Crack formation due to inhomogeneous moisture distribution (Bazant, 1988)

2.2.3   Autogenous Shrinkage

Concrete may also experience a phenomenon commonly referred to as autogenous shrinkage. In the past, there has been a lack of agreement and confusion with respect to the different terms used to describe this mechanism. One suggested definition for autogenous deformation is "the bulk deformation of a closed, isothermal, cementitious material system not subjected to any external forces" (Jensen & Hensen, 2001). The Japanese Concrete Institute labelled it as the macroscopic volume reduction that occurs to cementitious materials when cement hydrates after initial setting, ignoring the effects of any moisture exchange with the environment, temperature variation, and external forces and restraints (Tanzawa, 1999).

Several mechanisms can be used to describe autogenous shrinkage: self-desiccation, surface tension, disjoining pressure, and capillary tension (Lura, Jensen, & van Breugel, 2003). The most frequently associated mechanism is self desiccation, which is defined by Jensen and Hensen (2001) as the "deformation of a set cementitious material system caused by chemical shrinkage".

Chemical shrinkage is the internal volume reduction linked with the hydration reaction in a cementitious material amounting typically to 6-7mL/100g of cement reacted (Powers & Brownyard, 1948). Up until the point of setting, the chemical shrinkage in the concrete is synonymous with the autogenous shrinkage. Upon setting, chemical shrinkage results in the formation of internal voids within the cementitious matrix while autogenous shrinkage results in the bulk deformation of the cementitious mass. This is portrayed in Figure 2.4. Solid matter is represented by the dark grey areas, pore water by the light grey

areas, and the white spaces are the voids in the cement. Figure 2.4 (a) depicts a low degree of hydration, only forming internal voids from chemical shrinkage. Figure 2.4 (b) illustrates a higher degree of hydration: a decreased amount of pore water, increased solid matter, refinement of the pore structure, increase in air voids due to chemical shrinkage, and decrease of the menisci radius of curvature. The effects of self-desiccation are illustrated by the bulk volume change, illustrated by the dashed line representing the original volume.
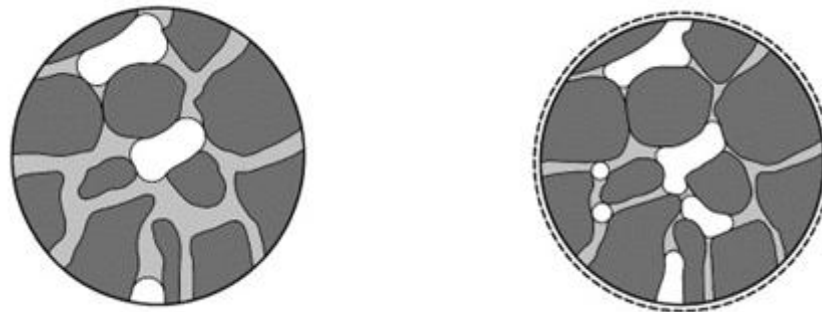
(a)   **(b)**
Figure 2.4 Schematic representation of hydrating cement (Jensen & Hensen, 2001)

The formation of internal voids is accompanied by the formation of water-air menisci and the RH decreases. This is described using Kelvin's Law, as presented in Equation 2.2. The relative humidity, *RH*, is a function of γ which is the water surface tension, the molar weight of water, *M*, the contact angle between water and solids, θ, the density of water, ρ, the radius of the meniscus, r, the ideal gas constant, *R*, and the absolute temperature, *T*. With the creation of the menisci, tensile stresses are developed. This is summarized by Laplace's law in Equation 2.3, where σ_{cap} is the tensile stress in the pore fluid (Acker & Ehrlacher, 1995).

$$\ln \text{RH} = \frac{2\gamma M\cos\theta}{\text{prRT}} \qquad\qquad 2.2$$

$$\sigma_{cap} = \frac{2\gamma}{r} \qquad\qquad 2.3$$

Autogenous shrinkage is most commonly associated with high performance concretes, or more accurately, when the water-to-cement ratio is less than 0.42 (Aitcin, Neville, & Acker, 1997). It was in the 1980's that laboratory investigations proved that the observed cracking phenomena in these high performance concretes was due to the increased autogenous deformation (Pailliere, Buil, & Serrano, 1987). Since then, the research of autogenous shrinkage has grown to better develop an understanding of the phenomena. Another observed variable that influences the amount of autogenous shrinkage is the inclusion of Silica Fume. The replacement of cement with 10% Silica

Fume can result in up to a 55% increase of the autogenous shrinkage (Zhang, Tam, & Leow, 2003).

2.2.4   Thermal Cracking

The approach used for examining the mechanisms of early thermal contraction is different from that of plastic and drying shrinkage. The effect of the loss of moisture could be explained on the microscopic level with the interactions of aggregates, CSH paste, and water. Thermal strains are the product of the heat of hydration that occurs with the production of the CSH. To adequately describe the driving forces it is necessary to closer examine the heat of hydration, and the diffusivity of the heat through the mass of concrete.

The hydration reaction acts as an exothermic reaction. With the process of hydration the concrete expands as the heat is dispersed throughout the matrix. The stress that develops depends on several factors of the concrete: the degree of restraint (K_r), the elastic modulus, E, the coefficient of thermal expansion, α, and the creep of concrete, ϕ. The following equation is used to calculate the thermal stresses (Mehta & Monteiro, 2006):

$$\sigma_t = K_r \frac{E}{1 + \varphi} \alpha \Delta T \qquad\qquad 2.4$$

The temperature change experienced in the concrete is influenced by the concrete material properties. Some variables used to define the temperature change include the specific heat capacity, thermal conductivity, and thermal diffusivity. The amount of heat liberated during hydration is controlled by the composition of the cement and its clinker phases. In contrast, the diffusivity and the stresses developed within the concrete highly depends on the type of aggregate used. For example, a quartzite aggregate has a thermal coefficient of expansion of 12 microns per ˚C while a limestone coefficient is 6 microns per ˚C (Mehta & Monteiro, 2006). This is often reflected in concrete standards where the limiting differential temperature is categorized by aggregate type such as in the British standards BS 8110.

In an attempt to model the behaviour of thermal cracking, it was observed that the varying degrees of axial and rotational restraint are integral (Emborg & Bernander, 1994). The temperature related criteria such as the heat capacity and thermal conductivity cannot describe the potential of cracking. During the hardening process, cracking does not occur with the expansion of concrete, but rather upon cooling when the shrinking strains induce tensile stresses. These stresses are also a result of the restraining action of movement. One type of restraint includes an external restraint caused by fixity of the concrete to its surroundings. Another form of restraint which is common in mass concrete structures is an internal restraint caused by a temperature gradient.

2.3   Influence of Cracks on Concrete Mass Transport Properties

To assess concrete in terms of its durability, the concrete mass transport properties are typically examined. Concrete transport properties can be divided into three separate mechanisms: permeability, diffusion, and capillary absorption. The permeability is the property that governs the rate of flow of a fluid due to a pressure gradient whereas diffusion is the property that governs the movement of substances due to a concentration gradient. Capillary absorption is the movement of water through the pores in concrete in the absence of externally hydraulic head. For this section only the implications of cracks on permeability and chloride diffusion are reviewed as they are most commonly related to reinforcement corrosion through chloride ingress and carbonation in the literature.

2.3.1   Permeability

Knowledge of the flow properties of water through cracked and uncracked sections is essential in predicting the extent of deterioration that is caused by subsequent mechanisms such as freezing and corrosion. Overall, the crack width or crack opening displacement (COD), may be directly related to the permeability of the concrete. However, when the COD is less than 50 microns the crack opening has little effect (Wang et al., 1997). Between 50 and 200 microns the water permeability increases rapidly. After the crack width reaches 200 microns the permeability becomes steady and less rapid. The results from Wang et al., as well as another series of similar experiments conducted by Aldea et al. (1999) are shown in Figure 2.5.

The material properties also influence the ingress of water. The permeability of normal strength concrete increases much more rapidly once a COD of 100 microns is reached. This was not observed in the other concrete materials (paste, mortar, and high strength concrete) subjected to cracking (Aldea et al., 1999). The permeability is expected to vary with the material based on uncracked sections, however in a cracked section this occurrence may be caused by the variation of the microstructure and its tendency for cracking. The interfacial transition zone in concrete is a point of weakness as it is highly porous and most susceptible to cracking. This may account for the permeability difference observed between normal strength concrete and mortar.

The experiments conducted by Wang (1997) and Aldea (1999) failed to fully examine the different variables affecting the cracked concrete permeability. In order to induce cracking in the concrete for permeability testing the splitting test was used. The approximately constant width that results from the testing method is not a true representative of in-situ cracks. The permeability coefficients are used as a means of measuring the permeability of the cracked concrete with respect to the COD. To obtain true representative values, the experimental design would need to include other factors not easily quantifiable such as: tortuosity and roughness. In the work of Akhavan et al. (2012), an attempt to include the tortuosity and roughness of the cracks was employed using surface metrology techniques. Including this measured parameter provided a more accurate estimation of the crack permeability.
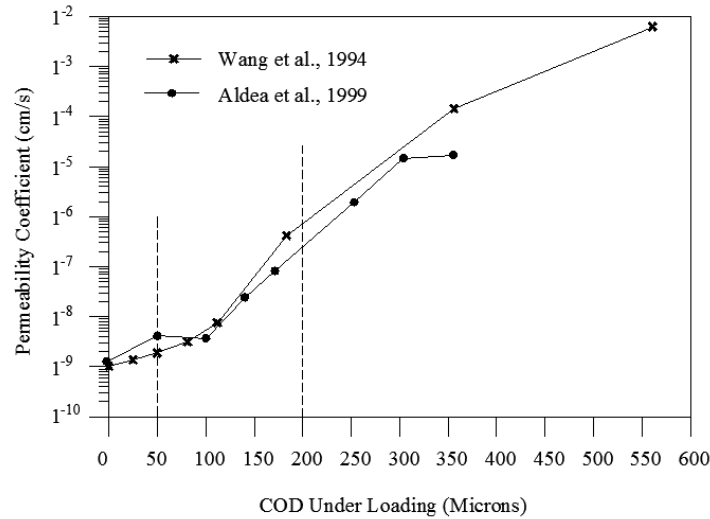
Figure 2.5 Crack width and material effect on permeability (Aldea et al., 1999)

Another factor that should be addressed when examining the cracked concrete permeability is concrete's self-healing nature. The introduction of water in a crack will allow for a phenomenon known as autogenous healing to occur. At a hydraulic gradient of 1 MPa/m of water, cracks less than 0.10 mm can be closed by self-healing processes (Reinhardt & Jooss, 2003). Also, the application and presence of mechanical stress also influences the cracked concrete's permeability properties (Hoseini, Bindiganavile, & Banthia, 2009). For concrete cracked under stress, there exists a threshold value for that applied stress. Other limitations on experiments conducted include constant properties of porosity and saturation and idealization of single cracks.

Primarily the focus of research has been on permeability of cracks with CODs less than 500 μm. Once the crack has a greater width than 1 mm the permeability is proportional to the cube of the crack width (Lawler, Zampini, & Shah, 2002). Thus the formation of one wide crack will be more permeable than several smaller cracks. An increase in the crack width consequently has a large impact on the permeability of concrete.

It is clear that the presence of cracks in concrete, depending on the crack width, will cause an increase in the permeability. The relation between concrete's permeability and its durability is not direct but interconnected by various mechanisms. First, cracks provide a direct path for aggressive agents such as siliceous solutions. Secondly, the overall increase in permeability in turn promotes deteriorating processes such as the carbonation and freeze-thaw.

Carbonation and freeze-thaw of concrete has been linked to the permeability of concrete. The square of the depth of carbonation shows a linear trend with the logarithm of the air permeability (Basheer, 1991). The relationship between air permeability and the mass loss during freeze-thaw damage was also found to be linear (Hilsdorf, Schonlin, & Burieke, 1992). Both of these mechanisms are damaging to concrete causing scaling, delamination, further cracking, and ultimately inducing corrosion of steel reinforcement.

Therefore, the permeability of concrete is indirectly a measure of its durability and longevity.

2.3.2 Chloride Diffusivity

Corrosion of reinforcement also depends on the diffusivity of chlorides in concrete. The exact quantitative relationship between chloride diffusivity and cracks remains still undetermined. Using a rapid penetration test, Aldea et al. (1999) concluded that the water permeability is more sensitive than diffusivity to the crack width. In a series of experiments conducted by Jang et al. (2011) the proposed theory of a threshold crack width was confirmed for chloride diffusion. Below a value of 55-80 microns the crack width has little influence on the diffusivity of chloride. Moreover, a linear relationship between crack width and diffusivity can be established after the threshold crack width is reached. The linear relationship was further defined by using a "crack geometry factor" to account for the variation due to tortuousness, connectivity, and constrictivity.

Several models have been developed in attempt to model the chloride diffusion in cracked concrete. In the model developed by Djerbi et al. (2008), the chloride diffusion coefficient is a function of the diffusion of uncracked concrete plus the effects of the crack. The effects of the crack are described as a linear function of the crack width from $30 - 80$ μm, and a constant when the crack width is greater than 80 μm. Gowripalan et al. (2000), theorize that it is more accurate to describe the chloride diffusivity with the crack width /cover ratio, W_{cr}/C. It was found that the chloride threshold level was related to W_{cr}/C by a hyperbolic function implying that the corrosion initiation of steel in concrete becomes more rapid with an increase in crack width. There exists extensive literature with models that examine various variables in the chloride diffusion of concrete: the effects of wet-dry cycles (Ye, Jin, Jin, & Fu, 2012), comparisons of experimental and numerical chloride penetration (Marsavina, Audenaert, De Schutter, Faur, & Marsavina, 2009) (Gerard & Marchand, 2000), and the effects of using recycled aggregate (Ying, Xiao, & Tam, 2013).

As previously discussed, the crack width significantly affects the permeability of cracked concrete. Thus with an increased permeability the ingress of corrosion agents such as chlorides will also increase. This will result in an overall increased corrosion rate. This conclusion has been justified by Vidal et al. (2004) who found that an increase in crack width generally resulted in an increased loss of steel area due to corrosion. Based on a parametric study of service life prediction in cracked concrete, it was found that an increase in crack width greatly decreased the service life of the concrete (Kwon, Na, Park, & Jung, 2009). The results of a probabilistic model and a deterministic model are shown in Table 2.1. The parameters of the model included a cover depth of 161 mm, a surface chloride concentration of 13.1 kg/m^3, a critical chloride content of 1.2 kg/m^3 and a diffusion coefficient of 3.87 x 10^{-12} m^2/s. The predicted service life values indicate that even hairline cracks less than 0.3 mm are capable of significantly reducing the service life of concrete.

Table 2.1 Service life predictions for cracked concrete for chloride diffusion (Kwon et al., 2009)

Crack Width (mm)	Service Life Prediction (Years)	
	Probabilistic Model	Deterministic Model
0.0 - Sound Concrete	84.5	118.5
0.1	44.5	65.0
0.2	22.5	35.5
0.3	13.0	20.5

2.4 Repair Techniques

2.4.1 Injection Repairs

The success of restoring the strength and stiffness of cracked concrete has been proven through years of experience and practice. The outcome of research has confirmed these results. In a simple experiment designed to test the performance of epoxy repairs, concrete blocks with simulated cracks were impregnated and tested in compression (Issa & Debs, 2007). The experimental results found that cracks reduce the strength of concrete in a range of 33% to 41%. The epoxy injection repaired bocks only experienced an 11% reduction in strength compared to the uncracked control block. The epoxy injections improved the performance of cracked concrete but not to the original capacity of the uncracked specimens.

Due to the simplicity of the experimental design the translation of the results to field repairs is often questionable. The cracks were simulated with greased steel plates and the specimens were loaded in compression parallel to the crack length. The effect of crack tortuosity on the performance of crack repairs is not well defined but it will influence bond between the epoxy and the concrete. In reality cracks will also vary in width along their depth and length. Where the cracks are not stable in their width the repair only becomes successful if the epoxies are compressed into the narrow slits. An epoxy resin with a higher elastic modulus will only allow for a small volume change when injected into cracks limiting their performance (Letsch, 1986). Moreover, crack repairs are most often subjected to flexural loading rather than direct compression. Under flexural loading the crack repairs will fail in the tension zones of the cross section.

The performance of crack repair methods under flexural loading has not gone untested. In an attempt to define the structural performance of various techniques, Thanoon et al. (2005) tested concrete slabs under four point bending. The resulting moments caused cracking in the slabs which were then repaired by cementitious grouting, epoxy grouting, and several other methods. The results were similar to those obtained with compressive loading. An epoxy injection repair experienced a 8.6 % reduction of the ultimate load when compared to the control specimen. With the exception of epoxy injection, all other techniques experienced an increase in the ultimate load as depicted in Figure 2.6. These experimental results suggest that epoxy repairs are a poor choice of

strengthening technique when compared to Carbon Fibre Reinforced Polymers (CFRP) and ferrocement layer repairs.
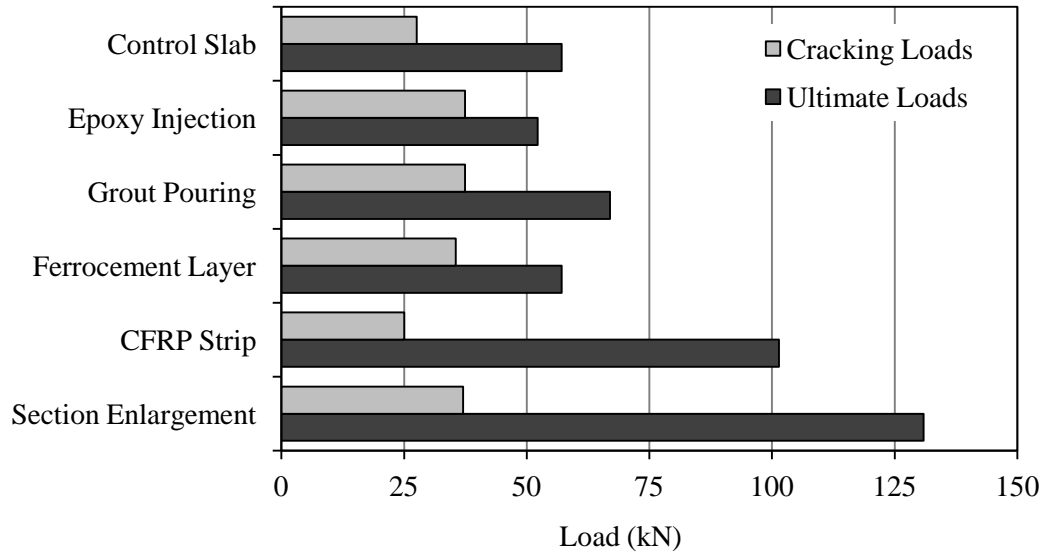
Figure 2.6 Structural performance of repaired concrete slabs (Thanoon et al., 2005)

Different materials are available for crack injections other than epoxies. Several other materials include: polyurethanes, methymethacrylates, cementitious grouts, modified cementitious grouts, etc. The choice of material used for the repair application depends on the different properties of the crack: crack width, whether the crack is active or dormant, depth and length, and whether the crack is leaking. Several technical guidelines have been published to aid in the selection of the type of repair material: "Guide for the Selection of Grouts to Control Leakage in Concrete Structures" published by the International Concrete Repair Institute (2006), "Guide for the Selection of Polymer Adhesives with Concrete" reported by the ACI Committee 503 (1992), "Guide for the Selection of Materials for the Repair of Concrete" made available by ACI Committee 546 (2006), and "Specification for Crack Repair by Epoxy Injection" by ACI Committee 503 (2007).

2.4.2   Concrete Overlays

Concrete overlays are a common method used in concrete rehabilitation, and in particular in the rehabilitation of bridge decks. Dependent on the type of material used and the depth of the overlay the repair can either be implemented to increase the structural capacity of the sections or to simply improve the concrete transport properties. As shown in Figure 2.6, a section enlargement, which can be achieved by the application of a thick overlay, is capable of increasing the structural capacity of concrete. From a durability standpoint, the overlay may be applied onto the concrete substrate to prevent the ingression of chlorides reduce the infiltration of water and other aggressive agents.

For example, the use of a high performance concrete overlay improves the concrete conditions in terms of rapid chloride permeability, gas permeability, and water permeability (Tayeh, Bakar, Johari, & Voo, 2012).

Regardless whether or not the overlay is applied as a structural repair or to preserve the concrete durability, the interfacial bonding or adhesion between the deteriorated concrete and the new overlay is one of the most important factors for a successful repair (Delatte, Fowler, McCullough, & Grater, 1998). In concrete rehabilitation, it is the bond between the two materials that results in failure of the repair (Yuan & Marosszeky, 1991).

A series of different tests are available to determine the bond strength of overlay repairs including: slant shear test, pull-off, and splitting prism. In an experimental investigation conducted by Momayez et al. (2005) it was found that the bond strength greatly depends on the type of test conducted. When in particular looking at the failure of laminated composite materials it is widely held that debonding occurs by shear along the base-overlay interface (Asad, M.H., & Al-Gadhib, 1997). Contrary to this, an investigation carried out by Granju (2001) found that in the application of thin cement based overlays, the governing failure mode is the built-in tensile stress perpendicular to the interface. The tensile debonding stress is developed by the combined effects of the bending of the structure, cracking of the overlay, and the peeling force induced by shear effects at the interface.

From the literature and through the use of the various testing methods, several variables were found to influence the bond strength of the concrete overlay material. The bond strength is capable of increasing up to 25% with the rough surface preparation and is more pronounced with low adhesive cementitious materials (Momayez, Ehsani, Ramezanianpoura, & Rajaiea, 2005). The inclusion of silica fume in the cementitious repair material increases the bond strength (Santos, Julio, & Silva, 2007). Moreover, the addition of polymers in the mortar and overlay mixtures has provided better adhesive properties, and ultimately greater structural and durability performance. The addition of latex and a combination of latex and methylcellulose both successfully restore the flexural capacity of cracked beams whereas plain or silica fume mortars experienced premature separation and reduced toughness and ductility (Ali & Ambalavanan, 1999). Various methods can be used to increase the adhesion between the adhesion of polymer mortars: the application of silane coupling agents (Gupta, Mani, & Krishnamoorthy, 1983), an increase in the polymer-cement ratio (Afridi, Ohama, Iqba, & Demura, 1995), and the use of different types of polymers (Brien & Mahboub, 2013).

Another failure mechanism of cement based concrete overlays for a durability repair is the cracking of the overlay material. This is primarily of concern with repairs applied to increase the durability and service life of the concrete. Shrinkage cracks can form caused by those mechanisms discussed in Sections 2.2. The potential for cracking increases with overlay materials because of the higher degree of shrinkage due to high cement contents needed for adhesion, and the high degree of restraint with substrate (Banthia & Gupta, 2009). The effects of shrinkage however are not limited to simply cracking, but may also result in the debonding of the overlay (Beaushausen & Alexander, 2006).

2.4.3 Self-Healing Repairs

With the advances in technology and materials, the concept of "smart" materials or self-healing materials has developed considerably over the past decade. This area of research has predominantly been for polymer materials and is now being explored for the implementation in the area of concrete materials (Ghosh, 2009). The mechanism triggering the self-healing may be passive, requiring no intervention, or may be active where a user is required to activate the healing process. A summary of the research being developed in the area self-healing of concrete is provided in Table 2.2. The technologies are subcategorized by microcapsules, tubular capsules, and other techniques. The theory and experimental work of encapsulation techniques and bacteria-based self healing is further discussed. The development of a self-healing prototype with the intent of implementation as part of the experimental work of this thesis is presented in Appendix D.

Table 2.2 Summary of research of self-healing in cementitious materials

Self-Healing Technique	Repair Material	Source
Microcapsules		
Oil core/silica gel shell - two component microcapsules	Methylmethacrylate monomer and triethylborane catalyst.	(Yang, Hollar, He, & Shi, 2011)
Poly(styrene-divinylbenzene) shell microcapsules	Epoxy.	(Ge, Wan, Lu, & Yu, 2011)
Silica shell microcapsules	Various organic compounds.	(Kaltzakorta & Erkizila, 2010)
Polyurethane shell microcapsules	Sodium silicate solution	(Pelletier, Brown, Shukla, & Bose, 2011)
Tubular Capsules		
Borosilicate glass / ceramic tubes	Polyurethane prepolymer and accelerator.	(Van Tittelboom K. , De Belie, Van Loo, & Jacobs, 2011)
	Cyanoacrylate.	(Joseph, Jefferson, & Cantoni, 2007)
Glass capillary tubes	Foam; Cyanoacrylate; 2 Part Epoxy; 3 Part Methylmethacrylate.	(Dry, Corsaw, & Bayer, 2003) (Dry & McMillan, 1996) (Dry, 1994)
	One-part epoxy	(Thao, Johnson, Tong, & Dai, 2009)
Other		
Bacteria	Strain *Bacillus pseudofirmus*	(Jonkers & Schlangen, 2007) (Jonkers & Schlangen, 2009) (Jonkers, A., Copuroglu, & Schlangen, 2010)
Superabsorbent Polymers		(Lee, Wong, & Buenfeld, 2010)

2.4.3.1 Encapsulation Techniques

One method of autonomous self-healing in concrete attempts to store the healing material in the cement matrix until required. Upon the initiation of cracking, the crack propagates through the vessel containing the repair material and the material flows into the crack. The repair system can either be a one-component system or a two-component system. In a one-component system the material acts readily with either already present moisture to solidify, whereas in a two component system the reactant must react with a second material, either another reactant or a catalyst. There are two methods of encapsulating the repair materials: microcapsules and tubular capsules.

Various methodologies exist for the encapsulation of materials, however polycondensation interfacial polymerization is most commonly used (Yang, Keller, Moore, White, & Sottos, 2008) (Huang & Yang, 2011) (McIlroy, et al., 2010). This process is produced typically using an oil-in-water emulsion, with two monomers dissolved in incompatible phases, meeting at the interface, and reacting immediately to form a membrane or shell which continues to grow (Yow & Routh, 2006). The shell encapsulates the core or repair material.

For the use in concrete microcapsules with silica-shell microcapsules have been developed containing two-component polymer repair materials (Yang, Hollar, He, & Shi, 2011) (Kaltzakorta & Erkizila, 2010). Other researchers have also considered a variation of different shell and core materials (Ge, Wan, Lu, & Yu, 2011) (Pelletier, Brown, Shukla, & Bose, 2011). In particular, the experiments conducted by Yang et al. (2011) found that the microcapsules decreased the permeability coefficient by 66.8% when loading 30-day old concrete to 80% of its compressive strength.

Tubular capillaries are another method of encapsulating the repair material within concrete. Repair material filled glass or ceramic capillaries varying anywhere from $2 - 5$ mm in diameter are cast within the concrete specimen. Dependant on the repair material, its adhesion and viscosity, cementitious materials containing tubular capsules with healing agents are capable of reducing the permeability of concrete. The self-healing of concrete is instituted for one of two reasons: to decrease the concrete's permeability or to increase the structural capacity. The decrease in permeability is achieved using expansive materials. A two-component expansive polyurethane foam encased in ceramic and glass capillary tubes saw a decrease in the water permeability of cracked concrete by a factor of $10^2 - 10^3$ and $10^3 - 10^4$ respectively (Van Tittelboom K. , De Belie, Van Loo, & Jacobs, 2011). For a structural repair, a strong adhesive is required. In the work of Joseph et al. (2007), it was found that the use of cyanoacrylate adhesive-filled glass capillary tubes witnessed an increase in the post-cracked stiffness, peak load, and ductility.

2.4.3.2 Bacteria

An environmentally friendly process of self-healing of cracked concrete includes the microbial precipitation of calcium carbonate ($CaCO_3$). The formation of $CaCO_3$ precipitate is the result of a series of biochemical reactions. The use of bacteria with cementitious materials is not a relatively new one. Bacterial concrete also has proven

capabilities of resistance to drying shrinkage, alkaline, sulphate, and freeze-thaw attack (Ramakrishnan, Panchalan, & Bang, 2001).

Recent research has progressed to include the bacterial spores within the cement paste. One specific process has been proposed by a team of researchers in the Netherlands. Jonkers et al. (2007) have developed a formulation involving the addition of organic compound substrates with bacterial spores to the concrete mix in order to activate the biochemical processes. The bacteria remain dormant within the concrete and at the onset of cracking are revived with the inflow of water. The bacterial spores then use the organic substrate also present in concrete to form the calcium precipitation which forms in the crack preventing further ingress of water.

The effectiveness of bacteria repaired cracks have been tested with injection and foam strip application methods (Van Tittelboom K. , De Belie, De Muynck, & Verstraete, 2010) (Bang, Galinat, & Ramakrishnan, 2001). With the proper protection in a silica gel, the bacteria are capable of reducing the permeability of cracked concrete from 10^{-7} m/s to as low as 10^{-12} m/s.

Several issues were observed with the use of bacterial spores in concrete. The inclusion of organic compounds within mixing water needed to activate the bacteria had negative impacts. Dependent on the type of organic compound, a 5-60% reduced strength was observed (Jonkers & Schlangen, 2007). Furthermore, the bacterial spores have proven to remain viable for up to 200 years within harsh environments (Schlegel, 1993). Despite this, Jonkers et al. (2010) found that the number of viable bacteria placed within the concrete decreases with time, leaving relatively no active bacteria spores after 135 days of curing suggesting that as the concrete cures and the pore sizes decrease, the bacteria which are approximately 0.8 μm are crushed.

2.5   Effects of Environmental Factors

2.5.1   Temperature and Thermal Cycling

Extreme temperatures and thermal cycling are environmental conditions capable of degrading concrete repairs. These two concepts need to be examined separately as each is caused by a distinct deterioration mechanism. Firstly, for the investigation of extreme temperatures, only epoxy repairs and in particular hot temperatures ranging up to 100 °C will be examined. Epoxy materials are thermosetting plastics, where their mechanical properties significantly change, when the epoxy goes from a hard glass like state to a rubber state. The observed softening of the material is caused by the weakening of cohesive forces between the molecules due to the vibrations of chain segments (Ehlers, 1964). The vibrations are initiated by the increase in temperature and lead to an overall decrease in the strength of the material.

Colak et al. (2009) found that epoxy injection repairs are influenced by the environmental temperature. The flexural strength of repaired beams were tested using three point bending at temperatures ranging from 40 to 100 °C, where the glass transition temperatures of the epoxies ranged from 75 to 100 °C. The load bearing capacity of four epoxy repairs were found to decline with an increasing temperature. At a temperature of 40°C, the four epoxies retained an average strength of 88% compared to those tested in

laboratory conditions , whereas at a temperature of 100°C, the same epoxies retained an average of 31% of the original strength.

In the same study by Colak et al. (2009) it was also found that at high temperatures greater than 80°C, the thickness of the epoxy injection became critical to the load-bearing capacity of the repaired beam. Concrete beams with a 5 mm adhesive demonstrated lower strength retention capability than those of 1 mm. In the case of adhesive joints, the fracture toughness of adhesive layers initially increase with the adhesive thickness then begin to decrease (Yan, Mai, & Ye, 2001). This suggests that there is an optimum adhesive thickness between 1 and 5 mm that could demonstrate greater strength retention.

One of the factors affecting the extent of damage caused by thermal cycling is the difference in the thermal coefficient of expansion (α) between the concrete and the repair material. Naderi (2008) investigated the response of a collection of overlay repair systems to a series of environmental conditions, including temperature cycling. The response of the repaired systems was evaluated by examining the repair/concrete bond. To do so, through a direct tensile test was employed. The repaired concrete slabs were 100 mm in depth with a 20 mm thick layer of repair mortar. One temperature cycle included raising the temperature to 80°C for 6 hours and cooling the specimens to 20°C for 18 hours. The environmental conditioning was continued for a total of 200 cycles.

The repair mortars contained a variety of polymer additives (polyester, styrene butadiene, etc.) with an array of thermal coefficients of expansions ranging from 8 to 55 x 10^{-6} mm/˚C. The resulting relationship of the direct tensile strength reduction with the thermal coefficients is reproduced in Figure 2.7. To calculate the bond strength reduction, the environmentally conditioned test results were compared to a control with 0 temperature cycles. In general, it was found that a positive correlation existed. A typical thermal coefficient of concrete varies from 6 to 12 x 10^{-6} mm/˚C (Mehta & Monteiro, 2006). The divergence of the repair material's thermal coefficient from that of the concrete substrate is an indication of the bond deterioration caused by the dimensional instability during temperature cycles.
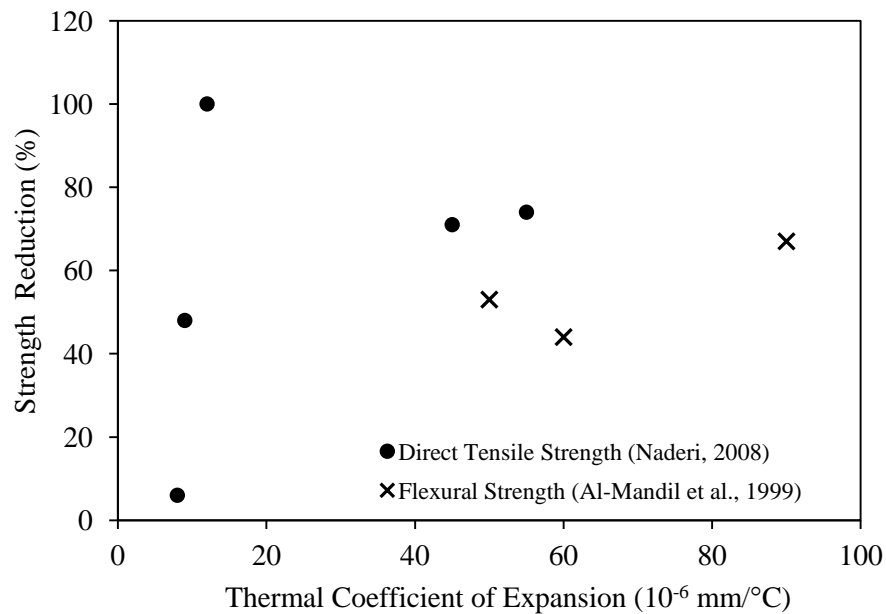
Figure 2.7 Repair systems strength reduction with temperature cycles

Al-Mandil et al. (1990) simulated cracks in concrete beams to examine the effects of temperature cycling on epoxy repairs. Three different epoxy materials with varying mechanical and thermal properties were injected in notches located at the middle of the beams and reaching mid depth. The thermal cycling regime consisted of 150 cycles, where one complete cycle consisted of 6 hours at 70˚C followed by another 6 hours at a temperature of 20˚C. The concrete beams were tested with third point loading in accordance with ASTM C78-84. Similar to the results of Naderi, it was found that the greater the thermal coefficient of expansion of the repair material, the greater the loss of the flexural strength of the concrete beam. The findings are replicated in Figure 2.7. The average flexural strength reduction of three different epoxies consisted of 44, 53, and 67%. With the temperature cycling regime, the bonding of the epoxy repairs became ineffective and the flexural strength began to approach that of a notched/unrepaired beam.

The effect of temperature cycling on the strength of the repaired system is also influenced by the types of stresses generated at the concrete/repair interface. By evaluating the flexural strength of an injection repair, the interface experiences a combination of shear and tension. Similarly, in a direct tensile strength test, an overlay repair only experiences tensile forces. Both Naderi (2008) and Al-Mandil et al. (1990) also evaluated the performance of repair materials subjected to temperature cycling using a slant shear test adapted from BS6319 developing a combination of compression and shear stress along the repair interface. After 30 temperature cycles Naderi found that 5 of the 6 different types of cementitious repairs experienced an increase in the shear bond strength by an average of 26%. However after a complete 200 cycles, the repair systems' shear bond strength had decreased by 89, 37, 21, 3, and 3%. In contrast, Al-Mandil found that for 3 different epoxy repairs the temperature cycles had no effect on the repair

system, where the compressive load increased by 27, 29, 111 %, and the failure was indicated by crushing the concrete rather than at the repair interface.

The temperature cycles generate stresses in the repair methods and the failure mode under the temperature cycles will also be dependent on the combination of the different material properties as well as the repair application and arrangement. In an analytical study conducted by O`Connor and Saiidi (1993) the stresses generated in a 19 mm thick cementitious and polymer modified cementitious overlays applied on bridge decks were examined. Using finite element modelling it was found that the failure occurred in tension with the polymer modified cementitious overlay at a temperature differential of 25˚C. Under the same conditions, the ordinary cementitious overlay proved to be successful. The coefficient of thermal expansion for the ordinary cement and the polymer modified were 9.0 and 23.4 μ/˚C respectively. The two overlays also had drastically different modulus of elasticity and modulus of rupture which affected the stresses developed and the criterion.

2.5.2   Freeze-Thaw Cycling

One of the most indicative environmental conditions on the durability of a repair is the action of freeze thaw (FT) cycles. In light of this, research has been conducted to determine the effects of freeze thaw on the durability of concrete repair systems. The deteriorating effects of FT on concrete as a material are well reviewed in literature and will only be briefly reviewed in this section before examining the effects on the repaired system.

Concrete is a porous material, and when water is readily available, the internal pore structure may be saturated. Upon freezing, water expands by approximately 9%. It was Powers (1958) who aptly described the FT damaging mechanism in concrete. During the FT process, when the pores are critically saturated, hydraulic pressure is developed as the frozen water forces the excess water out through the boundaries. The freezing water in turn also pushes against the capillary walls causing stress. In addition, an osmostic pressure is developed caused by the partial freezing of solutions due to the presence of substances such as chlorides, calcium hydroxide etc., which lower the freezing temperature. The stresses developed from the hydraulic, osmotic, and mechanical stresses created are released through micro-cracking of the concrete structure.

An examination of literature on the effects of FT on repaired systems shows how the damage mechanisms vary compared to those of plain concrete samples. In a study conducted by Tsiatas and Robinson (2002) the durability of concrete crack repairs subjected to FT cycles was evaluated using the fundamental transverse frequency. The six repair materials that were examined included: one modified cementious material, one cementitious material, two epoxies, and two high molecular-weight-methacrylates (HMWM). The repairs were subjected to FT cycles in accordance with ASTM 666 "Standard Test Method for Resistance of Concrete to Rapid Freezing and Thawing".

Examining Figure 2.8 it is evident that the performance of the concrete repaired system highly depends on the type of repair material used. The HMWM performed the best, exhibiting an increase in the fundamental frequency of 4.31 and 1.37 Hz after FT testing. The epoxy materials also performed well, showing only a slight decrease in the

fundamental frequency. The cementitious had the highest decrease in fundamental frequency, observing a decrease of 133.4 Hz, significantly lower that the uncracked control concrete

In the same investigation by Tsiatas and Robinson (2002) fatigue cycling was used to evaluate the concrete crack repairs. For this destructive method of testing, the results are representative of the structural effectiveness of the repair system after environmental conditioning. The results from the fundamental transverse frequency do not correspond to those of fatigue cycling. In this instance the best performing sample is the control with no cracks, and the HMWM which showed an improvement in fundamental frequency failed during the first fatigue cycle. The samples and respective fatigue cycles included: Control (154,229), Epoxy 2 (130,806), Epoxy 1 (100,574), HMWM 2 (99,929), Modified Cementitious (67,669), Cementitious (110), and HMWM 1 (0).
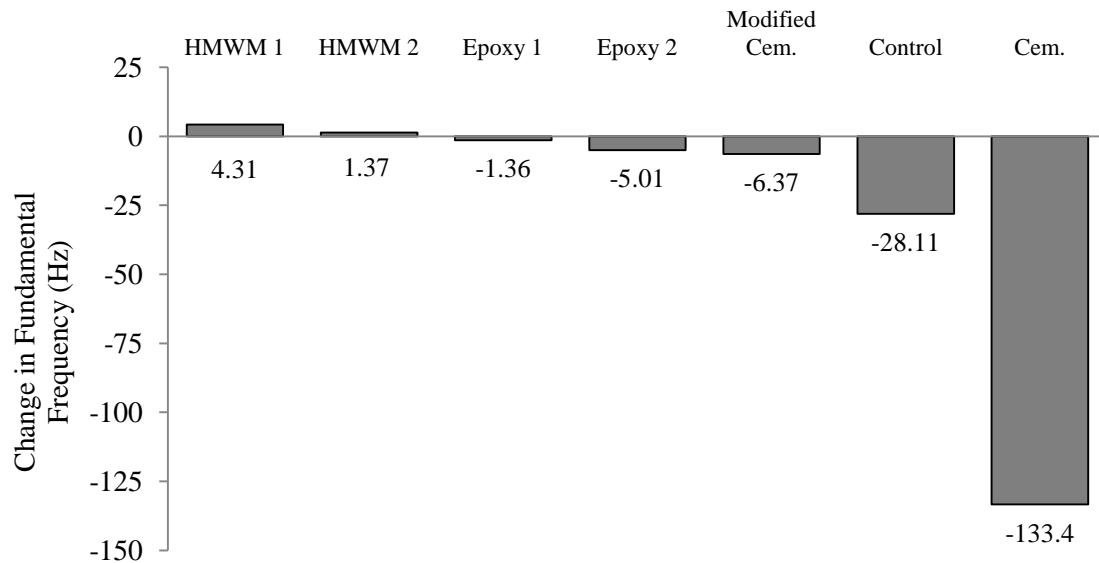
Figure 2.8 Change in fundamental frequency after 300 FT cycles (Tsiatas & Robinson, 2002)

The decrease in the performance of the cementitious repair material may be attributed to the poor compatibility between itself and the concrete substrate. One deteriorating mechanism includes the incompatibility of the pore structure. Similar incompatibilities and damaging consequences are seen in historic mortar repair (Klisińska-Kopacz, Tišlova, Adamski, & Kozłowski, 2010). Other potential causes include additional stresses on the materials due to drying shrinkage and differences of coefficients of thermal expansion (Emberson & Mays, 1996).

The resinous repair materials, epoxy and HMWM, both experienced changes in fundamental frequency less than that of the control, implying that these repairs suffered less damage. In the application of the resinous materials, during the solidification, there develops cracks at the adhesive interface (Bowers & Zisman, 1964). During the freezing

stage, these present microcracks provide relief during the hydraulic pressure development. In turn, there is less internal damage in the concrete repaired system.

Colak et al. (2009) also investigated the effects of FT cycles with salt solutions on epoxy crack repairs. Two categories of epoxies were used: a low molecular weight resin and the same resin with a quartz sand filler (74% by volume). In general, it was observed that the flexural capacity of the repaired systems decreased with an increasing number of FT cycles. Furthermore, it was determined that the epoxy resin repaired systems maintained bond stability up to 40 FT cycles. With an increase from 40 to 60 FT cycles, the epoxy repaired systems experienced adhesion failure exhibiting a 49% decrease in flexural capacity. The epoxy-filler repairs proved to be more effective, maintaining high flexural strengths at 60 FT cycles. The author attributed this maintaining in the bond stability to the decrease in magnitude of the stresses during the solidification process of the epoxy-filler adhesive.

The bond between the epoxy injection and the substrate is the cause of failure when subjected to freeze thaw cycles. This form of failure mode, however, does not impact the structural performance of the repaired system at ultimate loading. Ekenel and Myers (2007) found that epoxy repaired beams subject to laboratory and environmental conditions both exhibited the same flexural capacity. The environmental conditioning consisted of FT cycles as well as extreme temperature cycles and UV light exposure. An observation was made during experimentation that the concrete repairs that are loaded to failure under laboratory conditions commonly fail due to the formation of new cracks. When the same repair systems underwent environmental conditioning or accelerated testing, the repaired cracks reopened during failure.

Naderi (2008) examined the shear bond strength of concrete overlay systems subjected to FT cycles. Five different overlay systems consisted of: an epoxy resin mortar, a polyester resin mortar, a styrene butadiene rubber (SBR) modified cementitious mortar, a sand/cement mortar with epoxy bonding agent, and a sand/cement mortar with cement bonding. The repaired specimens were soaked in water for 48 hours prior to FT cycling which consisted of 17 hours at -20 ˚C and 7 hours in a 20 ˚C water tank. The shear bond strength was recorded at 33, 100, 200, and 300 cycles. The results are replicated in Figure 2.9. The highest loss in shear strength was that of the polyester resin mortar after 300 cycles (77%), followed by the SBR mortar (63%). Both the epoxy resin mortar and the mortar with epoxy bonding also experienced a loss of shear bond strength with FT cycles. However, the mortar with cement bonding showed an improvement in the shear bond strength, a total increase of 30% at 300 cycles.
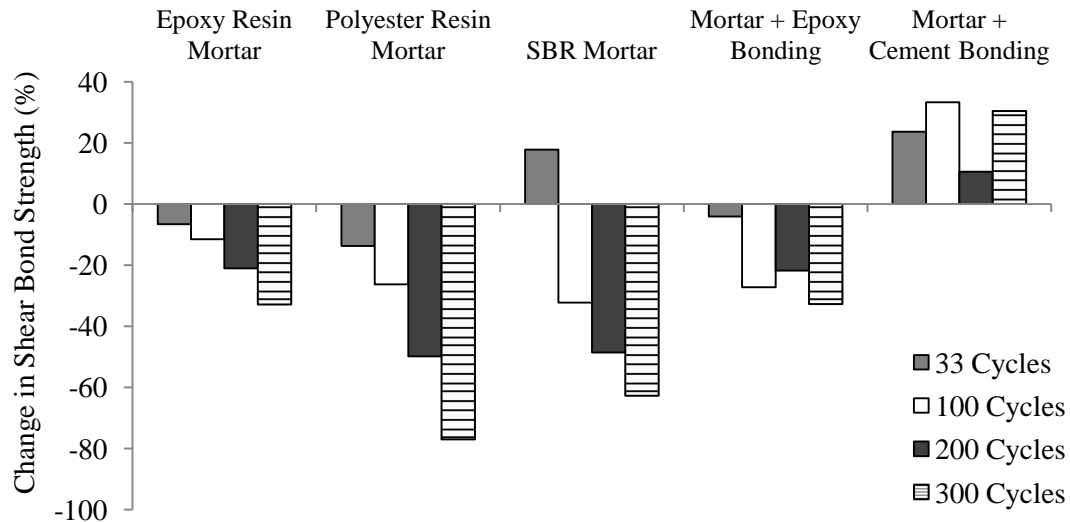
Figure 2.9 Effect of FT on shear bond strength of different repair systems (Naderi, 2008)

The loss of shear bond strength of the polyester resin mortar may be attributed to its high susceptibility to weathering, upon which it experiences embrittlement, shrinkage yellowing and crazing (Shashoua, 1992). Naderi attributed the deterioration of bond in the resinous repair systems to the water vapour flow in the specimens. The water from the saturation period of the cycling process is trapped in the concrete substrate underneath the impermeable repair material, building up to critically saturate the concrete. In turn, the layer of concrete at the repair interface experiences excessive deterioration due to FT. The increase in the shear bond strength of the cement bonded mortar may be a result of the continued hydration of the bonding cement and mortar.

2.5.3 Salt Solutions

During its service life, concrete will be exposed to corrosive environments in the presence of marine environments or through the use of deicing salts. The presence of salt solutions can deteriorate concrete by inducing mechanical stresses due to the crystallization of salts in the pores from their supersaturated solutions (Thaulow & Sahu, 2004). When coupled with freeze-thawing, salt solutions promote the development of osmotic pressure by lowering the freezing temperature in isolated regions. The damaging effects due to the presence of salts are worsened in a state of wetting and drying cycles (Spragg, et al., 2011). This section once again focuses on the literature presented on the influence of salts on repaired concrete rather than on plain concrete.

The integrity of epoxy crack repairs under two solutions: magnesium chloride ($MgCl_2$) and magnesium sulfate ($MgSO_4$) (Colak, Cosgun, & Bakirci, 2009). The samples were submersed in the solutions for a total of 120 days where upon they were tested under four point flexural bending. No deterioration was observed at the repair interface and only submersion in $MgCl_2$ solutions resulted in significant strength decrease. The concrete

observed a 12-29 % decrease of the flexural strength in epoxy-bonded specimens in a 10% $MgCl_2$ solution.

Colak et al. (2009) account for the decrease in flexural strength by the disruption of the interfacial zone between the cement and aggregate in the presence of the Mg atoms. The presence of $MgCl_2$ causes the replacement of CSH with non cementitious magnesium silicate hydrate, resulting in severe damage with scaling in concrete (Lee, Cody, Cody, & Spry, 2000). Due to the impregnation of concrete voids at the repair site, the formation of crystals occurs in the bulk of the concrete, leaving the repair-concrete interface in relatively undamaged.

In a further study conducted by El-Hawary et al. (1998) on epoxy repaired concrete exposed to salt water, it was found that for split and flexural tests failure occurred in the concrete, however, when exposed to for a duration longer than 6 months, the failure occurred within the epoxy. The bond test consistently found failure in the epoxy. Over a period of 18 months found that there was an initial decrease in strength of the repaired system due to salt crystallization, followed by an increase in strength due to continued hydration for the following strengths: tensile strength, compressive strength, flexural and bond strength.

While the presence of salts has a direct impact on the different strength properties of concrete, the effects can also be examined in terms of concrete's barrier properties. Accordingly, to protect concrete substrate samples, Mordallo et al. (2012) applied a series of concrete surface coatings that were placed in a highly saline tidal environment located along the Bandar-Abbas coast in South Iran. To determine the durability of the coatings, a chloride penetration test was conducted on core samples at the ages of 3, 6, 9, 36, and 60 months. From the results, the service life of the coating was predicted from empirical equations, assuming that failure occurred when the diffusion of the coating was equal to that of the reference concrete. The results are reproduced in Table 2.3. From these results it is clear that the polymer modified coatings have greater protective barrier properties than the plain cementitious coating with the exception of the acrylic modified cementitious coating.

Table 2.3 Overlay service life under salt solutions (Mordallo et al., 2012)

Coating Type	Coating Lifetime (Months)
Acrylic modified cementitious coating I	9
Epoxy polyurethane	46
Low viscosity silane primer & aliphatic acrylic top coat	48
Acrylic modified cementitious coating II	42
Cementitious coating	23
Low viscosity silane primer & styrene acrylate top coat	18

2.6   Summary

A review of the available literature on concrete crack repair was presented in this chapter. The mechanisms of different early age cracking in concrete were examined. Autogenous shrinkage in particular poses a problem with high performance concretes. These mechanisms which cause cracking are inherent to concrete, and although they can be mitigated they cannot be entirely avoided. Therefore, with proper restraint in a structure and the combined shrinkage deformation discussed, cracks may form in concrete.

Typically in practice, large crack widths can be the cause of structural deficiencies. Smaller cracks formed due to shrinkage cracking were proven to have implications on the mass transport properties of concrete, and ultimately on its durability. Crack widths as small as 50 microns begin to influence the concrete's permeability properties. The greater the permeability and diffusion of concrete leads to the penetration of aggressive agents through the concrete. This in turn leads to such mechanisms as the corrosion of reinforcement significantly reducing the service life.

To restore concrete's service life, different repair methods can be applied. An overview of three types of repairs is presented: injection repairs, overlay repairs, and autonomous self-healing repairs. The injection and overlay repairs being the more traditional techniques with well established and available materials of the three presented. The recent research of self-healing repairs in cementitious materials is also discussed to illustrate the direction of the future development of concrete crack repairs.

Finally, the effects of environmental conditions on concrete and repair materials are reviewed. These environmental conditions include: temperature cycles, freeze-thaw cycles, and the presence of salt solutions. For all three conditions the long term effects have negative impacts. The deteriorating effects include the reduction of tensile and flexural strength of the repaired systems, the loss of adhesion and bond strength between concrete and the repair material, the loss of fundamental frequency, and the reduction of fatigue cycles.

The literature available on the long term effects of concrete crack repairs from a durability perspective is however limited. The focus of research has been the structural capacity of concrete crack repairs or the durability of the repair has been implied to be synonymous to the structural effectiveness. Subsequently, this thesis aims to investigate the long term effectiveness of concrete crack repairs from a non-structural perspective by monitoring the mass transport properties of the repaired concrete.

CHAPTER 3 EXPERIMENTAL PROGRAM

3.1   Introduction

A comprehensive experimental program was developed to address the objectives of this study, namely to test the durability and longevity of repair methods of hairline cracks in concrete. The experimental program includes the selection of material, specimen preparation, selection of repair methods, and test methods for evaluating the long term performance of the repairs. Evaluation of the structural integrity of the repairs is not the intent but rather the air and water tightness of the repaired concrete section.   The following sections outline the materials selected for the experimental program, the procedures adopted for the fabrication of the concrete specimens, the various test methods conducted, and the evaluation techniques carried out.

3.2   Material

The materials selection includes those used for fabricating the concrete specimens and for repairing the cracked concrete specimen. For the repair, three different materials were selected; epoxy, polyurethane and polymer modified cementitious paste.

3.2.1   Concrete

Concrete mixtures consisted of fine and coarse aggregates, ordinary Portland cement (OPC), chemical and mineral admixtures, and water. The coarse aggregate used in the production of the concrete specimens is High Performance Bedding (HPB) obtained from Holcim Inc.'s Milton Quarry located in Milton, Ontario. The HPB is a crushed limestone aggregate with a nominal size of 6.7 mm that had been washed and graded. The aggregate's nominal aggregate size was smaller than that which is typically used in concrete production. Despite this, the particle distribution of the coarse aggregate, obtained in accordance with CSA Test Method A23.2-2A (2009), still met the CSA gradation limits shown in Figure 3.1. The oven dry bulk density of the coarse aggregate, measured according to CSA Test Method A23.2-10A (2009), was 1461 kg/m^3. The saturated surface dry moisture content and specific gravity, obtained using CSA Test Method A23.2-12A (2009), were found to be 2.60% and 2.63, respectively.

For the fine aggregate, a silicious sand with a fineness modulus of 2.69 was obtained from Lafarge North America's west Paris plant. The gradation of the sand, determined using CSA Test Method A23.2-2A (2009), was found to be well within the defined CSA limits as seen in Figure 3.2. The sand possessed an oven dry bulk density of 1614 kg/m^3 obtained using CSA Test Method A23.2-12A (2009). Using CSA Test Method A23.2-6A, the fine aggregate was found to have a saturated surface dry moisture content of 1.80% and a specific gravity of 2.65.
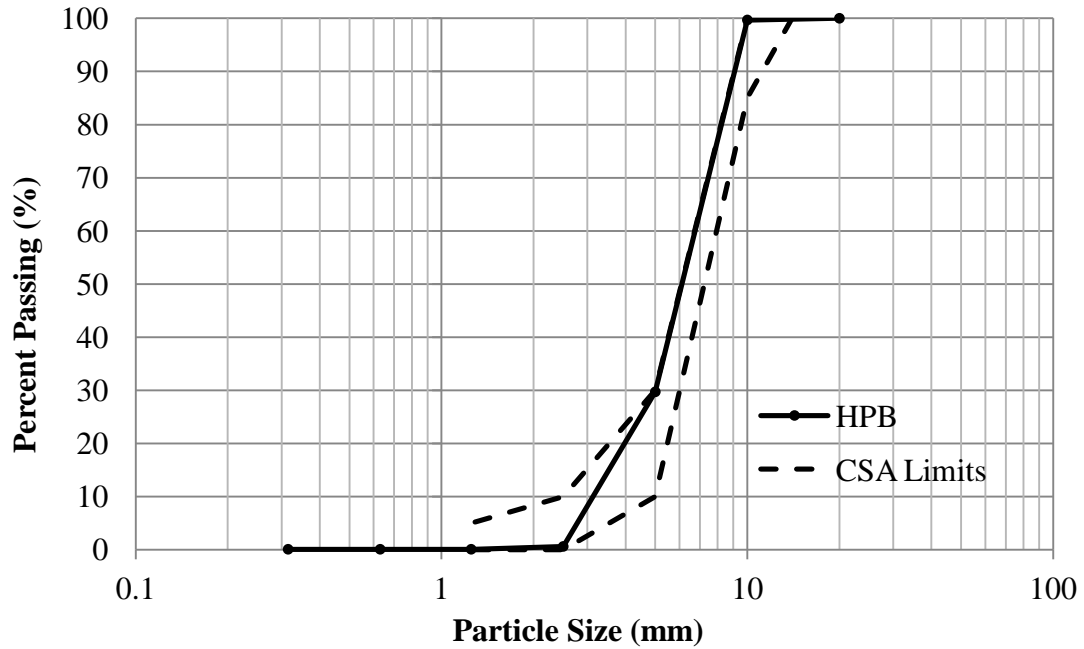
Figure 3.1 Gradation of coarse aggregate
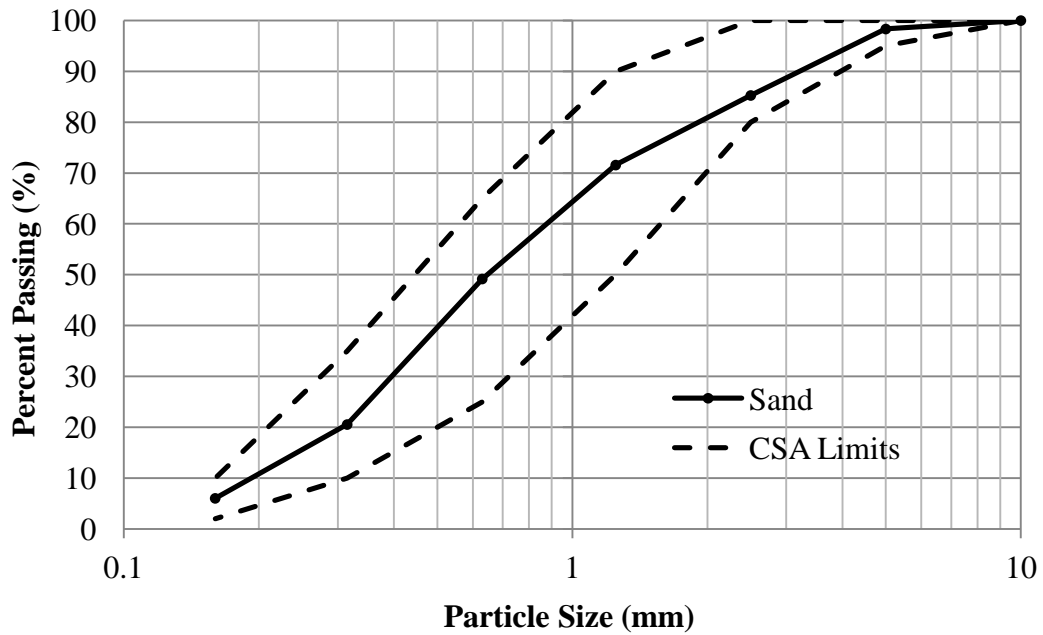
Figure 3.2 Gradation of sand

Two types of cement were used in the concrete specimen fabrication: Ordinary Portland Cement (OPC) (CSA type GU) and an 8% blended Silica Fume (SF) cement (CSA type GUb-SF). The Type GU cement was obtained from Lafarge North America's Bath plant in Ontario and the Type GUb-SF was acquired from the St. Constant plant in Quebec. The chemical and physical properties of the cement are listed in Table 3.1.

To achieve the desired workability of concrete, Glenium 770 manufactured by BASF Construction Chemicals was used in this study. This chemical admixture meets ASTM C494 provisional requirements for two types of admixtures: Type A ─ water reducing and Type F ─ high range water-reducing (BASF, 2010). The recommended dosage range of 130-975 mL/100 kg of cementitious materials was followed.

The air entraining agent, Micro Air, manufactured by BASF Construction Chemicals was used in the concrete mixtures. This product meets the requirements outlined in ASTM C260 (BASF, 2010). The manufacturer's recommended dosage of 35 mL per 45 kg/m^3 of cement content was used.

3.2.2 Steel Reinforcement

Each concrete specimen contained a 175 mm x 175 mm section of a galvanized steel welded hardware mesh fabricated by Peak Fencing. The mesh contained a 0.11 mm diameter wire with 12.7mm x 12.7 mm openings.

3.2.3 Repair Materials

Three repair methods were selected for this study. The first two methods are crack injection repairs and the third repair uses the overlay method. The three repair materials used are epoxy, polyurethane (PU), and polymer modified cement paste.

A two-component, 100% solids epoxy resin, Sikadur 55 SLV, manufactured by Sika was applied to the cracked concrete specimens. The product is a super-low viscosity, moisture insensitive, crack penetrating sealer that meets ASTM C881 specifications for epoxy-resin-base bonding systems for concrete (Sika, 2012). The two components consist of an epoxy compound and an amine compound mixed at a ratio of 2:1 by volume respectively. The viscosity of the mixed components is 105 cps with a pot life of 20 minutes, making it an ideal injection material for hairline cracks. The material properties as specified by the manufacturer are reproduced in Table 3.2.

A two-component, 100% solids and flexible polyurethane grout, SikaFix PU, manufactured by Sika was used as a non-structural repair material. The two components consist of a resin and hardner which are dispensed from a dual cartridge at a ratio of 1:1 by volume. The combined components have a specific gravity of 1.13 and a viscosity of 500 cps. A volume of 1 L of SikaFix PU grout will freely expand to approximately 25 L of foam. The pot life of a 200 g sample is approximately 60 minutes depending on the humidity and presence of moisture and has a reaction time of 39 s and a gel time of 460 s (Sika, 2012).

Table 3.1 Chemical and physical properties of cement (Lafarge Cement, 2011)

Chemical Properties	Type GU Cement	Type GUb-SF Cement
SiO_2 (%)	19.5	25.4
Al_2O_3 (%)	4.8	4.1
Fe_2O_3 (%)	3.1	3.1
CaO (%)	61.6	57.1
MgO (%)	2.9	2.7
SO_3 (%)	3.5	3.6
Loss on Ignition (%)	2.5	2.2
Insoluble Residue (%)	0.62	―
Equivalent Alkalis	0.7	―
Silica Fume Addition (%)	‒	8
Physical Properties		
Blaine Fineness (m^2/kg)	380	597
Retained on 325 Mesh (45um) (%)	3	8.6
Time of Setting (min)	105	148
Compressive Strength - 3 Day (MPa)	25.7	30.0
Compressive Strength - 7 Day (MPa)	32.3	38.4
Compressive Strength - 28 Day (MPa)	40.9	54.1

SikaTop Seal 107, a two component, polymer-modified, cementitious waterproof and protective slurry, produced by Sika was used as a repair overlay system. It is typically applied in layers on concrete surfaces to improve water tightness and protect against water penetration. To achieve a slurry consistency, the two components, an acrylic polymer compound and a cementitious component are mixed at a ratio of 1:4.1 by weight. The working time of the slurry is approximately 60 minutes at a temperature of 20°C. The material properties as specified by the manufacturer are listed in Table 3.3 (Sika, 2012).

Table 3.2 Material properties for Sikadur 55 SLV (Sika, 2012)

Properties at 23°C, 50% RH, and 7 Days	Values
Bond Strength – ASTM C882 (MPa)	17
Shear Strength – ASTM D732 (MPa)	40
Tensile Strength – ASTM D638 (MPa)	48
Compressive Strength – ASTM D695 (MPa)	75
Modulus of Elasticity – ASTM D695 (GPa)	2.0

Table 3.3 Material properties for SikaTop Seal 107 (Sika, 2012)

Properties at 23°C, 50% RH, and 28 Days	Values
Bond Strength – ACI 503R-30 (MPa)	1.0
Tensile Strength – ASTM C307 (MPa)	6.0
Compressive Strength – ASTM D695 (MPa)	20
Flexibility – ASTM D522 (%)	8

3.3   Specimen Fabrication

3.3.1   Concrete Mixture Design

The concrete mixture design was proportioned to resemble that of a possible concrete mixture used in bridge construction with the potential of acquiring shrinkage cracks. The concrete was designed on the basis of a type C-1 class of exposure according to the CSA Standard A23.1 (2009) which encompasses structurally reinforced concrete exposed to chlorides with or without freezing and thawing conditions. The design requirements for this class of concrete includes a maximum water-to-cementing ratio (w/c) of 0.40, a minimum compressive strength of 35 MPa at 28 days, and an air content range of 6-9% (Cement Association of Canada, 2011).

The same mixture design was used for the two batches of concrete, only varying the cement type (OPC or SF). The design proportions of materials were chosen based according to the concrete proportioning method of the Cement Association of Canada (CAC, 2011). The concrete was designed for a target compressive strength of 35 MPa, a slump of 150 mm, and a maximum air content of 9%. Based on these target requirements

and the recommendations listed by CAC, a w/c value of 0.38 and a coarse aggregate bulk volume of 0.47 were chosen. The material proportions are listed in Table 3.4.

Table 3.4 Concrete mixture proportions

Materials	Mass (kg/m^3 concrete)
Water Content	180
Cement Content	475
Dry Weight Coarse Aggregate	687
Dry Weight Fine Aggregate	882
Chemical Admixtures	**Volume (mL/100 kg cement)**
Air Entraining Agent	78
Superplasticizer	163

3.3.2   Specimen Design

The specimens used in the experimental program were designed largely for ease of handling. The specimen dimensions are 200 mm by 200 mm with a depth of 60 mm as depicted in Figure 3.3. The smallest dimension, 60 mm, meets the requirement that the nominal coarse aggregate size (6.7 mm) should not exceed one-fifth the narrowest dimension. The dimensions of the specimens were limited on two other accounts. First, enough surface area was necessary to allow for the Torrent air permeability testing (Section 3.5.1). The minimum distance between the external diameter of the two-chamber vacuum cell (105 mm) and the outer edge of the structural element must be a minimum of 20 mm, requiring a width of at least 145 mm. Secondly, the depth of the specimen requires a minimum depth of 50 mm to allow for the placement of the ultrasonic pulse velocity sensors (Section 3.5.2).

A steel mesh was placed in each specimen at a distance of 15 ± 5 mm from the top finished surface. The primary purpose of the steel reinforcement was to control the crack width opening in later stages of the experimental program and to prevent any sudden brittle failure which would cause the specimens to completely fracture.
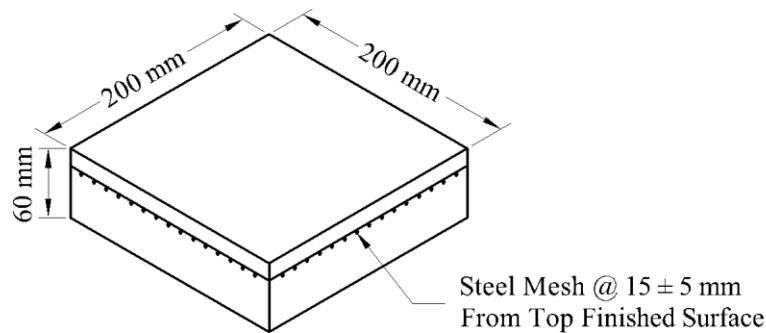
Figure 3.3 Concrete specimen dimensions

3.3.3   Concrete Specimen Production

The same concrete fabrication procedure including mixing, placing, and curing was followed for the two separate concrete pours. The first concrete batch using OPC produced a total of 42 specimens, and was cast on January 24, 2012 using a pan mixer at the Applied Dynamics Laboratory, McMaster University. The second set of specimens mixed with the OPC + SF cement was mixed and placed on February 22, 2012, also producing 42 specimens. The concrete was mixed according to the following procedure:

1. The air entraining agent and superplasticizer were added to the water and stirred for 30 seconds.
2. The dry materials: the coarse aggregate, fine aggregate, and cement, were added to the mixer and mixed for 1 minute.
3. Half of the water content was added to the dry mix while continuing to mix the dry ingredients. The contents were mixed for 2 minutes.
4. The remaining water was added and mixed for 2 minutes.
5. The mixing was paused for 1 minute.
6. The total contents were mixed for 1 minute.

The fresh properties of the concrete mixtures were evaluated using a slump test and according to the CSA Test Method A23.2-5C (2009). The density and the air content for each mixture was measured according to CSA Test Method A23.2-4C (2009).

For both concrete batches, six cylinders, 150 mm in diameter and 300 mm high were prepared for compressive strength testing in accordance with CSA A23.2-3C (2009). The cylinders were cast in three layers, pouring each layer of concrete and subsequently rodding 25 times into only the top layer. The cylinders were left to set and after 24 hours were demolded and placed in a saturated lime water bath at an average temperature of 15 ℃ for 7 days.

The fresh concrete mix was poured into wood forms in two stages. First the concrete was poured to a depth of 45 mm. A5mm thick steel plate was placed on top of the poured concrete, the vibrator head was placed on the steel plate and the entire surface

area of the concrete was vibrated for approximately 5 seconds. This was done to properly compact the concrete into place and avoid honeycombing. The steel mesh was then worked into the surface of the vibrated concrete, as shown in Figure 3.4. The second layer of concrete was immediately added on top of the steel mesh to avoid the formation of cold joints. The second layer of concrete was vibrated using the same procedure.

Figure 3.4 Steel mesh placement in concrete specimens

Once the concrete forms were filled and vibrated, the concrete surfaces were levelled and smoothed using a steel trowel. The concrete specimens were left until initial setting, where after an hour, the surface of the specimens were finished using a magnesium float. The specimens were removed from the forms after 24 hours and placed in a saturated lime water bath to cure for 7 days at an average temperature of 20ºC. After 7 days of moist curing, the specimens were removed from the water bath and left to dry at an average temperature of 22 ºC and RH of 50%.

3.3.4   Crack Formation

A three-point bending setup was adapted from RILEM's TC 162-TDF (2002) to generate cracks in the concrete specimens. Principally, this test method was developed to evaluate the tensile behaviour of steel fibre reinforced concrete beams by monitoring the load-displacement relationship for a notched beam. As such, several modifications have been made to accommodate the objectives of the experimental program. The first deviation includes the specimen dimensions and configuration. The standard requires a concrete beam with dimensions of 150 mm x150 mm x 550 mm. As previously discussed in Section 3.3.2, the dimensions of the concrete specimens in this experimental program were chosen primarily for ease of handling. Furthermore, the notch required at mid span in the RILEM was omitted in the experimental program to allow for a natural crack propagation throughout the entire concrete specimen depth.

At an age of 8-10 days the specimens were supported at a 190 mm span, with two fixed steel rods welded onto separate plates. The two rods were arranged on the base table

of a 2.224 kN MTS Testing system and fastened in place using steel angles placed around the corners and epoxied onto the base. The RILEM TC 162-TDF requires that one of the bottom rods be capable of rotating. However the primary objective for this test setup was to induce cracks, not to measure any of the fracture or tensile properties of the concrete.

A batch of hydrostone (gypsum cement) was mixed for each concrete sample tested and was placed along the length of the steel rods to avoid the development of stress concentrations due to any irregularities in specimen geometry. The specimen was then set on top of the rollers so that the finished surface was oriented along the bottom. The hydrostone was allowed to set before proceeding with the rest of the procedure.

The MTS machine, a static-hydraulic load frame was operated using a displacement-based control system. The frequency of the displacement readings was set to 3×10^{-3} Hz. A standard 0.001 mm scale dial gauge was attached to the MTS to manually monitor the displacement of the base table. The MTS setup is shown in Figure 3.5. The three point bending test operated undisturbed until the peak load was reached and subsequently began to decline. At this point the specimen had reached its cracking moment. Immediately after the peak load was recorded, the automated system was manually paused. The dial gauge was then zeroed and then the automated system testing recommenced. The test was continued until the vertical displacement increased by approximately 0.03 – 0.04 mm and a hairline crack was visible along the depth of the specimen. The relationship between the crack width opening and the vertical displacement is discussed in Section 3.3.5. This testing procedure was then repeated for a total of 72 specimens. An alternative method to generating cracks in concrete is presented in Appendix C.
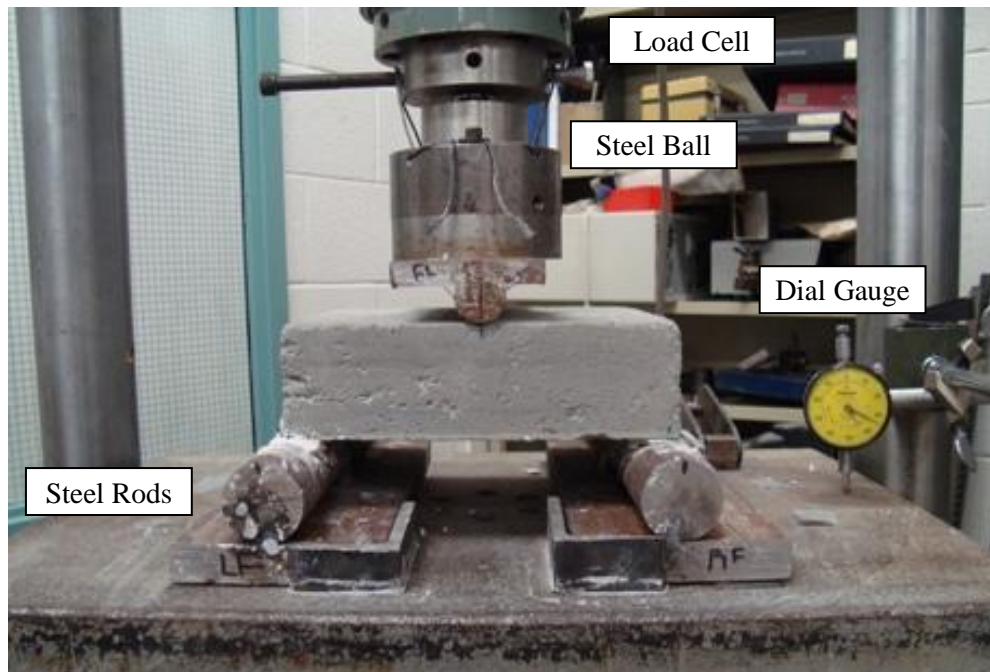
Figure 3.5 MTS three-point bending set-up

3.3.5   Crack Width Using Rigid Body Modes

Prior to cracking, the vertical displacement of the concrete at the midspan (*L/2*), is a function of the elastic modulus of concrete and the applied load. Post-fracture, it is possible to model the concrete using rigid body modes as shown in Figure 3.6. Using the following Equations 3.1 and 3.2, and combining them into Equation 3.3, a relationship between the vertical displacement and the crack width opening, *w*, is established. It is assumed that the crack propagates through the entire depth of the specimen, noting that the height *h*=60mm, and the length of the specimen *L*=190 mm. Accordingly, it is possible to approximately achieve the target crack widths based on the vertical displacement.

$$w = 2h\theta \qquad\qquad\qquad 3.1$$

$$\delta = \frac{L}{2}\theta \qquad\qquad\qquad 3.2$$

$$w = \frac{4h\delta}{L} \qquad\qquad\qquad 3.3$$
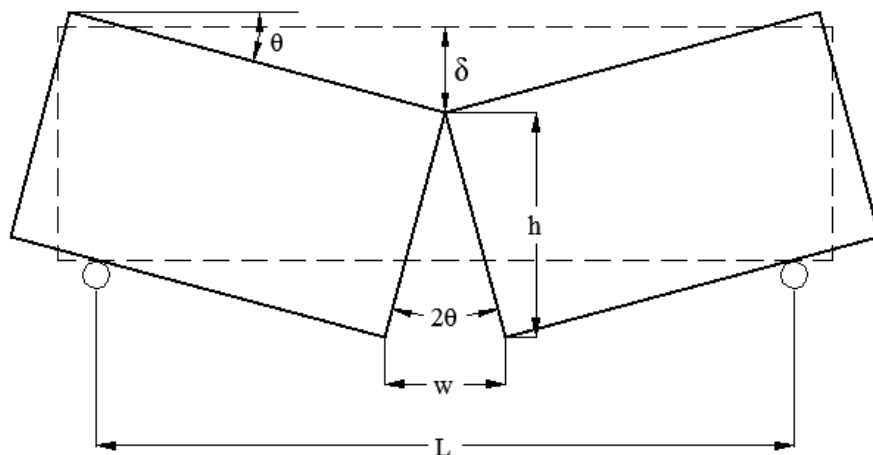
Figure 3.6 Crack width opening using rigid bodies

3.3.6   Repair Application

3.3.6.1   Epoxy

The epoxy repair,Sika's Sikadur 52 two component system, was applied using a gravity fed procedure in accordance with EN 1504-5: Concrete Injection, following method "M4.6 Filling of Cracks, Voids, and Interstices" (Danish Standards Association,

2004). First, a silicone barrier was formed to create a pond on the cracked surface. The dikes were placed at 40 mm from the crack. The sides of the specimen were left unsealed.

Once the silicone edge had set, the two components of the epoxy were mixed following the manufacturer's directions. The two liquid components were blended using a paddle mixer and a low speed drill at 400-600 rpm for 3 minutes. Immediately after mixing, the epoxy was poured into the silicone dikes as shown in Figure 3.7 . The epoxy resin was successfully injected into all the cracks which was made evident by the epoxy seeping out the sides of the cracks. A spatula was used to spread the epoxy within the dyke to ensure that the epoxy covered the entire marked area. The epoxy repaired specimens were then left to set overnight. In the following day, the silicone was removed from the specimens. All of the epoxied concrete surfaces were grinded down using a hand held electric grinder. In the case that the epoxy had seeped through the entire depth of the crack and pooled on the bottom surface, the bottom surfaces were also ground.

Figure 3.7 Epoxy poured into silicone dikes

3.3.6.2 Polyurethane

The SikaFix PU was dispensed using a low pressure procedure following the expectations of EN 1504-5: Concrete Injection, according to method "M1.4 Filling of Cracks" for the purpose of sealing the concrete (Danish Standards Association, 2004). The repair was carried out with the specimens resting horizontally, the cracked surface facing upwards. To prepare the specimens for the repair application, two holes with a diameter of 10 mm were drilled 100 mm apart along the crack propagating through the specimen. The holes were drilled to a depth of 50 mm. Afterwards, an air compressor was used to remove any residue. Water was then squirted into the two holes to moisten the crack in preparation for the polyurethane injection.

Sika Injection Ts were inserted into the two holes and using a dual cartridge gun, the two component mixture was administered through a static mixer according to the manufacturer's specification as seen in Figure 3.8 (a). The mixture was dispensed in both holes until it began to pool up on the top of the injection Ts, or until it was no longer able to dispense the two components. Minutes after injecting the cracks, the injection Ts were removed and the surface was wiped down to remove any of the mixture that had spilled from the ports. A successful repair would be indicated with water being displaced by the polyurethane and accumulating on the cracked surface as visible in Figure 3.8 (b). This however was not evident on all the specimens. For the specimens where the PU did not expand fully into the drilled holes after removing the T ports, additional PU was injected directly to seal the holes. Four days after applying the PU repair, the top repaired surfaces were grinded to remove any excess PU that had accumulated on the surface.

(a)   (b)
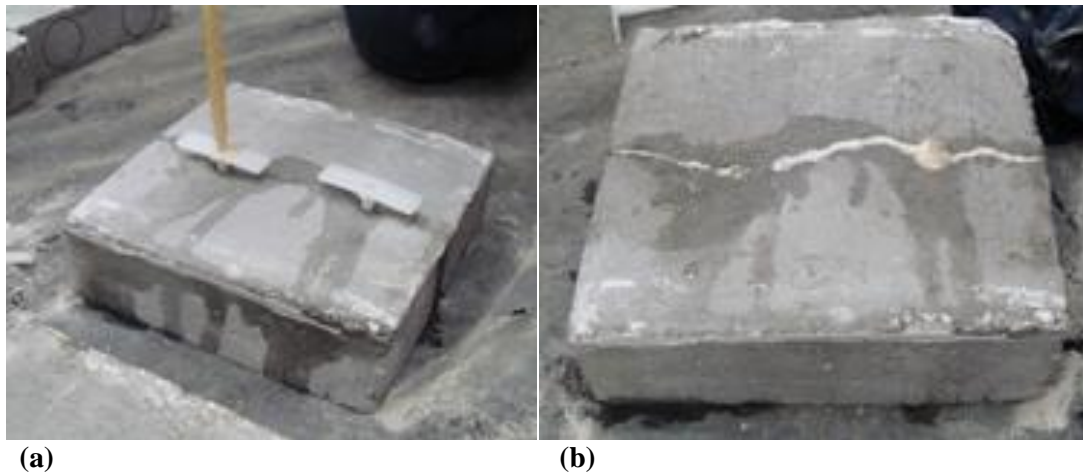
Figure 3.8 (a) SikaFix PU being injected using T-ports. (b) Polyurethane expanding and displacing water in the crack

3.3.6.3   Polymer-modified cementitious paste

The use of SikaTop Seal 107 was applied as a surface protection system as described in EN 1054-2: Surface Protection Systems for Sealing, following method "M1.2 Surface Protection by Sealing" (Danish Standards Association, 2004). The specimens were first prepared by lightly sandblasting the surface to a texture resembling sandpaper, or to a CSP 3 texture as specified by the International Concrete Repair Institute (ICRI). The repair material was applied in two stages. Before applying the first layer, the sandblasted surfaces were wet with a sponge to reach a saturated surface dry (SSD) state. No water was visible on the surface before proceeding with the application.

The two components, an acrylic polymer and a cementitious dry mix, were proportioned to achieve a slurry consistency at a ratio of 1:4.1 by weight, respectively, as recommended by the manufacturer. The acrylic polymer component was poured into to a bucket and the cementitious component was slowly added while stirring with an electric drill and paddle mixer at a speed of 300-450 rpm. The two components were mixed for 3 minutes. A 1 mm layer of the mixture was applied using a long nap roller as seen in

Figure 3.9. The overlay was left to cure indoors at room temperature for two days before applying the second layer.

After the two days of curing, the specimens were lightly sandblasted to a CSP3 texture. The sandblasted surface was wet to a Saturated Surface Dry state. Another batch of the overlay slurry mortar was mixed using the same procedure as indicated previously. A second layer of the overlay mixture was applied, rolling the material onto the surface in a direction perpendicular to that of the first layer. After all of the specimens were coated with a second layer, a clean short nap roller was used to smoothen and finish the final coat.

Figure 3.9 Application of the first layer of SikaTop Seal 107

3.4   Test Methods

3.4.1   Concrete Compressive Strength

The concrete's compressive strength was determined after 28 days as described in Section 3.3.3. For each concrete batch, three cylinders, were tested according to CSA Test Method A23.3-9C (2009) using a 300 kip Tinius Olsen Universal testing machine.

3.4.2   Measuring Crack Widths

The characterization of the generated cracks within the concrete specimens was carried out by measuring the crack widths using a magnifying crack comparator with a minimum scale of 0.1 mm. Four different readings were taken at equally spaced distances along the crack length as shown in Figure 3.10. The average of the readings was used to represent the average crack width.
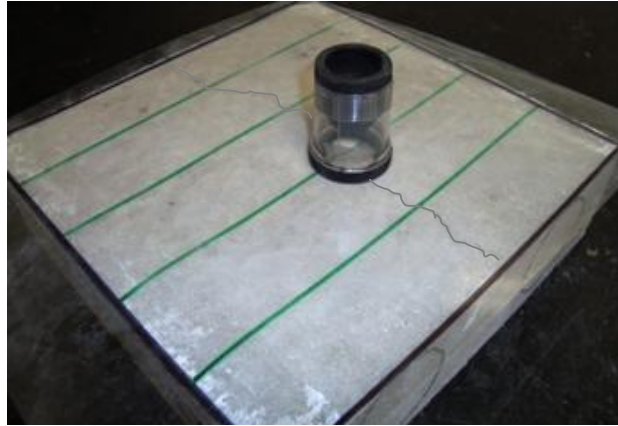
Figure 3.10 Measuring specimen crack width

3.4.3 Freeze-Thaw Testing

To examine the durability of the concrete crack repair systems, a series of environmental stressors, or freeze-thaw (FT) testing regimes were established. Three different regimes were chosen to represent various in situ environmental conditions that concrete could be subjected to through its service life in a Canadian environment: temperature cycles (T), freeze-thaw cycles with salt solutions (FTS), and freeze-thaw cycles with sustained loading (FTL). Each of these regimes exposed the repaired systems to different stresses which arise through different internal and external mechanisms.

The first environmental regime, temperature cycles, simply examines the mechanical compatibility between the concrete substrate and the repair material. The specimens are exposed to temperature variations which lead to dissimilar dimensional changes, caused by the difference in the thermal coefficients of expansion in both the materials. The result is the development of interfacial stresses at the substrate-repair boundary which may cause a loss of bond and deterioration.

Another environmental regime includes FT cycling with salt solutions. In contrast to the temperature cycling, the presence of water is included which increases the aspect of potential internal damage. By saturating the concrete samples, water is absorbed into the concrete pores, where, upon freezing, the water expands by 9%. In small capillary pores, hydraulic pressure is generated by the ice crystals pushing against the capillary walls. In the presence of de-icing salts, an additional destructive mechanism causes further damage. The presence of salt lowers the freezing temperature of the solution, therefore generating osmotic pressure developed due to the partial freezing regions (Mehta & Monteiro, 2006). FT with salt solutions leads to scaling of the concrete surface as well as to internal cracks caused by the formation of hydraulic and osmotic pressure. The repaired specimens were subjected to the FTS cycles to determine whether they exhibited any additional deterioration of the concrete or of the repair-substrate bond.

The third environmental stressor included FT cycles paired with a sustained load. The same damaging effects caused by hydraulic pressure discussed for the freezing and thawing of the FTS cycles applies to these cycles as well. However, while FT cycles

generate internal stresses, these specimens were also subjected to an additional sustained flexural applied load. For the injection repairs, the bond between the repair material and the concrete substrate was subjected to flexural tension and compression whereas for the overlay material the bond was put in a state of shear stress and tension. Generally, service loads should not lead to any considerable damage of concrete. Despite this, the coupling of external applied loads along with FT cycling has been shown to accelerate deterioration in plain concrete (Sun, Mu, Luo, & Miao, 2002).

For all three environmental conditioning regimes, the Ministry of Transportation of Ontario's LS-412 standard "Method of Test For Scaling Resistance of Concrete Surfaces Exposed to Deicing Chemicals" (1997) was adopted with some modifications for each of the regimes. The only variance included the dimensioning of the specimens where the standard requires the specimens to be 300 x 300 x 75 mm.

Temperature (T)

One of the conditions that the repaired specimens were subjected to included temperature cycling without any saturation in water. The temperature variations dictated by the LS-412 (1997) standard were adhered to. One temperature cycle consisted of storage in the industrial freezers for 17 hours at a temperature of -18 ± 2˚C followed by a thawing environment for 7 hours at a temperature of 23 ± 2˚C and relative humidity of 50 ± 5%. One modification included the overall length of testing. While the standard dictates a minimum of 50 cycles, the duration of the temperature cycles lasted for only 30 cycles due to time constraints of experimentation.

After each cycle the freezer racks were rotated 180˚ and were placed in one of four different locations within two separate freezers. After a round of 5 cycles, the specimens were removed from the freezers and the repaired surfaces were examined and photographed. Before proceeding with the next set of temperature cycles the specimens were rotated on the freezer rack to account for any variability of temperature within the freezers.

Freeze-Thaw Cycles and Salt Solutions (FTS)

The FTS testing procedure follows that of MTO Standard LS-412 (1997). To allow for the ponding of salt water on the repaired surface of the specimens a silicone dyke was applied at a distance of 15 mm from the outer edge and built up to a height of 20 mm as seen in Figure 3.11. As defined by the MTO LS-412 Standard, a 3% sodium chloride (NaCl) solution was prepared using distilled water and placed within the silicone dykes prior to the freezing regime. The test surface was covered with a minimum of 6 mm of the salt solution.

Figure 3.11 Freeze-thaw with salt solution specimens

After 5 FT cycles, the salt solution was drained and the specimens were visually examined and photographed. After every 5 cycles, the samples were then rotated on the freezer racks, a new salt solution was added into the ponds, and the FTS testing was resumed.

Freeze-Thaw Cycles and Sustained Load

The third testing regime that was included in the experimental program examined the influence of both freeze-thaw and sustained loads on the repaired systems. To apply the flexural load, a four point bending test set-up was adopted. Within a plastic container two painted steel rods were fixed to the base using a cyanoacrylate adhesive at a span (*L*) of 180 mm, centre to centre. The concrete specimens were placed on the two rods using a silicone sealant, ensuring that the repaired surface was facing downwards. Two additional steel rods were placed on the top of the specimen in the middle third of the specimen, at a distance of 60 mm from the two bottom rods. The two top steel rods were secured in placed by cutting slots into the sides of the plastic container and running the rods through the openings. On the top of the two steel rods, a 75 x 75 x 200 mm square steel section was placed. An illustration of the test set-up is shown in Figure 3.12.
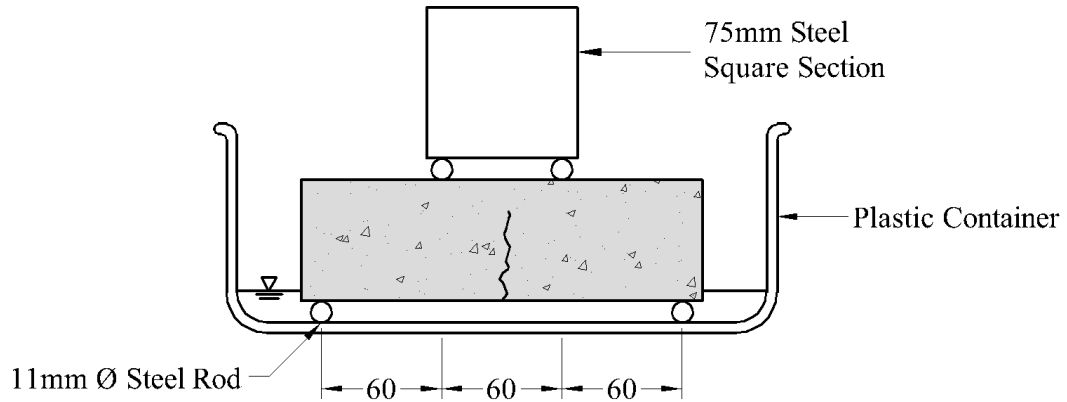
Figure 3.12 Freeze-thaw with a sustained load test set-up

Using the four point bending system, a constant bending moment was induced across the middle section of the specimen. This ensured that the cracked section was subjected to the same bending moment, since the crack was located anywhere within the middle third of the specimen. The weight, P, of each of the steel section was 91.5 N. The moment, M_L, produced across the cracked section can be calculated using the following equation:

$$M_L = \frac{P}{2}\left(\frac{L}{3}\right) = 2745 \text{ N. mm} \qquad 3.4$$

The FTL cycles, follow the same temperature cycles as that of the T and FTS cycles. The plastic container was filled with distilled water, so that the water level was approximately 5mm above the base of the specimen. The water was added one hour prior to placing the specimens in the freezing environment. After allowing an hour of absorption the water was drained to avoid the formation of a layer of ice capable of supporting the specimen along its base. After 5 cycles of testing the specimens were removed from the containers for the examination of the concrete repaired surface.

3.5 Evaluation Techniques

3.5.1 Air Permeability

The air permeability coefficient and affected depth of the concrete was measured at three different intervals during the experimental program: before the application of the repair, after applying the repair materials, and after the freeze-thaw conditioning regimes. The air permeability is an indication of the air tightness of the concrete which can be related back to the transport properties of the concrete and are often used as indicators of the durability of the material. Gas permeability measurements have indicated good

correlation with deterioration mechanisms such as chloride ingress (Romer & Leeman, 2005) and carbonation (Basheer, Kropp, & Cleland, 2001), both of which lead to reinforcement corrosion.

The equipment used to evaluate the air permeability is the Torrent permeability tester manufactured by Proceq. This non-destructive testing method operates with the creation of a vacuum within the concrete using a two chamber cell while measuring the rate of change of pressure as it returns back to the atmospheric value. Primarily, this test is used as an indication of the quality of the concrete cover. However since the specimens depth are limited to 60 mm, the results give a good indication of the overall condition of the concrete. The air permeability tests were conducted in accordance with the Swiss Standard SIA 505 262/1 - Annex E (2003).

A vacuum pump, with a suction capacity of 1.5 m^3/hr was attached to the control unit. From the control unit, two hoses fed into the inner and outer chambers of the vacuum cell. Finally, the control unit was also attached to the display unit via an input cable. The test setup is displayed in Figure 3.13.

Before each round of testing, the machine was calibrated by measuring the pressure loss of the unit with the vacuum cell placed on a polished steel plate. To start the test, first the atmospheric pressure was recorded, subsequently the vacuum cell was placed on the specimen. Using both the inner and outer cells, a vacuum within the specimen is created. After 1 min, the hose to the inner chamber is closed, and the pump can only act on the outer chamber while ensuring that the pressures between both chambers are always equal. The air flow is unidirectional into the inner chamber and the change in pressure within the system in recorded for up to 12 minutes. The test was repeated to a total of three times per specimen to determine an average air permeability coefficient and an average affected depth.

From the pressures recorded, the coefficient of permeability (*kT*) and the affected depth (*L$_a$*) is calculated using the following equations (Torrent R. , 1992):

$$kT = 4\left(\frac{V_c(dP_1/dt)}{A(P_a{}^2 - P_1{}^2)}\right)^2 \frac{\mu P_a}{\varepsilon} \int_{t_0}^t \left[1 - \left(\frac{P_1}{P_a}\right)^2\right] dt \qquad 3.5$$

$$L_a = \left\{\frac{kt \cdot P_a}{\varepsilon \mu} \int_{t_0}^t \left[1 - \left(\frac{P_1}{P_a}\right)^2\right] dt\right\} \qquad 3.6$$

Where *kt* is the coefficient of permeability to air (m^2), *L$_a$* is the affected depth (m), μ is the dynamic viscosity of air (N s m^{-2}), *V$_c$* is the volume of Torrent's test chamber (m^3), ε is the concrete porosity, *A* is the cross sectional area of the test chamber (m^2), *P$_1$* is the pressure of the inner chamber (N m^{-2}), and *P$_a$* is the atmospheric pressure (N m^{-2}). The Torrent testing machine records the change in pressure and calculates, and outputs the *kT* and *L$_a$* values.
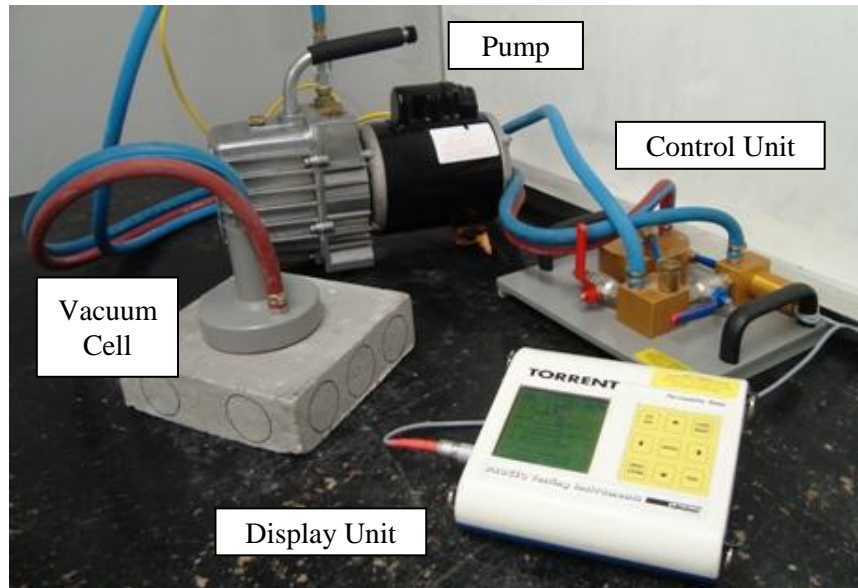
Figure 3.13 Air permeability test setup

3.5.2 Ultrasonic Pulse Velocity

To assess the durability of concrete crack repairs the use of ultrasonic pulse velocity (UPV), a non-destructive test method, was instituted using Proceq's Tico instrument. Typically UPV is used to indirectly determine the elastic modulus or the compressive strength of concrete. The use of non-destructive tests such as UPV has also become vital in areas of infrastructure quality assessment. Monitoring the changes in the UPV across cracked or deteriorated sections of concrete has become a common means of quantifying the damage (Qasrawi & Marie, 2003) (Zhong & Yao, 2008). The UPV method has also become a popular procedure for the quality assurance of concrete injection repairs (Bjegovic, Skazlic, & Jambresic, 2005) (Promboon, Olson, & Lund, 2002). In this experimental program, the UPV is used as a method of quantifying the damage caused by the introduction of cracks in concrete; to investigate the efficiency of injection repairs; and to monitor the deterioration of the injection repaired systems when exposed to the freeze-thaw conditioning regimes.

The Tico instrument consists of two 54 kHz transducers, one of which acts as a transmitter and the other a receiver. The transducers are connected to a display unit via two separate BNC cables. An ultrasonic pulse is transmitted from one of the transducers and the time of the pulse from the transmitter to the receiver is recorded. Based on the distance between the two transducers the UPV can be calculated. The setup of testing technique is shown in Figure 3.14.
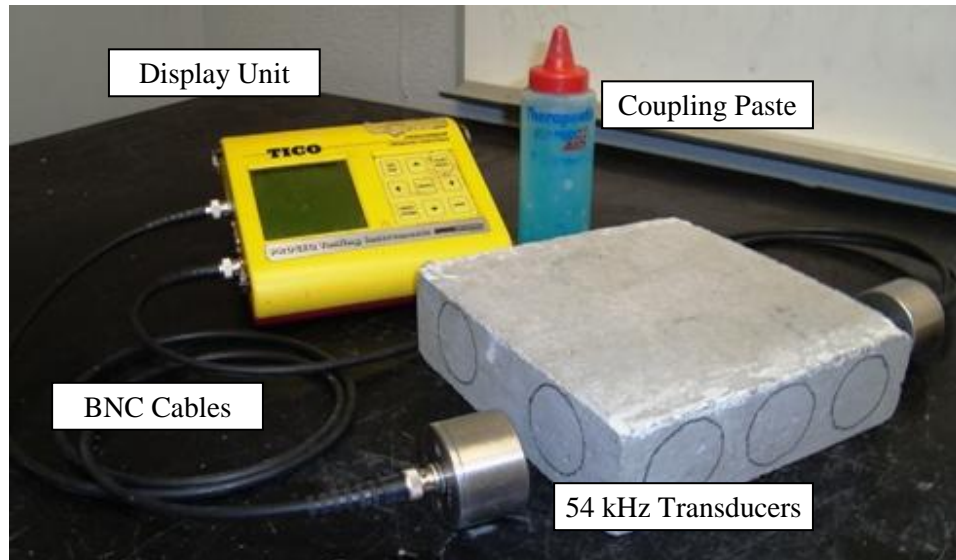
Figure 3.14 Ultrasonic Pulse Velocity test setup

There are three different techniques that can be used to measure the UPV: the direct, semi-indirect, and the indirect method. Of the three, the direct and indirect methods were used. Typically the direct transmission is preferred due to the straight-line path of the transducers. The use of the indirect method is typically used in the field, when evaluating a concrete structure where there is no access to opposite components, thus the transducers are both placed on the same surface of the concrete. In plain concrete, indirect surface measurements are equal to those obtained using the direct method (Yaman, Inci, Yesiller, & Aktan, 2001). Both direct and indirect methods were used to determine whether the inclusion of a crack in the concrete will impact the two readings in the same manner, and which of the two measurements is a better representation of the damage in the concrete.

The direct transmission method was performed on five different locations on each specimen. Three of the locations were on lengths passing through the cracked section of the concrete. The remaining two locations were through an uncracked section. The transducers, 50 mm in diameter, were placed at the centre of the depth with a clearance of 5mm above and below the transducers. The locations of the transmitters were marked so that the exact location could be used constantly throughout the experimental program. The locations are shown in Figure 3.15.

The indirect method was only used in evaluating the damage caused by the cracks in the concrete. Four locations were marked on the top surface of the specimen, two locations were through a cracked section and the other two were through uncracked sections. The transducer locations on the specimen are shown in Figure 3.15.

DIRECT TRANSMISSION   INDIRECT TRANSMISSION
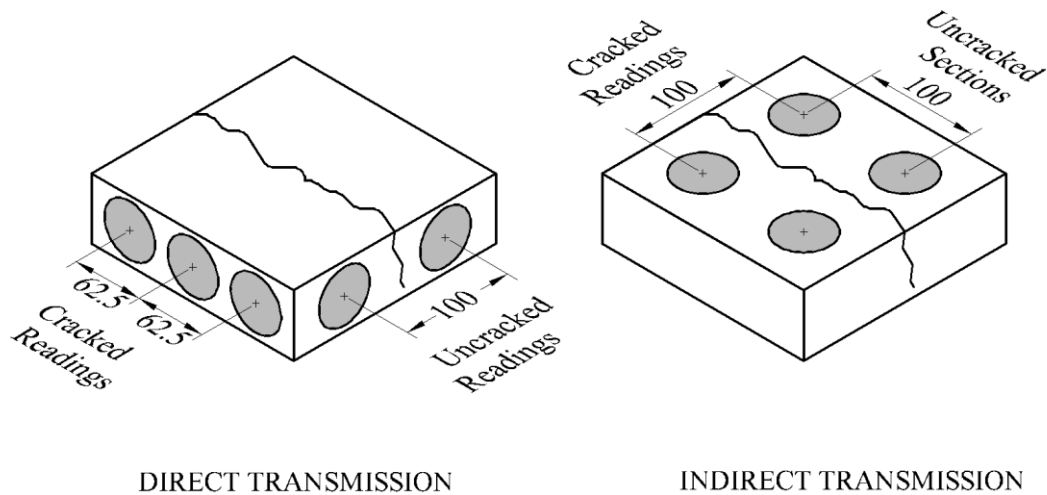
Figure 3.15 Transducer locations for direct UPV testing

The UPV readings were taken in accordance with ASTM C597 (2009). A calibration reading was taken on a reference cylinder to ensure proper operation of the Tico instrument. A thin layer of coupling paste was applied to the concrete surface as well as the transducers in order to avoid trapping any air between the two surfaces. While maintaining pressure on the transducers, the transmission time measurement was recorded. A total of five readings were taken at each location on the specimens in order to measure the UPV and its variance.

One factor affecting the UPV direct transmission reading was the steel mesh within the specimens. The UPV of steel is $1.4 - 1.7$ times that of unreinforced concrete which is in the typical range of 3700 to 4200 m/s (Naik & Malhotra, 2004). The steel mesh runs parallel to the ultrasonic waves being transmitted. If the sensors are placed far enough from the steel, it is possible to conclude that steel will have no influence on the transmission times. The distance in which the steel no longer has an effect on the UPV reading when the axis of the bar is parallel to the direction of propagation is given in Equation 3.7 where V_s and V_c are the ultrasonic pulse velocities of steel and concrete respectively, a is the clear distance between the sensor and the steel, and L_v is the total path length (Naik & Malhotra, 2004). Since the depth of the specimen is 60 mm and the diameter of the transducers is 50 mm, regardless of the location of the steel along the depth, and regardless of placement, the steel mesh will influence the transmission time.

$$\frac{a}{L_v} > \frac{1}{2}\sqrt{\frac{V_s - V_c}{V_s + V_c}} \qquad\qquad 3.7$$

CHAPTER 4 ANALYSIS OF RESULTS AND DISCUSSION

4.1 Introduction

The results from the experimental program are outlined in this chapter. A statistical analysis of the non-destructive testing data was used to determine the effectiveness of the crack repair methods and the effects of the freeze-thaw (FT) regimes. A discussion of the results is included to provide insight into the underlying concrete material mechanisms affecting the results.

4.2 Specimen Nomenclature

An identification system was implemented to distinguish between cement type, repair method, and FT conditioning regime. The specimens were labelled first by cement type, then by the repair method, followed by the FT conditioning regime, and by an identification number within its category. This system is defined in Table 4.1. For example, the identification of a specific specimen includes the following nomenclature: OPC-E-FTL.

Table 4.1 Specimen nomenclature

Concrete Cement Type	
OPC	Ordinary Portland Cement
SF	Blended Silica Fume Cement
Crack Repair Method	
CON	Control - No cracks and unrepaired
E	Epoxy Resin
PU	Polyurethane Injection
OV	Concrete Overlay
Freeze-Thaw Conditioning Regime	
N	None
T	Temperature
FTS	Freeze-Thaw and Salt Solutions
FTL	Freeze-Thaw with Sustained Load

4.3 Statistical Analysis

The data collected from the experimental program was organized and analyzed using several statistical methods. For the first sections; analysis of the concrete material properties, crack widths, effects of cracks in concrete, and the effectiveness of the repairs

(Sections 4.4 to 4.7), the sample sizes, *n*, typically have a value greater than 3. While this remains true, confidence intervals were developed to evaluate the data. When examining the data for the effectiveness of the repairs under environmental regimes (Section 4.8), sample sizes contain either 2 or 3 samples. Because of the limited data, hypothesis testing was carried out using non-parametric statistical tools, in particular the Kruskal-Wallis Test.

4.3.1 Parametric Testing

In the experimental program, several different variables varied across the concrete repaired specimens: cement type, crack width, repair material, and environmental condition. To evaluate whether there exists any significant differences between two parameters, confidence intervals were developed.

Data comes from a random data set or distribution. The Central Limit Theorem states that the average of that data set, $\bar{x}$, comes from a normal distribution assuming the data samples are independent (Dunn, 2011). This can also be denoted as $\bar{x} \sim N(\mu, \sigma^2/n)$, which shows that the sample average comes from a normal distribution with a mean of μ, and variance of σ/n., where n is the size of the sample. The Central Limit Theorem is used to develop the confidence intervals.

Several assumptions need to be made about the population distribution parameters of the data sets being examined. First, it is assumed that the data from the two samples have been independently sampled. Secondly, it is assumed that the two samples being examined are from populations that are normally distributed. Using the Central Limit Theorem, even though the sample data set may not be normally distributed, the sample averages ($\bar{x}_1$ and $\bar{x}_2$) will be much more normal, even for small sample sizes. Furthermore it is assumed that the sample 1 and sample 2 have the same population variance, $\sigma_1 = \sigma_2 = \sigma$. Independence is also assumed between groups, therefore the means $\bar{x}_1$ and $\bar{x}_2$ are also independent (Dunn, 2011).

Based on these assumptions, it is possible to define the z-deviate. The z-deviate is a parameter that defines the distribution of a sample. The z-deviate is defined as follows:

$$z = \frac{(\bar{x}_1 - \bar{x}_2) - (\mu_1 - \mu_2)}{\sqrt{\sigma^2 \left(\frac{1}{n_1} + \frac{1}{n_2}\right)}} \qquad 4.1$$

The variance of the data, σ^2, is not known so an internal estimate of spread is required. It is assumed that the sample variances (s_1^2 and s_2^2) of the two data sets are equivalent. The validity of this statement is first verified by calculating a ratio of the two variances, F_0, as shown in Equation 4.2 and constructing a confidence interval from the F-distribution (Montgomery & Runger, 1994). The interval defined in Equation 4.3 uses the statistic $f_{\alpha/2, n_1-1, +n_2-1}$ which is the point along the cumulative F-distribution that has an area of $\alpha/2$, and n_1-*1* degrees of freedom for sample 1 and n_2-*1* degrees of freedom for sample 2, where n_1 and n_2 are the sample sizes from sample 1 and sample 2 respectively. If F_0 lies within the confidence interval, it is possible to conclude that the variances are

similar. For the testing of difference of sample variances conducted in this thesis, a confidence interval of 95 % (α=0.05) was used.

$$F_0 = \frac{s_1{}^2}{s_2{}^2} \qquad\qquad 4.2$$

$$f_{\alpha/2, n_1-1, n_2-1} < F_0 < -f_{-\alpha/2, n_1-1, n_2-1} \qquad\qquad 4.3$$

In the instances where the variances were found to be similar, a pooled variance, $s_p{}^2$, a weighted sum of the sampled variances, was used as an estimate of the value as shown in Equation 4.4.

$$s_p{}^2 = \frac{(n_1 - 1)s_1{}^2 + (n_2 - 1)s_2{}^2}{n_1 + n_2 - 2} \qquad\qquad 4.4$$

In the instance that the variance of the two data samples are found to be unequal in accordance with Equation 4.3, the variances can no longer be pooled, and an approximate z-deviate, is calculated in Equation 4.5. The degrees of freedom become defined by *v* as defined in Equation 4.6. This statistical test is an approximate method, as one of the initial assumptions made has been violated, and does not guarantee a statistical significance. Despite this, it can be used to give some indication of the equality between the data samples (Montgomery & Runger, 1994).

$$z = \frac{(\bar{x}_1 - \bar{x}_2) - (\mu_1 - \mu_2)}{\sqrt{\dfrac{s_1{}^2}{n_1} + \dfrac{s_2{}^2}{n_2}}} \qquad\qquad 4.5$$

$$v = \frac{\left(\dfrac{s_1{}^2}{n_1} + \dfrac{s_2{}^2}{n_2}\right)}{\dfrac{\left(\dfrac{s_1{}^2}{n_1}\right)}{n_1 - 1} + \dfrac{\left(\dfrac{s_2{}^2}{n_2}\right)}{n_2 - 1}} \qquad\qquad 4.6$$

To define the two-sided confidence interval, the z-deviate varies according to the t-distribution as shown in Equation 4.7. To build the confidence interval, n_1+n_2-2 degrees of freedom is used along with a 95% confidence (α=0.05). With the z-deviate substituted into Equation 4.7, a confidence interval for the true means μ_1-μ_2, can be isolated as seen in Equation 4.8. In the case that the variance of the two data samples is found to be unequal, Equation 4.8 is modified accordingly using Equations 4.5 and 4.6.

If the confidence interval is centered about 0, it is concluded that there is no statistical difference between the two variables. If both the upper and lower limits of the

confidence interval are greater or less than 0, it is not possible to conclude that there is a statistical difference between the two values.

$$-t_{\alpha/2,\text{dof}} < z < t_{\alpha/2,\text{dof}} \qquad\qquad 4.7$$

$$(\bar{x}_1 - \bar{x}_2) - s_p\sqrt{\frac{1}{n_1} + \frac{1}{n_2}} \cdot t_{\alpha/2,} < \mu_1 - \mu_2 < (\bar{x}_1 - \bar{x}_2) - s_p\sqrt{\frac{1}{n_1} + \frac{1}{n_2}} \cdot t_{\alpha/2,} \qquad 4.8$$

4.3.2   Non-Parametric Testing

When the sample size is less than three, an assumption that the data stems from a normal distribution can no longer be validated, thus, the use of non-parametric testing is alternatively used. The violation of parametric statistical tests has devastating effects on the results for small sample sizes, and yet these effects are unlikely to be detected. The Mann-Whitney U test, and an extension of this test, the Kruskal-Wallis test, is applied to conduct hypothesis tests on the data presented in Section 4.8.

Several assumptions are made with respect to these tests; all the samples are random samples from their respective populations, independence within each sample is assumed, as well as mutual independence among the various samples. The measurement scale is at least ordinal, and finally, the population distributions functions of the different samples are identical (Conover, 1999).

When there are two samples, the Mann-Whitney U test is applied, or accordingly when there are three or more different sample groups, the Kruskal-Wallis test is adapted. To carry out the statistical tests, all of the data from the samples are ranked from smallest to largest, and assigned the rank 1 to N, where N is the total number of observations The data consists of k random samples, where the ith sample size, n_i, is calculated from the sample's data: X_{i1}, X_{i2},.. X_{in}. The rank assigned to X_{ij} is represented by $R(X_{ij})$. For each sample, the sum of the ranks is calculates as indicated in Equation 4.9.

$$R_i = \sum_{j=1}^{n_i} R(X_{ij}) \quad i = 1,2,\dots,k \qquad\qquad 4.9$$

The data being analyzed is continuous and not ordinal, therefore there is very little chance of there being tied ranks. Accordingly, the variance and test statistic are defined respectively by Equations 4.10 and 4.11.

$$S^2 = \frac{N(N+1)}{12} \qquad\qquad 4.10$$

$$T = \frac{12}{N(N+1)} \sum_{i=1}^{k} \frac{R_i^2}{n_i} - 3(N+1) \qquad 4.11$$

In hypothesis testing, the null hypothesis, H_0, states that all of the k populations distribution functions are identical. The alternative hypothesis, H_1, suggests that at least one population tends to yield larger observations than at least one other population. The distribution of T can be approximated by the chi-distribution with k-1 degrees of freedom, however for more accurate results, the quantiles of the Kruskal-Wallis test statistic quantiles calculated by Iman et al. (1975) are used when possible. A one-sided confidence interval of (1-α) is used. In the case that the null hypothesis is rejected, individual populations can be tested for differences. Populations i and j seem to be different when the following inequality is satisfied:

$$\left| \frac{R_i}{n_i} - \frac{R_j}{n_j} \right| > t_{1-\alpha/2} \left(S^2 \frac{N-1-T}{N-k} \right)^{1/2} \left(\frac{1}{n_i} + \frac{1}{n_j} \right)^{1/2} \qquad 4.12$$

Where R_i and R_j are the rank sums of the two samples, and $t_{1-\alpha/2}$ is the (1-$\alpha/2$) quantile from the t-distribution with (N-k) degrees of freedom.

4.4   Concrete Material Properties

For the two concrete mixes used in the experimental program, OPC concrete and SF concrete, the fresh and hardened concrete properties were recorded. All of the fresh concrete properties and the 7 day compressive strength are based on a single test, while the 28 day compressive strength is the average of three different compression tests. The results of the fresh and hardened concrete property tests are listed in Table 4.2.

Table 4.2 Concrete material properties

Fresh Concrete Properties	OPC	SF
Air Content (%)	13	12
Density (kg/m³)	2150	2163
Slump – Initial (mm)	200	115
Loss of Slump – Final (%)	23	26
Hardened Concrete Properties		
7 Day Compressive Strength (MPa)	18.3	28.3
28 Day Compressive Strength (MPa)	31.8 ± 0.77	39.3 ± 1.2

As previously stated in Section 3.2.1, the target air content and slump of both concrete mixes were 9% and 150 mm respectively. The OPC and SF concrete both surpassed the targeted air content by a significant amount, 4 and 3 %, respectively. The

coarse aggregate had a nominal aggregate size of 6.7 mm, which was smaller than the values used in the concrete industry which typically range from 9.5 to 40 mm. According to Pinto and Honover (2001), from a durability perspective, greater air content is desired as the maximum-size aggregate is reduced. Since the main focus of this experimental program was to evaluate the effectiveness of the specimens under different environmental condition, a higher air content was acceptable.

The effects of such relatively high air content are twofold: firstly, the concrete specimens will have a high FT resistance, and secondly, the increased air content will decrease the compressive strength of the concrete. A concrete mix that contains more air-entrained voids, acts as an effective escape boundary and provides the necessary relief to reduce the hydraulic pressure generated during FT. As the main focus of this research is to examine the effectiveness of the concrete repair and not specifically the concrete material itself, it is important to provide the necessary minimum air content. An increased air content results in a reduced compressive strength, where a typical relation is that for a 1% increase in the air entrained content, the compressive strength is reduced by 5% (Whiting & Mohmad, 1998). The implications of high air content are also reflected in the air permeability measurements as discussed later in this chapter.

Two slump readings were taken after mixing, the first being measured shortly after mixing as the concrete was being poured into the forms. The second reading was taken just as the last of the concrete was being poured into the final specimens. Both concrete mixes had the same w/c ratio of 0.38 and the same water content, however the SF concrete had a lower initial slump of 115 mm compared the OPC concrete which was 200 mm. The SF concrete did not meet the target slump of 150 mm. The cement blend contained 8% Silica Fume blended in with the ordinary Portland cement. SF, with a mean particles size of 0.26μm, increases the surface area of the cement consequently requiring more water. It was found that a 10% replacement of OPC with SF required an increase of superplasticizer by approximately 200 mL/m^3 of concrete to maintain the same workability at the OPC concrete. Not only was the high area of the SF particles attributed for the loss of workability, but also a possible affinity of the SF to absorb the superplasticizer molecules (Nedhi, Mindess, & Aitcin, 1998).

Finally, the examination of the hardened concrete properties show that while the SF concrete achieved the target compressive strength, the OPC concrete did not. As previously noted, both mixes had higher than expected air contents, which may have impeded the concrete mixes from attaining higher compressive stresses. Another factor that may have resulted in a lower strength than originally specified is the curing regime used. The concrete cylinders were only subject to moist curing for 7 days rather than the typical 28 days. Furthermore, the SF concrete had a higher strength than the OPC, which may be attributed the 8% blended silica fume within the cement.

4.5   Crack Width

For each cracked specimen, an average of four different crack width readings were taken at equally spaced intervals along the length of the crack. The average of the four widths was taken to represent the crack width in millimetres. The average of the all

the crack widths for OPC concrete was found to be 0.171 mm with a standard deviation of 0.0426 mm while the average crack width for the SF concrete was found to have an average 0.251 mm with a corresponding standard deviation of 0.0663 mm. A summary of the crack width measurements is presented in Table 4.3. Confidence intervals were created to assess any statistical difference in the crack width of OPC and SF concrete samples. The results revealed that there is a significant difference between the crack widths in the OPC and SF concrete.

Table 4.3 Crack width measurements

Concrete Mixture	Crack Width (mm)	SD (mm)	COV (%)
OPC Concrete	0.171	0.0426	24.9
SF Concrete	0.251	0.0663	26.5

The difference between the crack widths in the OPC and the SF are not a product of the concrete variables but are a product of the procedure used to create the cracks in concrete. A three-point bending experimental set-up was used to fracture the specimens and induce cracks. It was user operation that controlled the vertical displacement after fracture. The vertical displacement can be related back to the crack opening displacement, assuming rigid body motions (Section 3.3.5). This model is a simplification of the conditions.

Further examination into the fracture mechanics of concrete can more accurately account for the differences in the crack widths. SF concrete has both a greater stiffness and strength than OPC concrete. As the strength increases, the fracture energy and the fracture toughness of the concrete also increase but not proportionally to the strength. For example, in an experimental study where the concrete was fractured using three point bending, it was found that the high strength concrete had a strength increase of 160 % while the fracture energy and toughness only increased by 12 and 25 %, respectively (Gettu, Bazant, & Karr, 1990). It is beyond the scope of this thesis to use linear and non-linear fracture mechanics to analyze the post fracture mechanics, however, an unproportional increase in the strength of concrete when compared to the fracture energy and toughness, indicates a significantly greater brittleness, as proven by Gettu et al. (1990). The higher brittleness in the SF concrete makes it difficult to control the crack width opening through the displacement controlled equipment.

In practice, concrete cracks have high variation both along the crack width, and between the cracks themselves, as is made evident by the various studies examination of new innovative techniques to measure to evaluate crack widths using imagining processing techniques (Litorowicz, 2006) (Cai, Dong, & Zhang, 2012). Alternative methods have been developed to initiate fractures in concrete with controlled crack widths, as first proposed by Wang (1997). A concrete disk undergoes a splitting tension test, where LVDTs are used to measure the horizontal displacement, or the crack opening displacement. In this study, the crack width was not directly measured but assumed to be equal to the lateral displacement of the disk, leading to inaccuracy due to the effects of

crack branching, variability of crack width along the length, and the inelastic deformation of the matrix (Akhavan, Shafaatian, & Rajabipour, 2012).

4.6 Effects of Cracks in Concrete

In the damaged, cracked state, before the repairs were applied, the concrete specimens were evaluated using the air permeability and UPV testing. From these results it is possible to establish and test several different hypotheses: whether there is any relationship between the air permeability/UPV tests with the concrete crack widths and whether direct or indirect UPV testing is more adequate in evaluating cracked concrete. Furthermore, the measurements taken at this stage of the experimental program are used to further evaluate whether the repairs were effective in restoring the transport properties of the concrete specimens. In this section, only the "damage degree" of the concrete due to the existence of the cracks is evaluated, while the effectiveness of the repairs follows in Section 4.7.

To evaluate the damage degree, or the influence of the crack on the concrete's transport properties, three different variables were measured: ΔkTb_{cr}, $\Delta UPV(d)_{cr}$, and $\Delta UPV(i)_{cr}$.

$$\Delta kTb_{cr} = \frac{kTb_{cr}}{AVG\ kTb_{uncr}} \qquad 4.13$$

where ΔkTb_{cr} is the ratio of the air permeability coefficients between cracked (kT_{cr}) and the average of the uncracked specimens ($AVG\ kTb_{uncr}$), the average of the uncracked air permeability coefficients are based on the average of 6 control samples, and all measurements are taken on the bottom surface of the specimens.

$$\Delta UPV(d)_{cr} = \left[1 - \frac{UPV_{cr}}{UPV_{uncr}} \right] \cdot 100\% \qquad 4.14$$

where $\Delta UPV(d)_{cr}$ is the percent relative change in the UPV between cracked and uncracked specimens. UPV_{cr} is the average of the three UPV readings taken through the cracked sections in a specimen, and UPV_{uncr} is the average of the UPV readings taken through two different uncracked sections in the same specimen.

$$\Delta UPV(i)_{cr} = \left[1 - \frac{UPV_{cr}}{UPV_{uncr}} \right] \cdot 100\% \qquad 4.15$$

Where $\Delta UPV(i)_{cr}$ is the percent relative change in the UPV, UPV_{cr} is the average of the UPV readings through two different locations through cracked sections in a specimen, and UPV_{uncr} is the average of UPV readings through two different uncracked sections in the same specimen.

The air permeability of the cracked specimens was measured on the bottom uncracked surfaces primarily because the specimens were not air tight on the cracked top surface due to the presence of the crack. Measuring the air permeability on the bottom surface of the specimens may not only be influenced by the crack width but also by the crack depth which in this experimental program was immeasurable. Rigid body modes were assumed when specifying the crack width or crack mouth opening, and by this same model, it is assumed that the crack depth is through the entire section. While it is possible to measure the crack depth using such techniques as UPV, the 60 mm concrete depth prevented the collection of such measurements. Although the crack depth is a variable that affects the air permeability recorded on the uncracked surface, it was could not be accounted for. Several other variables which may have influenced the air permeability but could not be accounted for include: the crack tortuosity, placement of the steel wire fabric, and any possible hidden defects or voids in the concrete.

The variable ΔkTb_{cr} specifies the amount of the damage, in terms of the permeability of the concrete specimens. A value of 1.0 or greater signifies that the cracked specimen has a greater air permeability coefficient than an uncracked section, or identifies the damaged specimens. A greater value of ΔkTb_{cr} signifies an increase in permeability, which results in a less durable concrete. The air permeability coefficient is a logarithmic variable.

In Figure 4.1, ΔkTb_{cr} is plotted against the crack width, with the specimens grouped by type of concrete: OPC or SF. In general, an increase in the crack width will result in greater damage or a relative increase in the air permeability of the concrete. Conducting a test of difference, it was found that there is a statistical difference between the variable ΔkTb_{cr} for OPC and SF concrete, where the values are 7.81 and 51.9 respectively. The results of the statistical tests conducted on the air permeability are summarized in Table 4.4. The difference between OPC and SF concrete is also visible in Figure 4.1. In general, the SF cracked concrete demonstrates more damage than the OPC concrete. Further investigation into the air permeability results reveals why the SF has a higher damage degree.

Table 4.4 Summary of air permeability results for cracked specimens

Variable	OPC			SF			Statistically Different?
	n	AVG	SD	n	AVG	SD	
kTb_{cr} (10^{-16} m^2)	34	6.37	11.0	29	15.1	20.5	No
kTb_{uncr} (10^{-16} m^2)	6	0.810	0.111	6	0.292	0.0587	Yes
ΔkTb_{cr}	34	7.87	13.6	29	51.9	70.3	Yes

Examination of the air permeability for SF and OPC uncracked control concrete specimens shows that SF has a statistically lower air permeability than OPC, an average of 0.292 x10^{-16} m^2 and 0.810 x10^{-16} m^2 respectively. The addition of SF in cement generally creates a more dense concrete and ultimately a concrete microstructure with a lower permeability. Referring back to the fresh properties of the concrete mixes listed in Table 4.2, for the same concrete material proportions, the SF concrete had a slightly

higher fresh density of 2163 kg/m^2 compared to the 2150 kg/m^2 density of OPC. Further testing for differences between the cracked air permeability (kTb_{cr}) of OPC and SF cracked specimens reveals no statistical difference between the two. Therefore, the air permeability for the cracked concrete is highly dependent on the crack and its width. The crack width governs the air permeability and the permeability of the concrete material is insignificant. Since the SF concrete has a lower uncracked air permeability, the SF concrete exhibits a greater loss of durability when cracked, resulting in a larger ΔkTb_{cr} and consequently greater damage.

Further examination of the damage degree using the UPV results, $\Delta UPV(d)_{cr}$, show similar trends. From Figure 4.2, it is seen that the cracked SF concrete specimens exhibit a higher degree of damage, consistent with the results from air permeability testing. For a confidence of 95%, the results revealed that the damage degree in the SF sample, an average of 43.5%, was statistically higher than the OPC samples which had an average damage degree of 34.3 %.
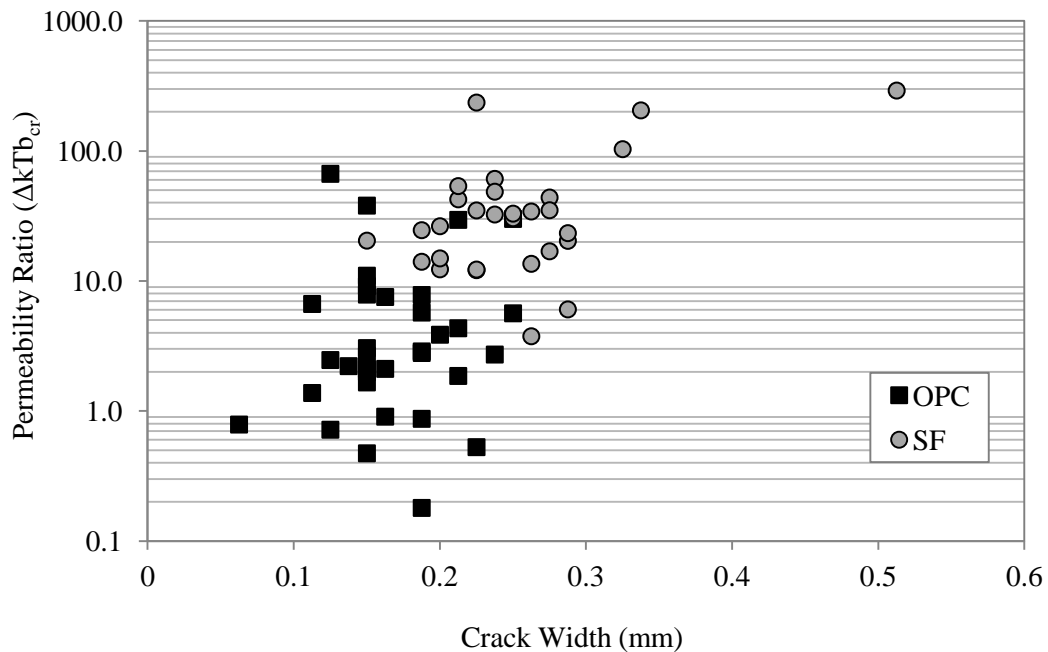
Figure 4.1 Effect of crack width on air permeability *(ΔkTb_{cr})*
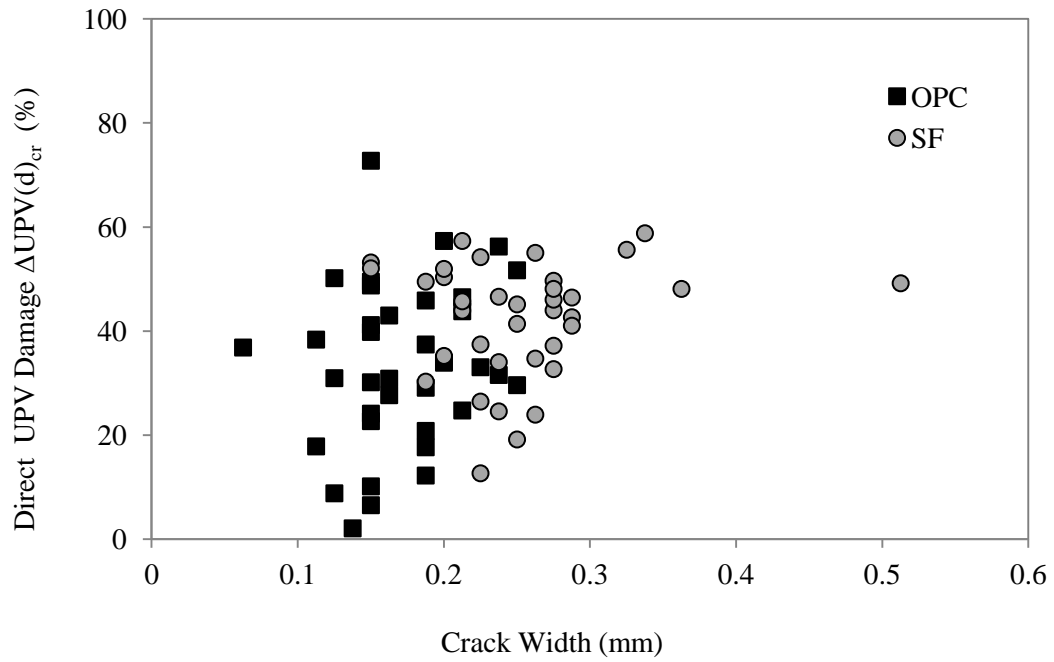
Figure 4.2 Effect of crack width on direct UPV readings *(ΔUPV(d)$_{cr}$)*
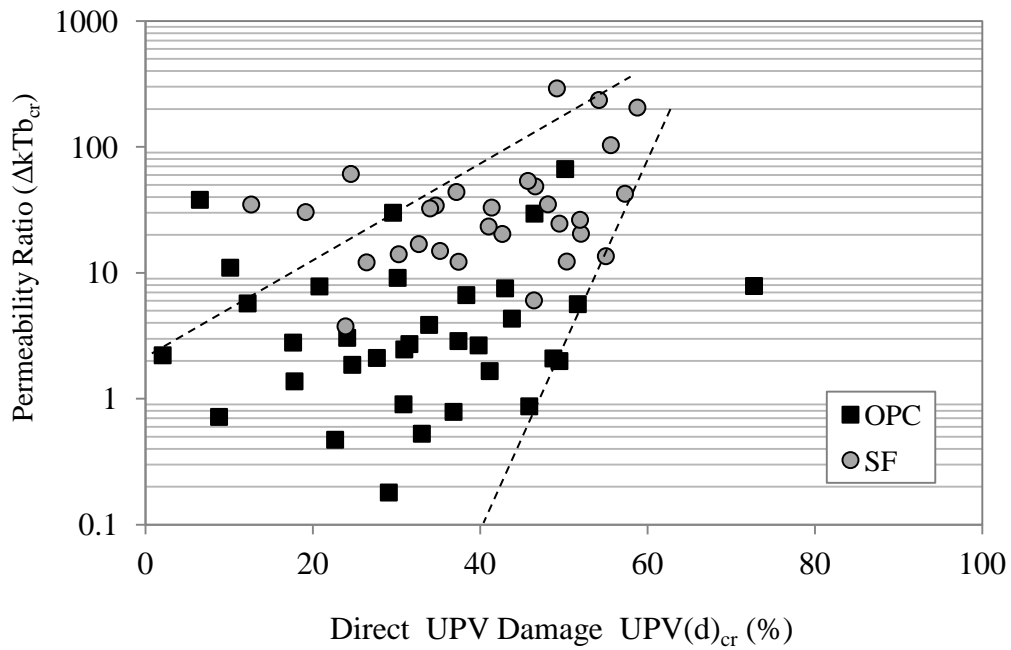
Figure 4.3 Comparison between air permeability and direct UPV

A direct comparison is made between the two variables ΔkTb_{cr} and $\Delta UPV(d)_{cr}$ in Figure 4.3. There exists a correlation between the two evaluation variables suggesting that either the UPV or the Torrent air permeability tests can be used to evaluate the damage induced by the crack in the concrete samples. As the UPV damage increases, so does the permeability ratio. At higher levels of damage, the correlation between the two variables is stronger. This is depicted by the converging dashed lines in Figure 4.3.

In the data, there exists one outlier that has a high UPV damage level, and does not follow the general trend. From the results, the previous conclusion that the air permeability results suggest SF have higher damage degrees is confirmed as the SF data points lie in the upper region of the graph. The same SF data points however have the same range across the x-axis as the OPC, suggesting that the UPV testing does not indicate a higher degree of damage in the OPC.

The weak correlation between the UPV and the air permeability results can be explained by the crack characteristics and the testing methods. The two non-destructive tests are governed by different principles. The UPV is a function of elastic properties and density while the Torrent air permeability coefficient is a function of the porosity and pore interconnectivity of the concrete. With the presence of the cracks in concrete, the UPV is more sensitive to the crack opening while the air permeability is more susceptible to the depth of the crack.

The effect of using different compositions of cement in concrete, is reflected in the properties of the microstructure, and ultimately in the difference of the slopes from the air permeability damage degree linear regression models. Similarly, in an experimental program measuring the relationship between the chloride penetration depth and the concrete crack density found that there existed different relationships between the two variables dependent on the cement used (Litorowicz, 2006).

By making these connections, the air permeability results agree with those of this study. A 95 % confidence interval indicates that the UPV could not detect any significant difference between the OPC and SF through uncracked sections indicating that the UPV test is less sensitive to the differences of OPC and SF matrices. Therefore, any differences between the damage observed in the OPC and SF samples may not be reflected through the UPV measurements.

In analyzing the relationship between the air permeability ratio and the ΔkTb_{cr}, an exponential relationship was assumed, or a linear relationship where the variable ΔkTb_{cr} was log transformed. According to Picandet et al. (2009) the presence of the crack in concrete can be modelled using Hagen-Poiseuille theory for viscous flow between rough parallel plates. A polynomial relationship is used to define the global permeability (k'_v) of the concrete with the following equation:

$$k'_v = \frac{\xi}{\Delta}\frac{w^3}{12} \qquad\qquad 4.16$$

Where ξ is the reduction factor due to the tortuosity and roughness of the crack, w is the crack width, and Δ is the mean distance between cracks. The relationship between

the crack width and the permeability is cubic. The data in Figure 4.1 does not reflect this model. This may be due to various factors not accounted for, such as the crack width variation along its length and the variation of the parameter ξ which is reflective of the conditions which according to the experimental results of Picandet et al. (2009) can vary from 0.1 to 0.001, several order of magnitude, and are not correlated to the geometry of the crack.

In the literature, the concept of a threshold crack width was proposed by Wang et al. (1997) where it was found that at crack widths less than 50 μm (0.05 mm), the crack width has little influence on the water permeability of concrete. Similarly, utilizing chloride diffusion as a means to evaluate the concrete's transport properties, it was found that there exists a threshold crack width at 55-80 μm (Jang, Kim, & Oh, 2011). For the evaluation $\Delta UPV(d)_{cr}$, there was no evidence of such a threshold. Even the smallest fracture would theoretically be reflected in the results, as the tests are characterized by the velocity of the elastic waves travelling through the concrete. The air permeability tests also did not have any indication of such a threshold level, which may be because the crack widths were not sufficiently small, or because the underlying cause of the threshold values is dependent on the presence of water and autogenous healing of the concrete. Evaluation of the gas permeability of cracked concrete found a much smaller threshold value of 15 μm (Picandet, Khelidj, & Bellegou, 2009), a value less than most of the measured crack widths during experimentation.

In terms of the UPV testing, the focus has been on the results from the direct testing method. The use of the indirect UPV has been ignored because it was found that this method is insufficient for detecting the influence of the crack in the concrete. The direct UPV variable, $\Delta UPV(d)_{cr}$, which has been shown to be correlated to the crack width, and which is in agreement with the air permeability results is plotted in Figure 4.4 against the indirect UPV method variable, $\Delta UPV(i)_{cr}$. There is no evidence of any correlation of $\Delta UPV(i)_{cr}$ to $\Delta UPV(d)_{cr}$. Approximately 85% of the data lies between 30 % < $\Delta UPV(i)_{cr}$ < 60 % and over a wide range of $\Delta UPV(i)_{cr}$. Therefore the results of the indirect method are not analyzed any further.
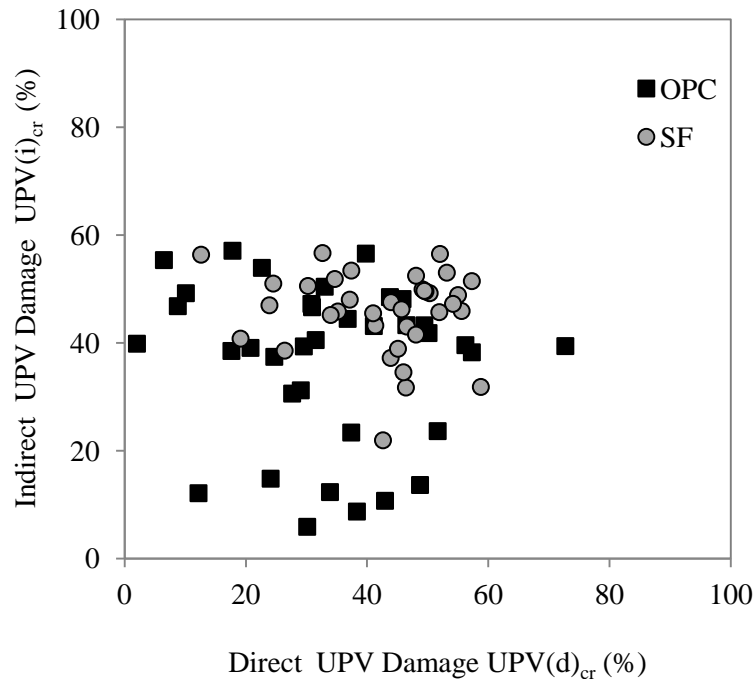
Figure 4.4 Comparison between direct and indirect UPV readings

4.7 Effectiveness of Repairs

4.7.1 Introduction

The effectiveness of the repair method was determined based on the two non-destructive tests completed: air permeability and UPV testing. The air permeability was used to evaluate all repairs while the results from the UPV tests were limited to examining the epoxy and polyurethane repairs. Measurements were taken before the repairs and afterwards to establish the effectiveness of the repair.

4.7.2 Air Permeability

The air permeability test results are presented using three different variables: kT_{rep} which is the air permeability coefficient measured on the cracked/repaired surface, ΔkTb_{rep} the ratio of the air permeability coefficient, measured on the bottom surface, of the repaired to the previously cracked air permeability coefficient, and ΔkTt_{rep}, the ratio of the air permeability coefficient measured on the repaired top surface compared to the bottom.The advantage to have the data presented within three different variables is that it indicates different aspects of the success of the repair. kT_{rep} gives a universal measurement of which repair results in the lowest air permeability, and effectively the most air tight concrete.

Another variable, ΔkTb_{rep}, gives the relative improvement of the concrete air permeability. This variable was used because in all of the cracked concrete specimens a reading could not be taken on the top cracked surface due to the lack of air tightness. Based on the measurements of the uncracked control specimens it was found, with 95% confidence, that there was no statistical difference between air permeability measurement on the top and bottom. The air permeability readings taken on the bottom of the specimens become more dependent on the crack depth. In spite of this, it is possible to justify using the bottom air permeability to evaluate the condition of the concrete specimen. This is again confirmed in Figure 4.1where there was a noticeable correlation between the bottom air permeability and the crack width measurements suggesting that measurements taken on the bottom are an indication of the overall state of the concrete.

Despite this, another variable, ΔkTt_{rep}, incorporating the air permeability of the repaired top surface is also evaluated. Both ΔkTb_{rep} and ΔkTt_{rep} are used to evaluate the degree of repair using a ratio of the repaired specimen air permeability to the cracked specimen permeability. The first variable analyze is the air permeability coefficient of the top surface, kTt_{rep}, (10^{-16} m^2) of the control and the repaired specimens.

Table 4.5 Air permeability - kT_{rep} (10^{-16} m^2)

Specimens	n	Mean	SD	COV (%)
OPC-CON	6	1.20	0.618	51.4
SF-CON	6	0.56	0.259	45.9
OPC-E	12	0.876	0.426	48.6
SF-E	12	0.655	0.209	32.0
OPC-PU	—	—	—	—
SF-PU	—	—	—	—
OPC-OV	11	24.1	12.0	49.7
SF-OV	12	38.9	18.8	48.5

The results presented in Table 4.5 show that the PU repair has failed to restore the air tightness, consequently no data is provided. Furthermore, the epoxy repaired specimens and the control specimens have the lowest air permeability. The average air permeability for epoxy repair is 0.876 x 10^{-16} and 0.655 x 10^{-16} m^2 for the OPC and SF concrete, respectively. The control specimens had an average of 1.20 x 10^{-16} and 0.56 x 10^{-16} m^2 for the OPC and SF concrete, respectively. Using 95% confidence intervals, it was found that there was no statistical difference between the control and the epoxy repairs for both OPC and SF concrete. The epoxy repair has successfully restored the permeability of the concrete to its original state. The air permeability indexes for the OV repair have the highest values of 24.1 x 10^{-16} and 38.9 x 10^{-16} m^2 for the OPC and SF concretes. Furthermore, it was found that the kTt_{rep} of the overlay repairs were greater than the control specimens. To better illustrate the range of air permeability between specimens and the variation, the results are plotted on a log bar graph in Figure 4.5.

Using confidence intervals to determine whether there was any statistical difference between the repaired specimens and the control samples, it was concluded that

the epoxy repair is able to restore the concrete's air permeability while the overlay repair fails to. The air permeability for the overlay material is significantly larger than the epoxy repair samples. The overlay material does not penetrate into the crack and its thickness is a meager 1 mm, not offering sufficient depth for air tightness protection. The epoxy repair proves to be a more effective repair strategy in terms of variable *kTrep*, because while the overlay does act as a protective barrier against water and other deleterious substances, the crack remains, providing a direct pathway for air movement. The air permeability is measured by creating an air vacuum within the concrete, and when the depth of the air vacuum created exceeds the depth of the overlay repair material, the crack still has a great influence on the air permeability.

By further examining the data in Table 4.5, it is evident that there is large variability within the sample of each repair. The control specimens, for both OPC and SF concrete, contain a high COV, indicating that although produced from the same concrete batch, there is great variability between specimens. The variability between reproduced readings for a control samples had on average a COV of 7.7% for the OPC concrete and 8.5% for the SF concrete. Precedence dictates that a coefficient of variation of approximately 6.6% can be expected between samples of the same concrete (Swiss Standard SIA 505 262/1 - Annex E, 2003). Therefore the high COV in the control group cannot be attributed towards the low precision of the Torrent testing machine. One possible cause for the high variation within the groups could in part be due to the concrete finishing process. All of the concrete specimens were finished at varying times. The quality of the concrete cover is highly dependent on the rate of bleeding, curing process, and finishing technique. The variation of the results is similar for CON, E, and OV specimens as visible in Figure 4.5.
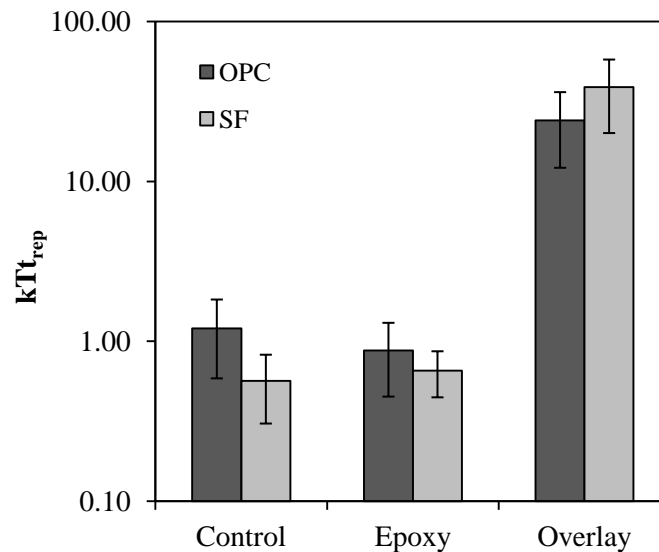
Figure 4.5 Air permeability of top surface

Further examination of the experimental results investigates the effectiveness of the repairs as a ratio of the air permeability after the repaired to the air permeability before the repair. This is done using two different variables, one of which incorporates the bottom repaired surface and the other the top surface. These variables are defined in Equations 4.17 and 4.19. For both of these variables, a value less than 1.0 indicates a decrease in the air permeability and likewise, for a value greater than 1.0, the concrete specimens have experienced an increase in air permeability:

$$\Delta kTb_{rep} = \frac{kTb_{rep}}{kTb_{cr}}$$

$$\text{4.17}$$

where ΔkTb_{rep} is the ratio of the air permeability coefficient, kTb_{rep}, of the repaired specimen measured on the bottom uncracked surface to air permeability coefficient, kTb_{cr}, of the same specimen before the repair, measured on the same surface.

$$\Delta kTt_{rep} = \frac{kTt_{rep}}{kTb_{cr}}$$

$$\text{4.18}$$

where ΔkTt_{rep} is the ratio of the air permeability coefficient, kTb_{rep}, of the repaired specimen measured on the bottom uncracked surface to air permeability coefficient, kTb_{cr}, of the same specimen before the repair, measured on the same surface.

The results of ΔkTb_{rep} and ΔkTt_{rep} are summarized in Table 4.6. Examining the results of ΔkTb_{rep}, several conclusions can be drawn. The results indicate that only the epoxy repairs show a decrease in the air permeability after the repair. Both the polyurethane and overlay repairs saw an increase in the air permeability of the specimens. Although the average of the epoxy repair shows an overall increase in the air tightness, the COV is quite high, even in comparison to the COV of the polyurethane and overlay repairs. Testing for difference between repairs for the variable ΔkTb_{rep} shows that there is no statistical difference between the OV and PU repairs, but that the E repair is different from both the OV and PU repairs.

The epoxy is the only repair that displayed any indication of improvement, which is indicated by the values of 0.309 and 0.0509 for the OPC and SF specimens respectively. Both the PU and OV average values were greater than 1.0, indicating that the repairs to these specimens saw an increase in the air permeability, which is counter intuitive of what is expected from repairing the concrete.

Conducting further statistical tests reveal that only the SF-E specimens demonstrated a statistical significant decrease in the air permeability after conducting the repair. Both the SF-OV and SF-PU showed a statistically significant increase in the air permeability whereas all other tests conducted on OPC-E, OPC-OV, and OPC-PU showed no statistically significant changes in the air permeability.

Table 4.6 Ratio of repaired to cracked air permeability

ΔkTb_{rep}				ΔkTt_{rep}			
Specimens	n	Mean	SD	COV (%)	Specimens	n	Mean	SD	COV (%)

Specimens	n	Mean	SD	COV (%)	Specimens	n	Mean	SD	COV (%)
OPC-E	12	0.309	0.240	77.8	OPC-E	12	0.427	0.441	103
SF-E	9	0.0509	0.0302	60.2	SF-E	8	0.127	0.086	67.8
OPC-PU	9	1.15	0.339	32.2	OPC-PU	—	—	—	—
SF-PU	7	1.69	0.751	44.5	SF-PU	—	—	—	—
OPC-OV	10	1.52	0.362	23.8	OPC-OV	10	9.80	9.05	92.3
SF-OV	11	1.55	0.236	15.3	SF-OV	10	4.87	3.04	62.5
OPC-CON	—	—	—	—	OPC-CON	6	1.56	0.963	61.8
OPC- CON	—	—	—	—	SF - CON	6	1.95	0.901	46.3

Further examination of the variable ΔkTt_{rep} demonstrates similar results. The epoxy repair demonstrated a decrease in the permeability in both the OPC and SF specimens. The repaired air permeability ratio for the uncracked control samples revealed an increase in the permeability. It must be noted that the values for the control actually indicate the ratio of the air permeability measurement of the top finished surface to the bottom surface. Theoretically, if the air permeability measurement is the same on the top and bottom, the control sample values should have a value of 1.0. However, the results show values of 1.56 and 1.95 for the OPC and SF samples respectively. Further tests revealed that there is no statistically significant difference in the air permeability measurements of the top and bottom surface measurements. Therefore it is not possible to conclude with any significance that the control samples have experienced an increase in the air permeability.

The overlay repair material shows a large increase in the air permeability after applying the repair. Both the ΔkTt_{rep} values are much larger than 1.0: values of 9.80 and 4.87 for OPC and SF. These repairs show a statistically significant difference with both the control and the epoxy repair. The polyurethane repaired specimens were not evaluated using this variable as the air permeability on the top surface could not be measured.

A comparison of the two variables ΔkTb_{rep} and ΔkTt_{rep} reveals that the results for both variables show similar trends. Both variables showed a decrease in air permeability for the epoxy repaired specimens and an increase in the overlay repaired specimens. The average value for the epoxy repaired specimens are similar, however there is larger difference between the two variables for the overlay repair. ΔkTb_{rep} indicates a ratio of 0.362 and 0.236 while ΔkTt_{rep} shows a value of 9.80 and 4.87 for the OPC and SF samples. Figure 4.6 plots the averages of the two variables.

Furthermore, the COV for the ΔkTt_{rep} values are much higher than those for ΔkTb_{rep}. The initial assumption that there is no difference between the air permeability measured on the top and bottom surface, although justified using statistical tests, should not be applied in the analysis of the data. The measurement of the air permeability measured on the top surface is influenced more heavily by the presence and effect of the crack in the concrete. Overall, when looking at the changes in the air permeability of the specimen, the ratios should compare the air permeability measured on the same surface of

the specimens. Thus for further analysis, only the ΔkTb_{rep} should be considered. From analyzing the variables kT_{rep}, $\Delta kTt_{rep,}$ and ΔkTb_{rep} the epoxy material is the only repair that proved to be effective in decreasing the air permeability of the cracked concrete. For the variable $kT_{rep,}$ the epoxy repaired specimens had an air permeability coefficient similar to or smaller than that of the control specimens. The epoxy repairs were the only specimens to see a decrease in the air permeability using the air permeability ratios $\Delta kTt_{rep,}$ and ΔkTb_{rep}.

The overlay material successfully restored the air tightness to the top of the specimen as made evident by the values for kT_{rep}, although considerably greater than the controls and epoxy repairs. For the variables $\Delta kTt_{rep,}$ and ΔkTb_{rep}, the overlay repair showed no signs of decrease in the air permeability. The repair therefore does not have a significant effect on the air permeability as the overlay material is too thin of a section for the Torrent testing device to sustain air pressure.

The polyurethane repair was unsuccessful at restoring the air tightness is the cracked specimens. The top surfaces of the polyurethane materials were not airtight after the repair application.
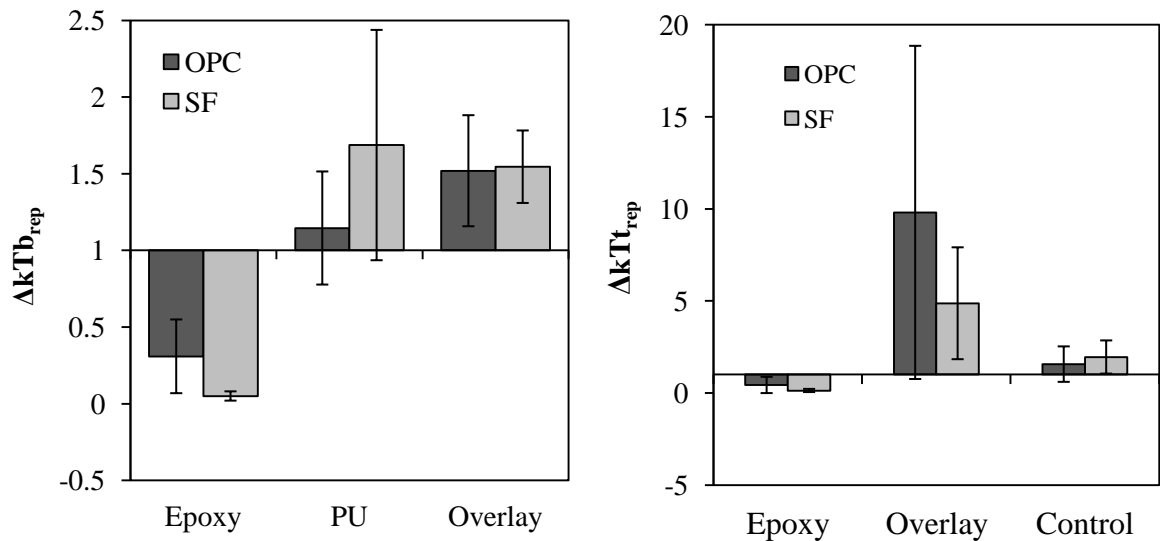
Figure 4.6 Ratio of repaired to cracked air permeability (ΔkTb_{rep} **and** ΔkTt_{rep})

4.7.3 Ultrasonic Pulse Velocity

The UPV of the injection repairs was measured to determine the effectiveness of the injection repairs by determining the success of impregnation of the crack with the repair material. The change in the UPV of the repaired material is defined by variable ΔUPV_{rep} which is presented in Equation 4.19:

$$\Delta UPV_{rep} = \left[\frac{UPV_{rep} - UPV_{cr}}{UPV_{cr}} \right] \cdot 100\% \qquad\qquad 4.19$$

where ΔUPV_{rep} is the percent change of the direct-UPV from the damaged cracked condition (UPV_{cr}) to the repaired state (UPV_{rep}). This variable for each specimen is based on the average of the change in the UPV in three locations through the cracked section. The indirect measurement of UPV, as previously discussed was found to be unreliable in measuring any changes across the specimens and not used in the analysis of the effectiveness of the concrete crack repairs.

The ΔUPV_{rep} was measured for only two types of repairs, without any controls: epoxy and polyurethane repairs. A summary of the results is presented in Table 4.7. A value of ΔUPV_{rep} greater than 0.0 implies that the UPV reading has increased, and that the repair material has been successful in impregnating the crack.

Table 4.7 Percent change in UPV after repairs (ΔUPV_{rep} (%))

Specimens	n	Mean	SD	COV (%)
OPC-E	11	52.8	29.7	56.3
SF-E	12	75.1	38.1	50.8
OPC-PU	11	-3.08	14.6	475
SF-PU	12	41.3	28.1	68.1

Several conclusions can be drawn from the UPV testing results. First, the epoxy repair was successful in impregnating the crack. Both the OPC and the SF showed an increase in the UPV greater than 50%. The SF-PU specimens also exhibited an increase in the UPV reading also suggesting that in general the PU was also successful. These results are reflected in Figure 4.7.

The only group of specimens that showed a decrease in the UPV after conducting the injection repairs was the OPC-PU group of specimens. On average, these specimens observed a decrease in the UPV reading by 3.08%. A high COV of 457% implies that the results are not reliable.
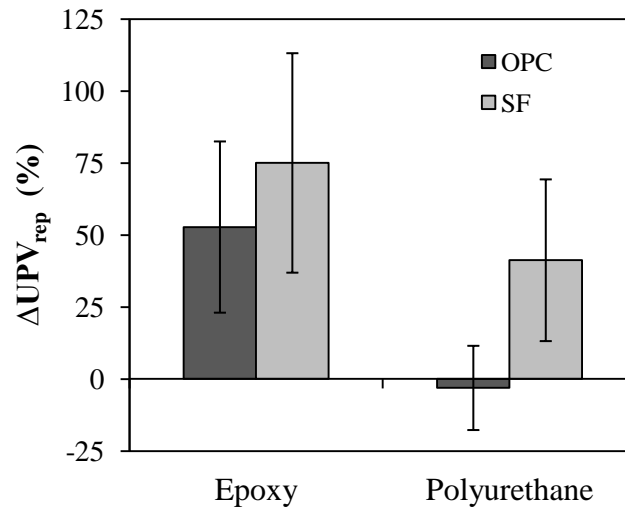
Figure 4.7 Repair effectiveness using UPV

For the polyurethane repair, it is apparent that only the SF specimens saw an increase in the UPV readings suggesting that they were successfully impregnated while the OPC specimens were not. The type of concrete however is not the causation for the apparent inability of the PU to fill in the crack. As previously concluded, the SF specimens had larger crack widths than the OPC specimens (Table 4.3). In addition, the viscosity of the PU repair was greater than that of the E, 500 cps compared to 105 cps. Both these factors may have contributed to the overall failure of impregnating the OPC specimens.

The average of 5 UPV readings was taken through each location on the concrete specimens. The average COV from 141 different concrete locations through uncracked was 2.60%. Likewise, the average COV from readings taken through cracked sections, based on 212 locations, was 26.3%. The UPV readings had a significantly higher COV for cracked sections compared to uncracked sections. The cracked sections have more variability in terms of the crack width, possible aggregate interlock, etc. which can be seen as the cause for the high COV. Furthermore, the average COV through the cracked-repaired sections had an average COV of 20.2% based on 156 locations. Overall the repaired UPV readings saw a decrease in the COV, but were still greater than the calculated COV through an uncracked section.

4.8 Effectiveness of Repairs: Freeze-Thaw Testing

4.8.1 Introduction

This section of the analysis and discussion examines the effectiveness of the repairs under freeze-thaw testing using air permeability and UPV testing similarly to the previous section. Measurements were taken prior to the FT regimes and after the completion of the FT cycles. The results are analyzed first by examining the individual

trends of the different repairs under the FT regimes using three different variables. A comparison of the results is done using non parametric statistical tests. In addition, the samples were also monitored for any visual degradation during testing.

4.8.2 Air Permeability

The results of the air permeability testing are presented using two variables ΔkTb_{env} and ΔkTt_{env}, which represent ratios of the air permeability of the environmentally conditioned specimens to the air permeability of the repaired specimens prior to FT testing. For both these variables, a value greater than 1.0 is an indication that the specimen's air permeability coefficient has increased, and can be considered degradation in the repaired concrete's transportation properties. Likewise, a value less than 1.0 is representative of a specimen where its air permeability coefficient has decreased, indicating an improvement in the air tightness of the specimen. The equations for the two variables are presented in Equations 4.20 and 4.21.

$$\Delta kTb_{env} = \frac{kTb_{env}}{kTb_{rep}} \qquad\qquad 4.20$$

Where ΔkTb_{env} is the ratio of the air permeability coefficients, kTb_{env} is the air permeability coefficient of the environmentally conditioned specimen measured on the bottom uncracked surface, and kTb_{rep} is the air permeability coefficient of the same repaired specimen prior to F/T testing, also measured on the bottom uncracked surface.

$$\Delta kTt_{env} = \frac{kTt_{env}}{kTt_{rep}} \qquad\qquad 4.21$$

Where ΔkTt_{env} is the ratio of the air permeability coefficients, kTt_{env} is the air permeability coefficient of the environmentally conditioned specimen measured on the top repaired surface, and kTt_{rep} is the air permeability coefficient of the same specimen prior to F/T testing, measured on the top repaired surface.

It is possible to relate the variable ΔkTb_{env} back to the variable defined in Equation 4.17, ΔkTb_{rep}. Both variables solely use the air permeability of the bottom uncracked surfaces as a reference point of unrepaired, repaired, and repaired/environmentally conditioned state of the specimen. In contrast, ΔkTt_{env} does not correspond to the variable ΔkTt_{rep} because it solely uses the top repaired surface as a point of reference. Previously, as described in Section 4.7.2, to calculate the $\Delta kTt_{rep,}$ the air permeability of unrepaired specimen was measured on the bottom surface since the top surface was not air tight, and no measurements could be taken. Using the air permeability measured on the same top surface eliminates any potential error due to differences in air permeability coefficients of the top and bottom surfaces.

The results of $\varDelta kTb_{env}$ are presented in Table 4.8. The specimens are categorized initially by type of cement and repair followed by the FT regime. As indicated in the experimental program, uncracked concrete control samples were subjected only to FTL and FTS regimes. The results for the OPC samples are replicated as bar graphs in Figure 4.8 and likewise the SF samples are presented in Figure 4.9. The sample size n for several of the specimen categories is 2. While 3 replicates were created for each category, it was not possible to get air permeability readings on all the samples, as several of the samples were found not to be air tight when measuring on the top or bottom surface. Similarly, the numerical results for $\varDelta kTt_{env}$ are presented in Table 4.9 and are also translated into bar graphs in Figure 4.10 and Figure 4.11 for OPC and SF samples respectively.

The results are discussed by examining the FT regimes individually, and analyzing the effects of the regime on the air tightness of the different repaired systems. To better interpret the results a series of parametric statistical tests were conducted on the data. Three different tests were conducted as follows.

First, a test was conducted to determine whether there was a statistically significant increase or decrease in the air permeability coefficient per specimen group. A two-sided confidence interval was created with a confidence of 95%. Because of the small sample size (n=2 or 3), the confidence interval gives a poor indication of that statistical significance, but is used as a general indication of the trend. A confidence interval is developed for each group. The air permeability has increased, $\varDelta kTb_{env}$ or $\varDelta kTt_{env} >1.0$, if the lower bound value of the interval is greater than 1.0, and it can be concluded that the specimens did see an increase in air permeability coefficients. The air permeability has decreased, $\varDelta kTb_{env}$ or $\varDelta kTt_{env}<1.0$, if the upper bound value of the interval is less than 1.0.

The same logic is applied for the second test which is used to examine whether the OPC or SF samples have either seen a statistically significant increase or decrease in the air permeability. The sample population consists of all different repairs categorized only by the cement type and F/T regime. In this case the sample size ranges from $6 - 12$ giving more validity to the significance of the results.

The final statistical test used is to test whether there is any statistical difference between the variable $\varDelta kTb_{env}$ and the variable $\varDelta kTt_{env}$. Once again, the data is grouped by cement type and FT regimes, but does not differentiate between the types of repairs. The sample size of these tests range from n= 6 to 12.

A comparison of the FT regimes is later discussed in Section 4.8.4.2 followed by a comparison of the different repaired systems in Section 4.8.4.2.

Table 4.8 Ratio of environmentally conditioned to repaired air permeability measured on the bottom surface (ΔkTb_{env})

Specimens	Regime	n	Mean	SD	COV (%)
OPC-CON	FTL	3	0.210	0.088	41.9
	FTS	3	0.287	0.057	19.9
SF-CON	FTL	3	0.369	0.0478	13.0
	FTS	3	0.512	0.129	25.2
OPC-E	FTL	3	0.199	0.0373	18.7
	FTS	3	0.227	0.095	41.7
	T	3	0.348	0.0439	12.6
	N	3	1.66	0.281	16.9
SF-E	FTL	3	0.501	0.064	12.7
	FTS	3	0.439	0.371	84.5
	T	3	0.652	0.139	21.4
	N	3	1.04	0.102	9.80
OPC-OV	FTL	3	0.079	0.054	68.7
	FTS	3	0.242	0.161	66.6
	T	3	0.227	0.103	45.4
	N	2	1.36	0.350	25.8
SF-OV	FTL	3	0.223	0.182	81.6
	FTS	3	0.168	0.101	60.1
	T	3	0.320	0.081	25.3
	N	2	1.05	0.0041	0.389
OPC-PU	FTL	3	0.101	0.0216	21.3
	FTS	3	0.144	0.133	92.3
	T	3	0.219	0.0343	15.7
	N	2	1.38	0.0359	2.60
SF-PU	FTL	2	0.594	0.342	57.5
	FTS	2	0.154	0.193	125
	T	2	0.500	0.0292	5.84
	N	2	0.869	0.284	32.7

Table 4.9 Ratio of environmentally conditioned to repaired air permeability measured on the top surface (ΔkTt_{env})

Specimens	Regime	n	Mean	SD	COV (%)
OPC-CON	FTL	3	0.306	0.148	48.3
	FTS	3	0.0887	0.075	85.0
SF-CON	FTL	3	0.501	0.398	79.5
	FTS	3	0.102	0.0319	31.2
OPC-E	FTL	3	0.247	0.0183	7.42
	FTS	3	0.0774	0.00600	7.76
	T	3	0.589	0.272	46.1
	N	3	1.263	0.108	8.57
SF-E	FTL	3	0.351	0.105	29.9
	FTS	3	0.0425	0.0103	24.2
	T	3	0.706	0.139	19.7
	N	3	1.050	0.163	15.5
OPC-OV	FTL	3	0.0106	0.00570	53.9
	FTS	3	0.0113	0.00496	43.7
	T	3	0.487	0.317	65.2
	N	3	1.398	0.248	17.7
SF-OV	FTL	3	0.0055	0.00365	66.4
	FTS	3	0.00307	0.00130	42.4
	T	3	0.427	0.319	74.7
	N	3	1.151	0.161	14.0
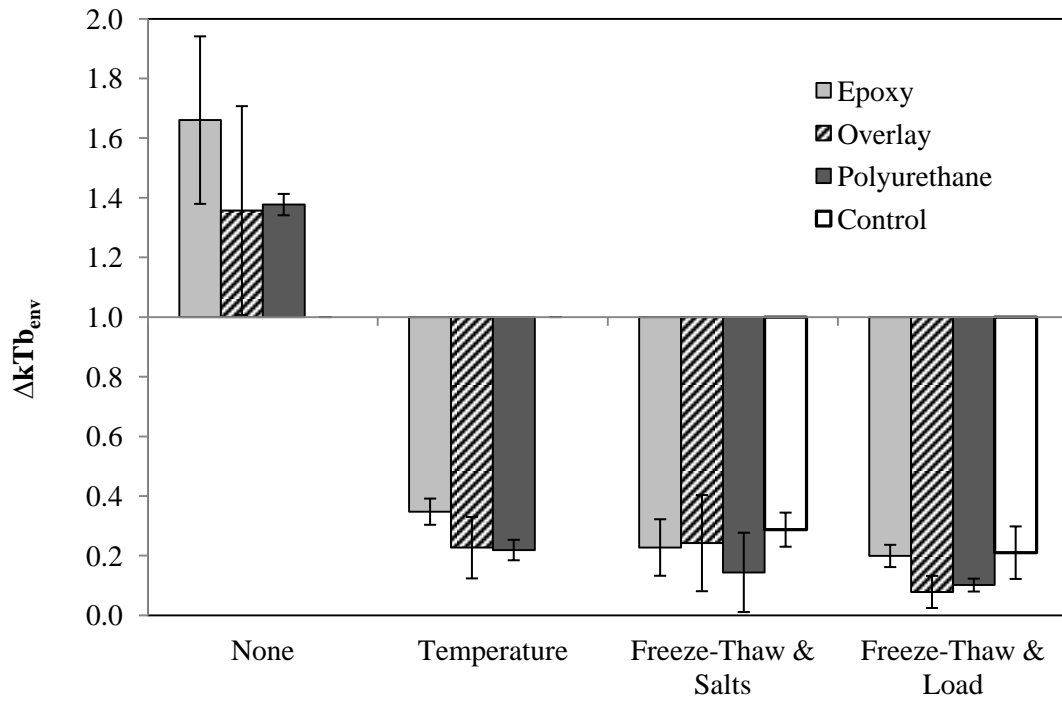
Figure 4.8 *ΔkTb$_{env}$* for OPC concrete specimens
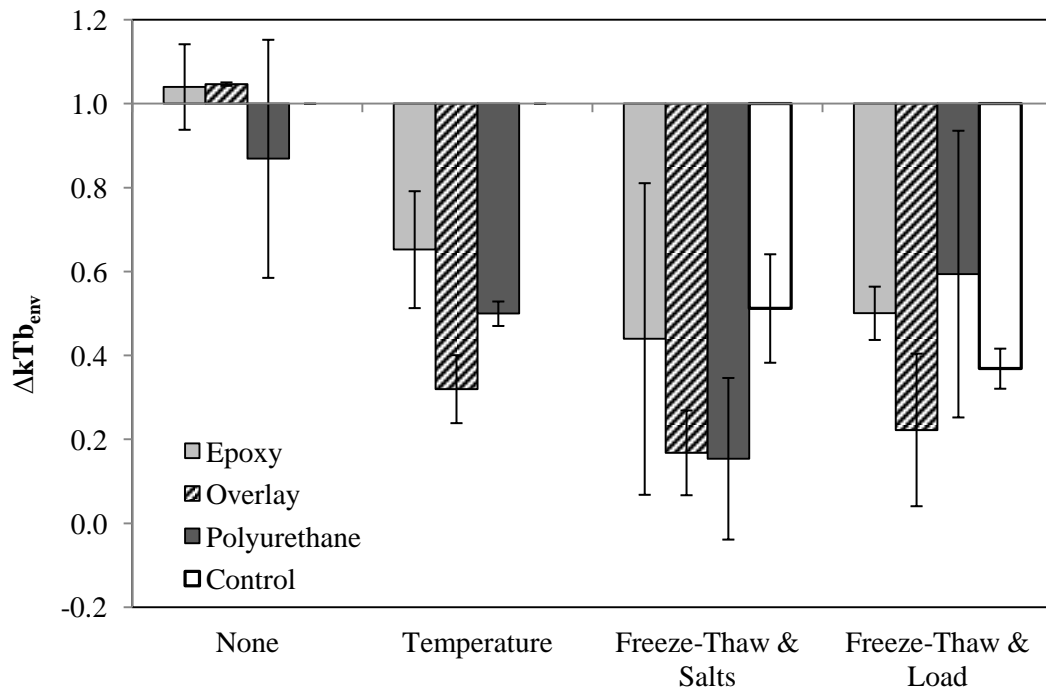
Figure 4.9 *ΔkTb$_{env}$* for SF concrete specimens
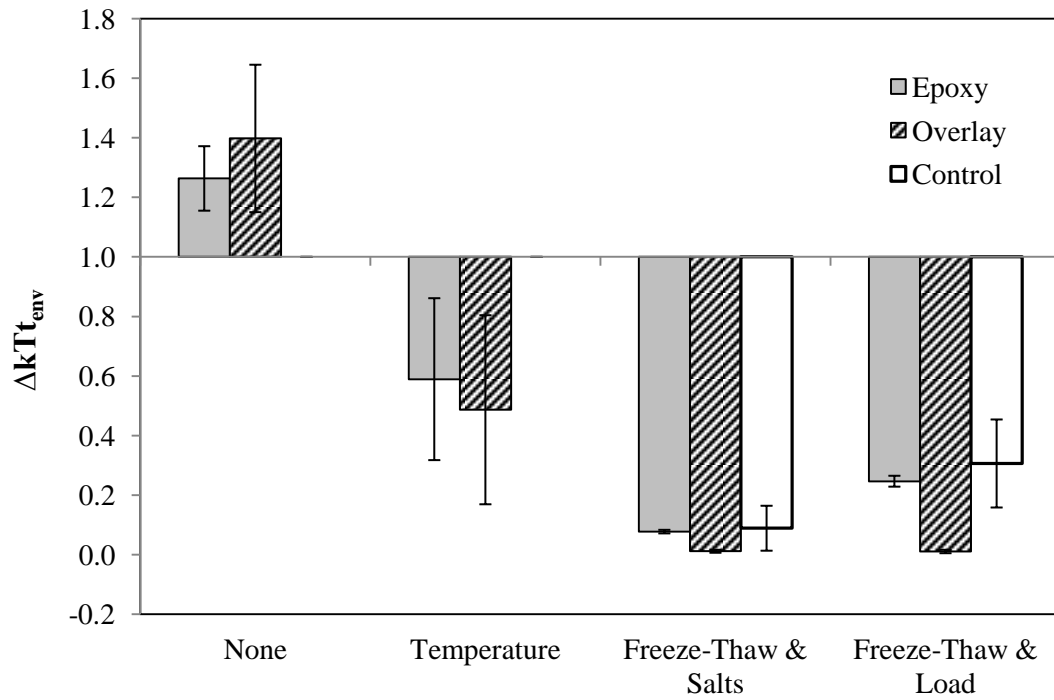
Figure 4.10 *ΔkTt$_{env}$* for OPC concrete specimens
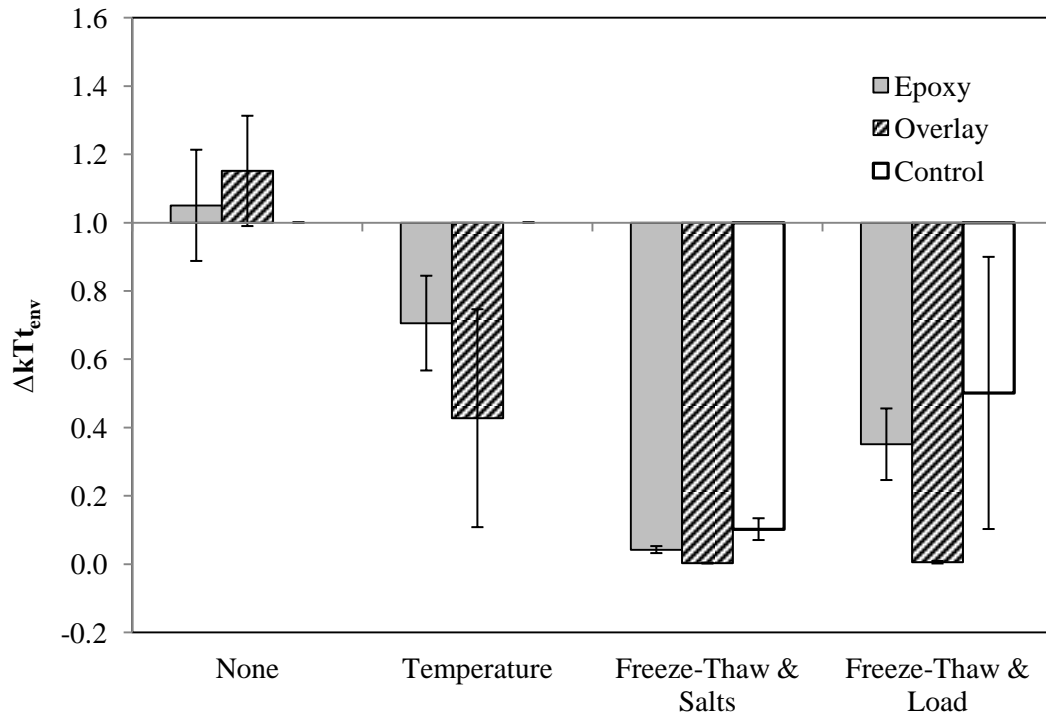
Figure 4.11 *ΔkTt$_{env}$* for SF concrete specimens

4.8.2.1 None

The most notable observation is all the specimens subjected to a FT regime (T, FTL, or FTS) observed a decrease in the air tightness, or what could be considered an improvement in the repaired system. The only samples which experienced an increase in air tightness are those specimens which were not subjected to any FT cycle (None) as is visible in Figure 4.8 to Figure 4.11.

These specimens were kept at laboratory conditions, which had an average temperature of 21˚C. The specimens were not exposed to any stressors intentionally for the duration of the other FT testing. For both variables, ΔkTt_{env} and ΔkTb_{env}, it was found that the OPC repaired system did see a statistically significant decrease in the air tightness while the results from the SF specimens were not statistically significant. One exception to this general trend includes specimen SF-PU-N which has a ΔkTb_{env} of 0.869, indicating an overall decrease in the air permeability coefficient.

There is no indication of what may have caused the OPC specimens to see a statistically significant decrease in the air tightness of the OPC specimens. One possible explanation may relate back to the concrete's microstructure and the degree of hydration. The difference in cement composition and the differences in microstructure properties and development may also account for the difference in the statistical test results between the OPC and SF samples. The two variables ΔkTt_{env} and ΔkTb_{env} both indicate similar trends, there is no indication of statistical difference between the two variables for both the OPC and the SF specimens.

By examining each repaired system individually, it was found that none of the results indicated a statistically significant increase or decrease in the air permeability coefficients. At the control conditions this is what is expected, as the specimens were not subjected to any conditions which would lead to an increase or decrease in air permeability conditions. This however contradicts the results grouped by cement type where the OPC specimens saw a significant increase in air permeability coefficients. The results of the latter test hold more influence since the sample size is 6 compared to 3.

The repaired systems under no environmental conditions also indicate a relative low COV in comparison to the variation of results of specimens subjected to other environmental regimes. The greatest COV is 32.7% for SF-PU-N specimens compared to the overall greatest COV of 92.3% for the OPC-PU-FTS specimens. One possible reason for the high COV for the PU specimens can be attributed to the repair method application. Due to the high viscosity of the polyurethane material and the range of crack widths, many of the PU repairs were unsuccessful at impregnating the cracks as previously discussed and shown through the low values of ΔUPV_{rep} when compared to the epoxy material.

4.8.2.2 Temperature (T)

All of the repairs under the temperature cycling regime have air permeability ratios less than 1.0, indicating an overall decrease in the air tightness, or an improvement in conditions. This is true for all repairs (E, OV, and PU) for both types of concrete (OPC and SF). Examining the individual repaired specimens separately, it was found that for

the variable ΔkTt_{env}, none of the results were statistically significant. For the variable ΔkTb_{env}, the specimens that saw a statistically significant decrease in the air permeability coefficient includes: OPC-E-T, OPC-OV-T, SF-OV-T, and OPC-PU-T. By examining the specimens grouped by cement type, it was found that for both variables, ΔkTt_{env} and ΔkTb_{env}, the OPC and SF saw statistically significant decreases in the air permeability coefficients. Both variables ΔkTt_{env} and ΔkTb_{env} show no statistical difference between the results for OPC and SF specimens.

Examining Table 4.8 and Table 4.9, none of the specimens undergoing T cycles have values greater than 1.0. The COV for the values varies with relatively high values for the SF specimens ranging from 19.7 - 74.7 %, in contrast to the OPC COV values which range from 5.84 - 45.4 %. The general trend, as reinforced by the statistical tests, and values presented suggests that the specimens in fact observe a decrease in the air permeability after undergoing temperature cycling. This in turn implies that the repaired samples are experiencing an improvement in properties when subjected to temperature cycles. These results contradict what is expected when examining the underlying mechanisms.

The temperature cycles consisted of increasing the temperature from -18°C to 23°C and back down again. The total change in temperature is $\Delta T = 41°C$. The thermal coefficient of expansion (CTE), α, of concrete is highly dependent of the type of aggregate used in the composition. The coefficient of thermal expansion typically ranges from 6 to 12 microns per °C (Mehta & Monteiro, 2006). The coarse aggregate is this experiment was limestone, and therefore the CTE of the concrete can be estimated as 6 x 10^{-6} °C.

Similarly, it is possible to estimate approximate values of CTE for the repair materials: epoxy, polyurethane, and a polymer modified cementitious paste. The CTE for the two component epoxy material used can be estimated to be 89 x 10^{-6} per °C from the product sheet of Sikadur-52 Injection Type-N, another epoxy material used for the same purposes, of concrete crack injection repairs (Sika, 2012; Sika, 2012). The polyurethane material can be approximated by 128 x 10^{-6}, the value of Loctite Hysol Polyurethane System 3173/3182 (Henkel Corporation, 2011). This value falls into the typical range expected for polyurethane adhesives used in concrete construction which typically range from 100 to 200 (ACI Committe 503, 1992). The coefficient for polymer modified mortars and pastes are typically close to that of concrete or slightly larger, therefore a realistic approximation of the CTE for the polymer modified paste is 9 x 10^{-6} (Ohama, 1998).

It is the differential strain between the materials that induces stress in both the repair material and the concrete. The stress that is induced in the injection repaired systems is different than that of the overlay repaired system. To calculate the induced stresses several assumptions and simplifications are made.

First, the properties of the concrete and materials must be estimated. The CTE of the materials are approximated for various sources of literature and product material sheets. The elastic modulus, E, of the materials must also be identified. For concrete, the elastic modulus can be calculated using the compressive strength. CAN/CSA A23.3-04 (2010) specifies the elastic modulus may be approximated by Equation 4.22, where f'$_c$ is

the compressive strength of concrete in MPa. The elastic modulus of the epoxy material was provided in the material product sheet for Sikadur 55 SLV (Sika, 2012). The elastic modulus for polymer modified mortars and concrete range from 0.001 to 10 GPa (Ohama, 1998). For the analysis, a median value of 5.0 GPa will be used. The polyurethane elastic modulus is estimated to be 0.6 GPa, as indicated on the data sheet for a similar product – Polyurethane 50FC (Larsen Building Products, 2012). These values are summarized in Table 4.10.

$$E_c = 4500\sqrt{f'_c} \qquad\qquad 4.22$$

For both injection and overlay repairs, a one dimensional linear elastic model is used to simplify the analysis, where the stresses developed are parallel to the concrete-repair material interface boundary. The final deformation of the repair material δ_{rep} and the concrete δ_c is equal to the addition of the unrestrained deformation due to the temperature change ($\delta_{rep(T)}$, $\delta_{c(T)}$) and the deformation due to the induced forces (F_{rep}, F_c) caused by the differential thermal expansion ($\delta_{rep(F)}$, $\delta_{c(F)}$). The unrestrained thermal deformation is calculated using Equation 4.23 and the deformation due to the developed forces is calculated using Equation 4.24, where L is the length in the direction of the deformation and A is the cross sectional area.

$$\delta_{(T)} = \alpha\,(\Delta T)L \qquad\qquad 4.23$$

$$\delta_{(F)} = \frac{FL}{EA} \qquad\qquad 4.24$$

From compatibility, the total deformation of repair must equal that of the concrete. Using equilibrium, and assuming no external forces, the forces must equate to zero. The deformations and forces are illustrated for an injection repair in Figure 4.12 for clarity. Using these two conditions it is possible to determine the forces and stressed developed in the repaired materials. Both the injection repairs (α_{inj}, δ_{inj}, E_{inj}, A_{inj}, F_{inj}) and the overlay repairs (α_{ov}, δ_{ov}, E_{ov}, A_{ov}, F_{ov}) are modeled in the same fashion. For the injection repairs and overlay repairs, equilibrium is defined in Equations 4.25 and 4.26 respectively.

$$F_{rep} = F_{inj} = 2F_c \qquad\qquad 4.25$$

$$F_{rep} = F_{ov} = F_c \qquad\qquad 4.26$$

To solve for the forces and respective stresses, compatibility and equilibrium conditions are enforced as shown in Equations 4.27 to 4.30.

$$\delta_{rep} = \delta_c \tag{4.27}$$

$$\delta_{rep\,(T)} + \delta_{rep\,(F)} = \delta_{c\,(T)} + \delta_{c\,(F)} \tag{4.28}$$

$$\alpha_{rep}\,(\Delta T)L - \frac{F_{rep}L}{E_{rep}A_{rep}} = rep = \alpha_c\,(\Delta T)L + \frac{F_c L}{E_c A_c} \tag{4.29}$$

Substituting Equations 4.25 and 4.26 in Equation 4.29, it is possible to solve for the forces developed. The forces generated in injection and overlay repairs are given in Equations 4.30 and 4.31 respectively. To determine the tensile and compressive stresses for injection materials, the area of the epoxy or polyurethane are estimated based on the average crack widths (w). Therefore for OPC samples the cross sectional area can be defined as 0.171 x 200 mm, similarly, the SF sample cross sectional area is 0.251 x 200 mm. For the overlay repair, the depth of the material is approximated as 2 mm, and therefore has a cross sectional area of 2 x 200 mm. The cross sectional area of the concrete for the injection repairs is 100 – (w/2) mm. For the overlay repairs, the concrete cross sectional area is 200 x 200 mm.

$$F_c = \frac{(\alpha_{inj} - \alpha_c)(\Delta T)}{\left(\dfrac{2}{E_{inj}A_{inj}} + \dfrac{1}{E_c A_c}\right)} \tag{4.30}$$

$$F_c = \frac{(\alpha_{ov} - \alpha_c)(\Delta T)}{\left(\dfrac{1}{E_{ov}A_{ov}} + \dfrac{1}{E_c A_c}\right)} \tag{4.31}$$

The stresses due to the temperature cycles are summarized in Table 4.10. They are categorized by type of repair and concrete. The normal stresses for both the repairs and the concrete are provided, the negative sign indicating tensile stresses. In addition the resulting bond shear stress, τ, at the repair interface is provided.

Using this simple model, some further assumptions need to be discussed. First, it is assumed that the only stresses developed are in one dimension. Furthermore, the injection repair has been idealized as a strip with a constant width across the whole depth of the specimen. It is also assumed that the repair material is fully bonded to the concrete.

From this model, there exists three different failure modes: failure of concrete in tension, failure of the repair material in compression, and failure of the bond strength. Examining the results, the stresses developed with the overlay material are minimal, primarily because the CTE of the concrete and the polymer modified cementitous overlay are similar. The concrete reached a maximum tensile stress of 1.68 MPa which is well below the tensile strength of concrete, which is approximately 10% of its compressive strength. Therefore the OPC and SF concrete tensile strength is estimated to be 3.18 and 3.93 MPa respectively. The epoxy reached a maximum of 6.72 MPa while the

polyurethane reaches a maximum of 2.99 MPa. The compressive strength of the epoxy is 75 MPa as listed in Table 3.2. The compressive strength of the polyurethane foam is not known, however it can be estimated as 11 MPa (Milosevski, Bossert, Milosevski, & Gruevska, 1999) which is well above the experienced stress.

It is not expected that solely the temperature differential will cause failure in the repaired concrete. The effects of fatigue or repeated cycles will also influence the failure mechanism. The concrete-repair stresses degrade with the increasing number of fatigue cycles caused by the cyclic temperature variation. The change in stress under fatigue loading is a function of the temperature variation, repair material properties, and concrete crack width (Shin, Miyauchi, & Tanaka, 2011). The effects of fatigue are not considered in this model as the number of cycles conducted is relatively small, so it is expected that fatigue will have little to no impact on the stresses generated.

The potential still exists for failure at the repair bond. The bond strength of the epoxy material to concrete is 17 MPa whereas the overlay material bond strength is 1 MPa (Table 3.2 and Table 3.3). The values of the shear bond stress in both cases are far from failure. In addition, the polyurethane material is a non-structural repair and is used primarily to stop the inflow of water into concrete. The bond strength, although not specified on the product's data sheet, is expected to be significantly lower than the epoxy, and the potential of failure at the bond is expected for the polyurethane repair. In a study conducted on polyurethane-based coatings used to protect concrete, the average bond strength of polyurethane materials to concrete ranged from 0.42 MPa to 0.78 MPa (Vipulanandan & Liu, 2005).

Figure 4.12 Stresses developed in injection repairs due to temperature cycles

Table 4.10 Stresses due to temperature cycles

Material		CTE α, (μ/°C)	Elastic Modulus, E (GPa)	Stress in Concrete σ_c (MPa)		Stress in Repair σ_{rep} (MPa)		Shear Bond Stress, τ (10^{-3} MPa)	
				OPC	SF	OPC	SF	OPC	SF
Concrete	OPC	6.0	25.4	–	–	–	–	–	–
	SF	6.0	28.2	–	–	–	–	–	–
Epoxy		89	2.0	-1.15	-1.68	6.72	6.69	9.57	14.0
Polyurethane		128	0.6	-0.512	-0.750	2.99	2.99	4.26	6.24
Modified Cem. Paste		9.0	5.0	-0.0204	-0.0204	0.611	0.611	6.11	6.11

4.8.2.3 Freeze-Thaw and Salts (FTS)

The effect of FT with salt indicates a decrease in the air tightness of the repaired systems. In Table 4.8 and Table 4.9 all the values of ΔkTb_{env} and ΔkTt_{env} associated with FTS are less than 1.0. Using confidence intervals on each of the individually repaired systems it is found that all the repairs saw a statistically significant decrease, for both variables, except for the following specimens: SF-E-FTS (ΔkTb_{env}) and SF-PU-FTS (ΔkTb_{env}). Similarily, when determining the confidence intervals on the specimens grouped by cement type, it was found that both the OPC and the SF samples saw a decrease in the air tightness for ΔkTt_{env} and ΔkTb_{env}.

When comparing the values of ΔkTt_{env} to ΔkTb_{env} it was found that for both SF and OPC specimens ΔkTt_{env} was statistically lower than ΔkTb_{env}. The air tightness measurements on the top surface decreased significantly when compared to those on the top surface. For example, the values of ΔkTt_{env} vs. ΔkTb_{env} for samples OPC-E and SF-OV are 0.0774 vs. 0.227 and 0.168 vs. 0.0113 respectively.

For the FTS regime the salt water ponded on the top surface of the specimens. Therefore the top surface was directly exposed to water, and dependent of the permeability of the samples, the water could migrate down towards the bottom surface. The COV values for the ΔkTb_{env} for the repairs are: 19.9%, 25.2%, 41.7%, 84.5%, 66.6%, 60.1% for the OPC-C, SF-C, OPC-E, SF-E, OPC-OV, and SF-OV respectively. The COV values for the ΔkTt_{env} for the respective repairs are: 85.0%, 31.2%, 7.76%, 24.2%, 43.7%, 42.4%. In general, the COV for ΔkTt_{env} is lower than for ΔkTb_{env}. This suggests that there is less variation in ΔkTt_{env}. For the FTS regime, ΔkTb_{env} shows greater variation in the results, which could be attributed to additional factors such as the permeability of the specimens which dictate how far the salt water penetrates into the samples. The one exception are the control samples whose COV for ΔkTt_{env} were higher than ΔkTb_{env} .

The presence of water on the surface of the specimens is providing a source for the continuing hydration process. Unhydrated cement particles when exposed to water will react and continue in producing Calcium Silica Hydrate. The curing process, as outlined in the experimental program, only consisted of 7 days of moist curing, after

which the specimens were cracked. This was done in order to prevent the effects of autogenous healing of the concrete, a process by which cracks are repaired in the presence of water due to the formation of crystalline $CaCO_3$ (Edvardsen, 1999). Similar logic can be applied to the overlay material which was not moist cured, but then exposed to water during the FTS regime. The effects are also amplified due to the high air entrainment as noted in Section 4.4. The continued hydration in the highly porous concrete becomes evident in the results due to the reduction of the porosity.

The MTO test standard LS-412 "Method of Test For Scaling Resistance of Concrete Surfaces Exposed to Deicing Chemicals" (1997) was adopted for the FTS regime. The standard specifies 50 cycles. In this experimental program, due to time constraints, only 30 cycles were completed. The FT cycles are meant to impose a deteriorating mechanism in the concrete. However, due to the competing effects of the continuing hydration, the deterioration is not evident in the specimens through air permeability testing. The deterioration was evident through the observed surface scaling and is further discussed in Section 4.8.5.

4.8.2.4   Freeze-Thaw and Loads (FTL)

The effects of the FTL regime resulted in an overall decrease of the variables ΔkTb_{env} and ΔkTt_{env} indicating a decrease in the air tightness, or an improvement in the concrete's transportation properties. For both types of specimens, OPC and SF, a statistically significant decrease in the air tightness was observed for ΔkTb_{env} and ΔkTt_{env}. Examining each of the sample groups, it was found that all repairs for both OPC and SF samples experienced a statistically significant decrease in the air tightness with one exception. Using the confidence intervals, the sample group SF-PU-FTL did not show a statistically significant decrease in the air tightness for ΔkTb_{env}.

Comparing the results of ΔkTb_{env} and ΔkTt_{env}, it was found that for OPC and SF samples there was no statistically significant difference between the two variables. While the FTL shows similar trends to FTS regime, the FTL regime shows similar decreases in air tightness for both the top and the bottom. This conclusion is based on not differentiating between the different repairs. The SF-E-FTL values for ΔkTb_{env} and ΔkTt_{env} are 0.501 and 0.247 respectively. Similarly, the sample SF-OV-FTL values are 0.223 and 0.0055. Overall there is no statistically significant difference between the air tightness of the top and bottom when grouping the different repairs, however examining the repairs individually, the OV repair shows an apparent difference in values.

The decrease in value of ΔkTb_{env} and ΔkTt_{env} can be attributed to the continuing hydration process in the presence of water as previously discussed for the FTS regime in Section 4.8.2.3. The effects of continued hydration are more prevalent than the FT cycles combined with the sustained load. The sustained load, using four point bending, induced a moment (M_L) of 2745 N.mm as previously calculated in Equation 3.3. For both the overlay and injection repairs the maximum tensile stress (σ_L) can be calculated using applied mechanics, where y is the distance to the outermost tension fibre (30 mm), and I_x is the moment of inertia about the neutral axis (3.6×10^6 mm^4). Substituting these values into Equation 4.32, the maximum tensile stress is equal to 0.02 MPa.

$$\sigma_L = \frac{M_L y}{I_x} \qquad\qquad 4.32$$

Comparing this value to the stress induced by the temperature cycling, it is almost negligible. However, the flexural tensile stress is perpendicular to the injected repair interface, putting the repair-concrete boundary in direct tension. For the stress induced by T cycles, the injection repair was modeled with a constant width throughout the entire specimen depth. In this case the stresses developed were along the repair-concrete interface boundary. For the overlay material, the T cycles and the load in the FTL cycles develop the stresses in the same plane, parallel to the overlay-concrete interface.

The transport of the water in the concrete differed between the FTL and the FTS regimes. For the FTL regime, the specimens were only saturated in the water for an hour before being placed in a freezing environment. For the FTL regime the specimen was in a container, with the water level reaching only 10 mm above the bottom surface. The water was absorbed into the concrete rather than permeating into the concrete under gravity as in the FTS regime. By the time the specimens were placed into the freezing environment, by visual inspection, it was noted that more than 30 mm of the 60 mm depth had been saturated. This may account for why ΔkTb_{env} and ΔkTt_{env} were statistically different for FTS but not for FTS.

4.8.3   Ultrasonic Pulse Velocity

For the injection repairs, the UPV testing measured after the environmental regimes to monitor any changes in the samples. To evaluate the internal damage in the specimens the variable defined in Equation 4.33 is utilized.

$$\Delta UPV_{env} = \left[\frac{UPV_{env} - UPV_{rep}}{UPV_{rep}} \right] \cdot 100\% \qquad\qquad 4.33$$

ΔUPV_{env} is the percent change of the direct-UPV from the damaged cracked condition (UPV_{rep}) to the environmentally regimented state (UPV_{env}). This variable for each specimen is based on the average of the change in the UPV in three locations through the repaired-cracked section. As a comparison, the percent change of the UPV in two uncracked sections is also included. These results are presented in Table 4.11. The results are also presented in Figure 4.13 and Figure 4.14.

Table 4.11 ΔUPV_{env} - Repaired and uncracked sections

Specimens	Regime	Repaired Sections				Uncracked Sections			
		n	Mean	SD	COV (%)	n	Mean	SD	COV (%)
OPC-E	FTL	2	23.1	2.0	8.5	3	3.88	3.16	81.4
	FTS	3	3.73	7.0	188.7	3	8.38	8.15	97.2
	T	3	10.9	11.5	105.6	3	-0.244	0.675	-277
	N	3	1.87	1.7	92.4	3	-0.074	2.11	-2,839
SF-E	FTL	3	5.61	2.6	46.1	3	1.53	1.94	127
	FTS	3	2.24	11.4	510.2	3	0.0540	9.44	17,471
	T	3	13.9	6.7	48.0	3	-1.61	7.43	-461
	N	3	19.9	11.5	57.7	3	-1.46	1.5	-99.7
OPC-PU	FTL	3	24.7	41.3	167.4	3	4.01	2.24	55.8
	FTS	3	41.7	17.7	42.3	3	5.93	4.40	74.3
	T	3	7.84	17.5	223.4	3	-0.00309	2.12	-68,481
	N	3	10.8	16.1	149.2	3	-1.597	0.800	-50.1
SF-PU	FTL	3	20.1	27.3	136.2	3	3.75	1.43	38.2
	FTS	3	54.3	32.0	59.0	3	-12.5	29.4	-235
	T	3	7.20	3.3	46.5	3	0.591	5.08	859
	N	3	12.1	10.3	84.7	3	3.04	1.10	36.4

The use of UPV to evaluate the effects of the environmental regimes on the repaired specimens is a poor measure of the conditions. The results show inconsistency as made evident by the data presented in Table 4.11. For both the repaired and uncracked sections there are specimens with high COV of over 100 %. No statistically significant and confident conclusions can be drawn from the data.
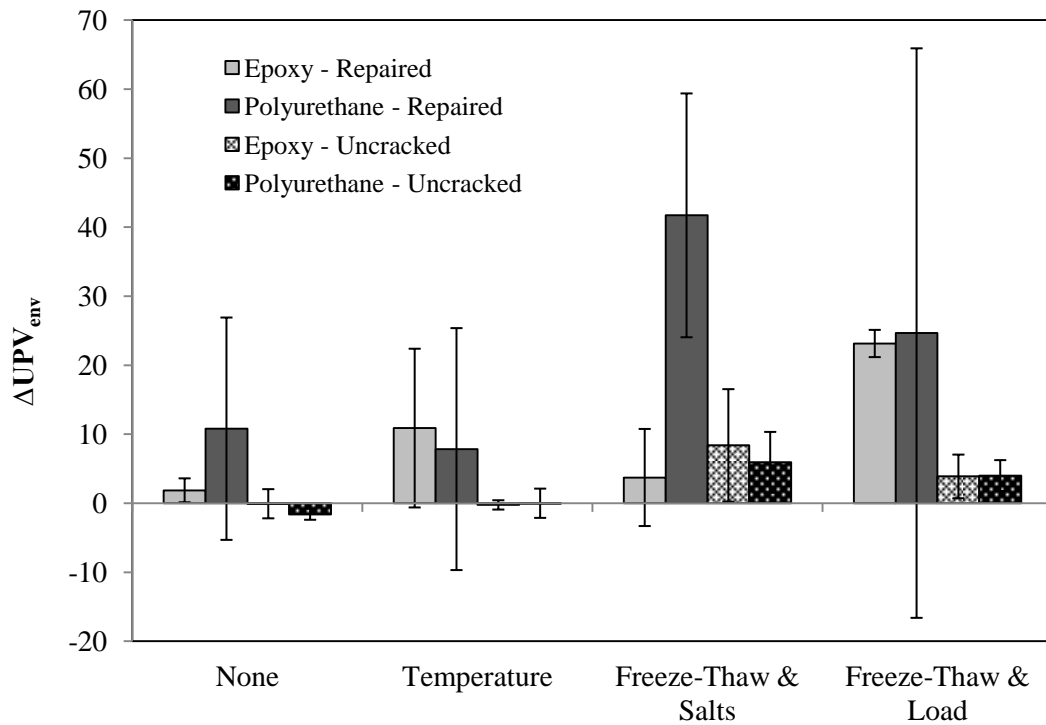
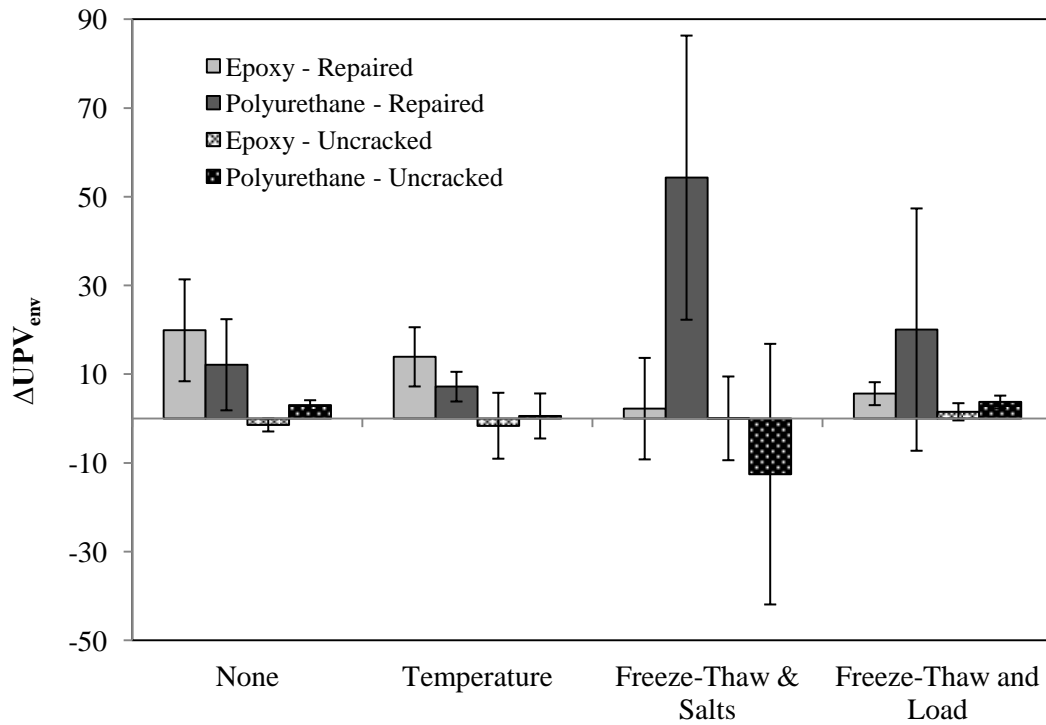**Figure 4.13 ΔUPV_{env} for OPC concrete**

Figure 4.14 ΔUPV_{env} for SF concrete

4.8.4   Comparison of the Results under FT Testing

Additional statistical tests were carried out using the Kruskal-Wallis technique to analyze the data in two different fashions. First, the results using the three different variables (ΔkTb_{env}, ΔkTt_{env}, ΔUPV_{env}) were used to relate how the concrete crack repairs compare to one another under the separate FT Regimes. These results are presented in Table 4.12. The variable ΔUPV_{env} was included in the comparison in order to relate its results to the air permeability testing, despite this testing method was found to be unreliable in evaluating the effectiveness of the repairs. Secondly, the results were also categorized by repair method to investigate the impact of the different FT regimes on the type of repair as presented in Table 4.13.

When interpreting the results from Table 4.12 and Table 4.13, there are several key points that need to be addressed. The statistical test used is based on a limited number of samples as previously mentioned when defining the Kruskal-Wallis statistical test in Section 4.3.2. Furthermore, a higher value of air permeability coefficient, ΔkTb_{env} and $\Delta kTt_{env,}$, indicates a loss of air permeability, or a worsening in the repaired concrete properties. For the variable ΔUPV_{env}, the opposite is true. A greater value implies an increase in the UPV reading, indicating an improvement in the repaired concrete properties.

4.8.4.1   Comparison of the Repair Techniques

By examining the results in Table 4.12 several observations can be made. To begin with, there is no statistical difference between the E, OV and PU repairs under the control condition (None) the temperature cycling regime (T). This is true for all three variables examined. As both of these condition cause little to no stress on the repairs and the repaired systems, little change would be expected in the air permeability and UPV readings. The one exception to this statement is that the SF-OV was found to have a lower ΔkTb_{env} than the other repairs under the T regime. As the OV material was applied on the top surface, it is unlikely that this material would indicate a greater improvement than the other repairs for this variable. These results may be the result of the small sample size and poor results using the Kruskal-Wallis test.

Under the FTS regime, the OV and PU repairs statistically performed better than the E repair and the CON. In general there was no statistical difference between the E and the CON samples, suggesting that the FT regimes have the same effect on the epoxy repair as they do on the control samples. In the case of the SF specimens, the variable ΔkTb_{env} found no statistical significance between any of the repairs and the ΔkTb_{env} found that the E repair was statistically greater than that of the CON sample.

These results are confirmed with the UPV results, the PU repairs saw a statistically greater improvement than the E repairs. In Table 4.7, it was shown that the E repairs had higher ΔUPV_{rep} values than the PU repairs. Overall the epoxy material was more successful in penetrating the crack than the polyurethane material. However, under the FTS regime, when the repaired system is exposed to water, the polyurethane material exhibits a greater improvement. The reactants to the formation of polyurethane include diisocyanates, polyols, amines, and catalysts. Two component polyurethanes rely on the

reaction of isocyanates and polyols to the formation of polyurethane polymers. However, the process can be further continued in the presence of water, where the isocyanates and water yield amines which then continue to further react with water to produce urea chains (Noble, 1997). The presence of water is capable of furthering the polyurethane curing process, resulting in an increase in the UPV reading. The same mechanism can be used to describe why the OV repair saw greater improvement in the air permeability ratio than the other repairs. The polymer modified cementitous material was applied on the surface of the specimens which was not followed by a curing period. The access to water during the FTS regime provided a source for continued hydration as previously mentioned,

Similar patterns to the FTS regime are observed in the results of the FTL regime. The ΔkTt_{env} variable found no statistical difference between the E repairs and the CON samples and the OV repairs saw a greater improvement in air tightness than the E and CON samples. The SF samples, when evaluated using the air permeability on the bottom found no statistical difference between the repairs, in contrast, the OPC concrete samples repaired with the PU saw the greatest relative improvement in air tightness, followed by the OV and E repairs.

Table 4.12 Comparison of the effectiveness of repairs under FT regimes using Kruskal-Wallis statistical tests

Regime	Type	Variable		
		ΔkTb_{env}	ΔkTt_{env}	ΔUPV_{env}
None	OPC	Similar	Similar	Similar
	SF	Similar	Similar	Similar
T	OPC	Similar	Similar	Similar
	SF	OV < E/PU	Similar	Similar
FTS	OPC	OV/PU < E/CON	OV < E/CON	E < PU
	SF	Similar	OV < E < CON	E < PU
FTL	OPC	PU < OV/E < CON	OV < E/CON	Similar
	SF	Similar	OV < E/CON	Similar

4.8.4.2 Comparison of the FT Regimes

For each of the repairs analyzed using UPV, it was found that there was no statistical significance between the FT regimes. This can be attributed to the high variation in readings and the overall inability of the UPV as an ineffective means of quantifying the change in the repaired concrete's conditions.

Using the change in the air permeability of the bottom surface of the concrete specimens (ΔkTb_{env}), also found no statistical significance between the types of FT regimes for the CON samples, E and PU repaired specimens. In contrast, the air permeability measured on the top of the specimen indicated that there existed FT regimes that were statistically significant.

For the CON specimens, as well as the E and OV repairs, it was found the FTS regimes resulted in the greatest improvement of conditions based on the air permeability

of the top surface. The next greatest improvement of properties was produced by the FTL regime, followed by the T regimes, and subsequently by no regime (N). The FTS caused the greatest improvement in conditions can once again be attributed to the presence of water and the continuing hydration process of the cement in the concrete. This same mechanism can be used to explain why the FTL regime saw a greater improvement than the T and N regimes. The FTL, unlike the FTS regime, however had an additional stressor of the steel bar, maintaining a constant moment on the specimens allowing for a tensile stress to develop between the repair material and the concrete substrate.

For all the repairs, the N regime saw the smallest improvement of air permeability properties, and actually demonstrated a worsening in the conditions when referring back to Figure 4.8 to Figure 4.11. The T regime typically saw less improvement of properties when compares to the FTL and FTS regimes, but demonstrated an improvement in the air permeability properties when compares to the N regime. The T and N regimes were not saturated in water and therefore should not exhibit the effects of continued hydration.

Table 4.13 Comparison of the effects of environmental regimes on repairs using Kruskal-Wallis statistical tests

Repair	Type	Variable		
		ΔkTb_{env}	ΔkTt_{env}	ΔUPV_{env}
CON	OPC	Similar	FTS < FTL	–
	SF	Similar	FTS < FTL	–
E	OPC	Similar	FTS < FTL & T < N	Similar
	SF	Similar	FTS < FTL < T < N	Similar
OV	OPC	–	FTS & FTL < T & N	–
	SF	–	FTS < FTL < T < N	–
PU	OPC	Similar	–	Similar
	SF	Similar	–	Similar

While statistical significance of the different environmental regimes is evident with the variable ΔkTt_{env} it is not evident with the variable ΔkTb_{env}. In the case of the FTL and FTS regimes it was the top surface that was exposed to water, which could in turn explain why the top surface air permeability readings for these regimes were found to be statistically significant. The top surface is also the location of the overlay material, and for the injection materials the top portion of the specimen contains a greater proportion of the injection material. This is assuming that the top surface contains the largest width of the crack, as proven using rigid body modes. Therefore under the T and FTL regimes, the location of the greatest stress is at the top surface and therefore the effects of the FT regimes are more likely to be reflected based of the air permeability readings on this surface.

4.8.5   Visual Observations

In addition to using non-destructive test methods, the specimens were also monitored for any visual signs of deterioration: scaling of the concrete, discolouration of

the repair materials, etc. Visually, the only signs of deterioration that were visible included scaling of the concrete surface for the specimens subjected to FTS and the FTL cycles.

By comparison, the specimens subjected to the FTS regime exhibited more scaling than the FTL specimens. Scaling was observed in the FTS specimens after only 5 cycles, while scaling was very minimal to nonexistent in FTL specimens after 30 cycles. The presence of the salts in the form of a 3 % NaCl solution had obvious implications on the amount of scaling observed. Both the FTS and FTL cycles will induce FT damage mechanisms in the specimens due to the expansion of the water in the capillary pores, however due to the additional osmotic pressures that develop with the presence of salts (Mehta & Monteiro, 2006), the FTS regimes are expected to exhibit more damage.

One exception included the OV repaired specimens which exhibited no scaling after 30 cycles when subjected to either the FTL or the FTS regimes. The OV-FTS specimens however did contain a white crusted film layer on the surface of the specimens as seen in Figure 4.15 (a), suggesting that the OV layer prohibited the NaCl from diffusing into the specimens. The OV repair material was a modified cementitious material incorporating an acrylic polymer. The addition of polymer in concrete results in a linearly increasing scaling resistance despite an observed decrease in the compressive strength (Bordeleau, Pigeon, & Banthia, 1992). The improved quality of concrete cover is attributed to the existence of a continuous polymer film bound within the CSH matrix hindering the penetration of water and chloride ions (Eash & Shafer, 1975).

When contrasting the SF and the OPC specimens undergoing the FTS regime, the SF concrete specimens revealed a higher amount of scaling than the OPC specimens, disregarding the OV repaired specimens which exhibited no scaling. Studies have mixed conclusions on the effects of silica fume on the scaling resistance of concrete: at a w/c $\geq$ 0.4 SF was proven to increase the scaling resistance (Aitcin & Pigeon, 1986) however at a w/c < 0.35 the effects of SF were marginal (Sorenson, 1983). Further investigations have proven that the curing conditions can significantly impact the scaling resistance of the SF concrete, and when cured at temperatures of 70 ˚C and above, the SF scaling resistance decreases (Langlois, Beaupre, Pigeon, & Foy, 1989). This suggests that specific pouring and curing conditions used in this experimental program, may have been the cause of the poor scaling resistance of the SF concrete.
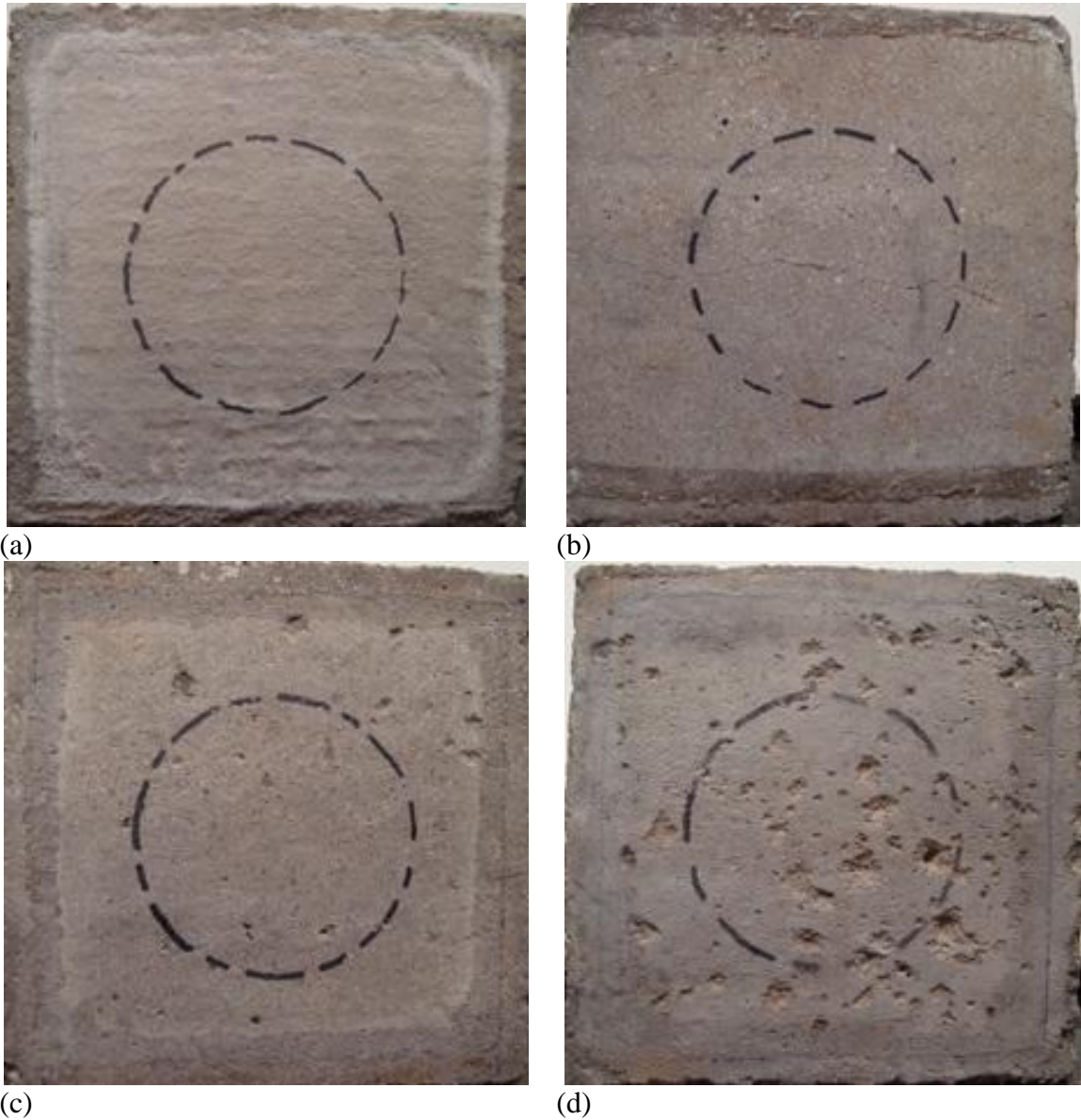
Figure 4.15 No evidence of scaling in the SF-OV-FTS (a) and SF-E-FTL (b) specimens; only moderate scaling in the OPC-E-FTS (c) specimens; and excessive scaling in the SF-CON-FTS (d) specimens after 30 cycles.

4.9   Service Life Predictions

It has been recognized that deterioration in reinforced concrete structures is caused primarily by concrete's insufficient durability. In light of this, action has been taken to implement concrete durability indexes, such as Torrent's air permeability coefficient (*kT*), in performance based specifications for reinforced concrete structures (Alexander, Ballim, & Stanish, 2008). In particular, the Swiss Standard SIA 262 on "Concrete Construction" recommends checking the impermeability of the cover concrete on site (Torrent, Denarie, Jacobs, Leeman, & Teruzzi, 2012). One of the results of this movement is the development of service life predictions based on the durability indexes.

4.9.1   Carbonation Service Life Model

Utilizing the presented results in Section 4.8.2 from the Torrent permeability testing, the values can be correlated to other concrete properties, such as the carbonation depth and chloride diffusivity. Based on the experimental work of Torrent and Ebensperger (1993) as well as Torrent and Frenzer (1995), the air permeability index kT (10^{-16} m^2) has been experimentally correlated to the carbonation depth, d_{co} (mm), using the empirical formula presented in Equation 4.34 and summarized by Torrent (2007) where *t* is the time in years.

This model is based on data collected from both OPC and SF concrete samples which have been cured for 0 and 7 days, and exposed to natural conditions (20 °C, 50 RH) for 500 days. The determination of the carbonation depth is an empirical formula based primarily on the results of experimental data. The failure of the concrete due to carbonation or the end of its service life is reached when the carbonation depth is equal to the concrete reinforcement cover. In Canadian concrete construction, when the concrete is exposed to chlorides as well as freeze-thaw cycles, (Class of Exposure C-1), the CSA (CSA A23.1, 2009) recommends a minimum cover of 60 mm. Therefore Equation 4.34 is rearranged to solve for t, or the service life of the concrete (*SL*), assuming a reinforcement cover of 60 mm.

.

$$d_{co}\ (\text{mm}) = 2.2\ln\left(\frac{kT}{0.01}\right)t^{0.5} \qquad\qquad 4.34$$

$$SL\ (\text{Years}) = \left[\frac{27.27}{\ln\left(\frac{kT}{0.01}\right)}\right]^2 \qquad\qquad 4.35$$

The service life predictions for carbonation are presented in Figure 4.16.

4.9.2   Chloride Service Life Model

Similarly, the chloride diffusivity has been correlated to the Torrent air permeability by Torrent (2007). Through the use of Fick's second law for chloride diffusion as well as the empirical relationship between air permeability measurements and

chloride diffusion, it is possible to create an equation to estimate the depth of chloride ingress.

Fick's second law of diffusion is presented in Equation 4.36 where x is the distance from the concrete surface (mm), t is the time in seconds (s), D_c is the diffusion coefficient (mm^2/s), C_0 is the equilibrium chloride concentration on the concrete surface, and $C_{(x,t)}$ is the chloride concentration at position x, and time, t.

$$C_{(x,t)} = C_0 \left[1 - erf\left(\frac{x}{2\sqrt{D_c t}} \right) \right] \qquad 4.36$$

$$t = \frac{x^2}{4D_c \left[erf^{-1}\left(1 - \frac{C_{(x,t)}}{C_0} \right) \right]^2} \qquad 4.37$$

An empirical relationship between the chloride diffusivity, D_c, and the Torrent air-permeability are established by Torrent (2007) through the means of experimental data. The relationship is defined in Equation 4.38 where kT is the coefficient of air permeability (10^{-16} m^2).

$$D_c = 56 \, kT^{0.70} \, 10^{-6} \, (mm^2/s) \qquad 4.38$$

To determine the service life of the repaired concrete due to chloride ingress, Equation 4.39 is substituted into Equation 4.36. Similar to the carbonation service life development, a reinforcement cover of 60 mm is assumed, and subsequently is substituted for x. The values of C_0 and $C_{(x,t)}$ must be approximated based on the environmental conditions, as well as the type of concrete and reinforcement used.

The surface chloride concentration (C_o) is dependent on the exposure conditions of the concrete. For this study, the concrete structure is presumed to be a bridge located in Ontario, Canada, specifically examining the concrete deck surface. The environment presented for such a location would be classified as a severe environment. Consequently a surface chloride concentration of 3.95 kg/m^3 is assumed based on a location with moderate to high corrosive environment which is suggested from the statistical data collected by the Strategic Highway Research program in the United States (Weyers, Prowell, Sprinkel, & Vortser, 1993).

The value of $C_{(x,t)}$ becomes the *threshold chloride* concentration at which the reinforcement is expected to start corroding. This value is primarily influenced by the type of reinforcement used in the concrete, but is also influenced by such factors such as humidity, w/c ratio, and the aggregates quantity and properties (Zhang & Lounis, 2006). Various values are suggested throughout literature. Trejo and Pillai (2003) found that a chloride threshold value of 0.27 kg/m^3 assuming standard A615 –ASTM deformed plain carbon-steel reinforcing bars. However, to be consistent with the chosen C_o concentration, a value of 0.708 kg/m^3 was used as recommended by Weyers et al. (1993).

Substitution of these assumed variables, as well as Equation 4.28 into Equation 4.36 results in the service life, *SL,* presented in Equation 4.39 as a function of *kT* (10^{-16} m^2).

The service life predictions for chloride ingress are presented in Figure 4.16. The service life of carbonation and chloride ingress are shown on two different scales, as the predicted service life for carbonation is significantly greater than that of chloride ingress.

$$SL = \frac{(60)^2}{224[erf^{-1}(0.82)]^2} \cdot kT^{-0.70} \qquad 4.39$$

$$SL = 0.55 \cdot kT^{-0.70} \qquad 4.40$$

4.9.3 Service Life Results

Examining the results of the service life predictions shown in Figure 4.16, one observes that the chloride penetration service life is consistently less than that of the carbonation. In terms of chloride ingress, no specimen has a service life greater than 8 years. In contrast, the concrete carbonation service life reaches a maximum of 700 years. Therefore it can be concluded that the process of chloride ingress is more aggressive than that of carbonation, and that the repaired concrete will first fail due to chloride ingression. The significant difference between the chloride service life and the carbonation service life may in part be attributed to the development of the models. The carbonation model was based solely on the experimental work of Torrent (2007), which included samples with specified curing conditions and cement type. The chloride service life model was developed using several estimated parameters (chloride concentration, chloride threshold, etc.) which contain high variability.

The service life of the control specimens and those samples subjected to temperature cycles, have not been included in these results. The calculated service lives of the N and T samples demonstrate the effects of the high air content in concrete and its porous nature. These samples had greater air permeability coefficients than those specimens subjected to the FTL and FTS cycles, resulting in underestimated service lives. Also, continuing hydration was dominant in the FTL and FTS samples, which is reflected in smaller air permeability coefficients and longer service lives.

 In the results, the PU repair has been omitted as it was not possible to obtain air permeability readings on the top surfaces of the repaired specimens, also indicating failure of the repair. Despite the poor interpretation of the results between the FT regimes, it is still possible to examine the service life of the different repairs. Except for those repairs exposed to FTL, the epoxy injection repair indicates the longest service life. Therefore, an epoxy repair should be specified as the repair method for cracks in concrete, so as to increase the durability of the concrete and prolong the service life of the structure.

Overall, the service life results reinforce the experimental results. The data from the experimental program does not yield the anticipated results for the performance of the repair materials when subjected to various environmental conditions. This is primarily attributed to the high air content of the concrete, that is, the high porosity resulted in poor air tightness of the concrete specimens. The air permeability coefficients were primarily influenced by this factor and the effects of the concrete repairs became secondary. Secondly, hydration was a dominant factor in the results. Continuing hydration resulted in the reduction of porosity, an effect that was amplified by the original high porosity of the concrete. In the experimental program, an insufficient number of environmental cycles were provided to effectively measure the performance of the repairs due to the competing effects of continuing hydration.
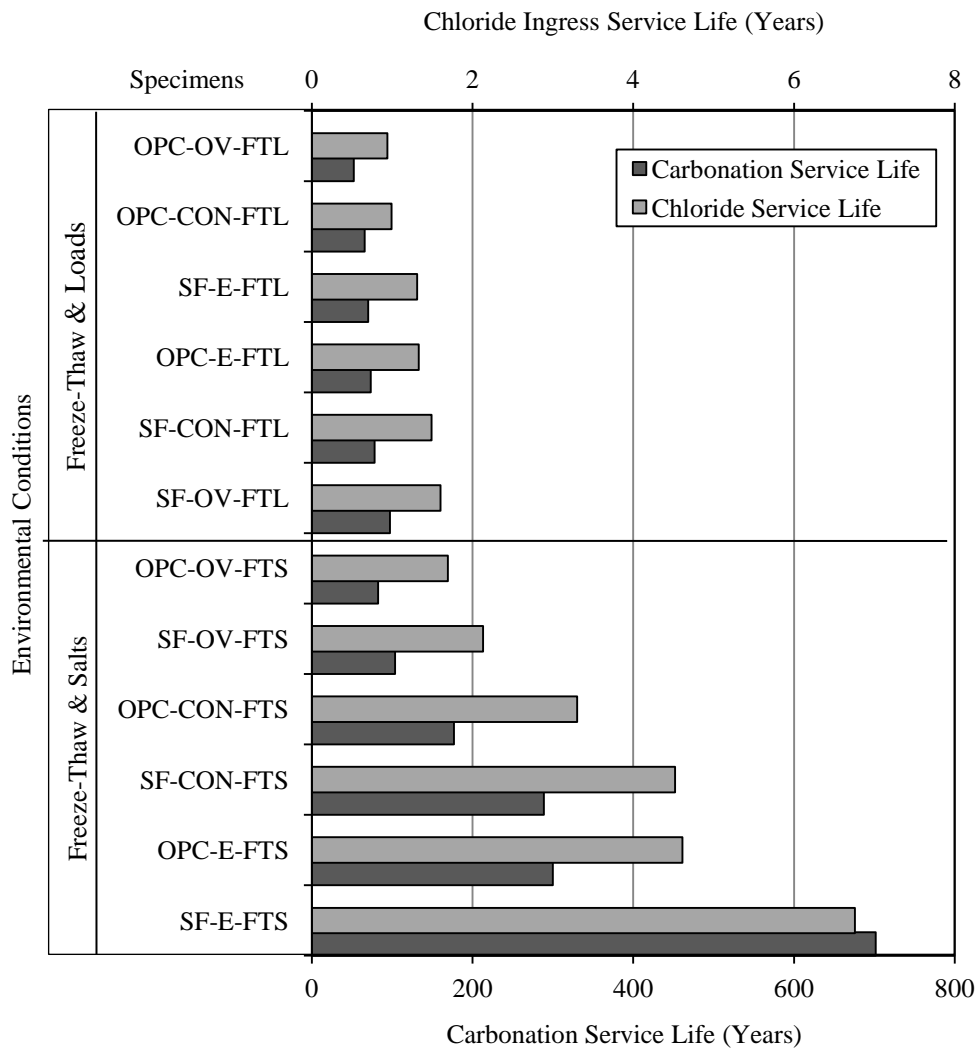

Figure 4.16 Service life prediction of concrete subjected to environmental conditions

A comparison of the service life of the repaired specimens can be made with cracked concrete. The influence of cracks on the chloride diffusivity was presented in the literature review. In an experimental study conducted by Djerbi et al. (2008), a simple relationship was found between the crack width and chloride diffusion coefficient in concrete. The established relationship is dependent of the type of concrete, whether OPC or SF. The coefficient of diffusion in cracked concrete is equal to the coefficient of diffusion in uncracked concrete (D_0) plus the additional diffusion due to the crack (D_{cr}) whose relationship to the crack width is established in Equation 4.41.

$$\begin{aligned} D_{cr} \ (mm^2/s) &= \ 2 \times 10^{-5} \cdot w - 4 \times 10^{-4} \quad 30\mu m \leq w \leq 80\mu m \\ D_{cr} \ (mm^2/s) &= \ 14 \times 10^{-4} \qquad\qquad\qquad\quad w \geq 80\mu m \end{aligned} \qquad 4.41$$

Using this relationship, the chloride diffusion for the cracked concrete samples can be estimated using the same procedure established in Section 4.9.2. The results of the estimated service life of the cracked concrete (SL_{cr}) and a comparison to the service life of the repaired samples (SL_{rep}) is shown in Table 4.14. The values suggest that the repairs are capable of prolonging the service life of cracked concrete.

Table 4.14 Comparison of repaired concrete service life

FT Regime	Concrete	Repair	SL_{rep}/SL_{cr} (Year/Year)
Freeze Thaw & Salts	OPC	Epoxy	210
		Overlay	77
	SF	Epoxy	307
		Overlay	97
Freeze-Thaw & Load	OPC	Epoxy	68
		Overlay	45
	SF	Epoxy	43
		Overlay	60

CHAPTER 5 CONCLUSIONS AND RECOMMENDATIONS

5.1   Introduction

This chapter summarize the main conclusions that were drawn from the data analyzed in the previous chapter on the evaluation of cracks in concrete, the effectiveness of repair methods, and the effects of the environmental regimes.

5.2   Evaluating Cracks in Concrete

Cracks were introduced in concrete specimens using three-point bending, and the crack widths were measured using a crack comparator. Two non-destructive techniques were used to evaluate the damage in concrete. The following effects of cracks on the concrete are as follows:

1. The silica fume concrete specimens had statistically significant greater crack widths than the ordinary Portland cement specimens: 0.251 and 0.171 mm respectively.
2. The cracked specimens were not air tight on the cracked surface.
3. An exponential relationship between the air permeability ratio ΔkTb_{cr} and the crack width was established with a weak correlation.
4. A linear relationship between the percent change in the direct UPV readings, $UPV(d)_{cr}$ was established with the crack width with a weak correlation.
5. The indirect UPV readings were found to be a poor indicator of the damage in the cracked concrete specimens.

5.3   Concrete Crack Repairs

The cracked concrete specimens were repaired with three different methods, and using the same non-destructive testing methods, the repairs were evaluated and are summarized in this section:

1. The epoxy and overlay repairs were capable of restoring the air tightness to the top of the concrete specimens.
2. The epoxy repair was the most effective repair, with kT_{rep} statistically similar to that of the uncracked control samples, and with ratios ΔkTb_{rep} and ΔkTt_{rep} less than 1.0 for SF and OPC specimens.
3. The overlay material did not have a significant effect of the air tightness of the specimens, as the ratios ΔkTb_{rep} and ΔkTt_{rep} were statistically greater than 1.0 for OPC and SF samples.
4. The polyurethane repair was unsuccessful at restoring the air tightness of the cracked concrete.
5. The epoxy repairs successfully impregnated the cracks, showing an increase of 52.8 % and 75.1 % for the OPC and SF specimens, respectively.

6. The polyurethane repairs were only successful in impregnating the SF specimens, which on average had greater crack widths.
7. There was no strong correlation for the degree of repair between the air permeability tests (ΔkTb_{rep}) and the UPV tests (ΔUPV_{rep}), suggesting that the successful infiltration of an injection repair material will not necessarily decrease the air permeability of the repaired concrete.

5.4 Effects of Freeze-Thaw Testing

The repaired specimens were subjected to one of three types of freeze-thaw environmental conditions: temperature cycles, freeze-thaw with salt solutions, and freez-thaw with sustained loads. The following conclusions were deduced regarding the effects of the various regimes on the different repairs:

1. The control specimens (E, OV, and PU), which were not exposed to any environmental conditioning regimes, saw an increase in the air permeability coefficient.
2. All the repairs (E, OV, and PU), including both SF and OPC samples, which were subjected to temperature cycles demonstrated a decrease in the air permeability. Using an one dimensional model, the temperature cycles generate stress in the concrete and repair materials. The effect of the stress developed is not evident in the results.
3. All the repairs (E, OV, and PU), for both SF and OPC samples, undergoing freeze-thaw cycles with salts saw a decrease in the air permeability. The internal pressures generated by the volumetric expansion of water upon freezing as well as the osmotic pressure generated by the presence of salts, were overshadowed by the effects of continuing hydration of the cement.
4. The freeze-thaw cycles with sustained loads, for the repairs E, PU, and OV, all demonstrated a decrease in the air permeability for both OPC and SF specimens. Similarly, the exposure to water in this regime promoted the ongoing hydration which dominated any effects of freeze-thaw and stresses generated by the sustained load.
5. The UPV was found to be inadequate in assessing the effects of the FT regimes due to sample size.
6. For the temperature regime, the only significant result was that the OV repair saw the greatest decrease in the air permeability for the temperature cycles.
7. Under FTS regime, the OV repair was statistically the most effective repair in decreasing the air permeability.
8. The OV repair was the most effective repair when subjected to F/T with loads, observing the statistically greatest decrease in air permeability.
9. The epoxy repair faired best under the FTS regime. The second greatest improvement in air tightness was observed in the specimens subjected to the FTL regime followed by the T regime.

10. The overlay repair saw the greatest improvement of air permeability under the FTS regimes, followed the FTL and T regimes progressively.
11. Relating the air permeability coefficients to the mass transport properties of concrete the results find that none of the concrete repairs have a service life greater than 8 years when solely examining chloride ingress. This is due to high porosity of the concrete.

5.5 Future Research

The main objective of this thesis was to evaluate the effectiveness of fine crack repairs in concrete for the long term. The experimental program was designed to include the examination of two types of concrete, three different repair methods, and three environmental conditioning regimes. From the experimental work presented, several recommendations can be made:

1. Repeat the experiment with a concrete whose air content is between 5 and 7%.
2. To fully understand the long term effects of the environmental stresses, a minimum of 60 additional environmental cycles should be conducted.
3. Future work needs to examine other repair techniques and materials that are available for fine concrete crack repairs.
4. Use other non-destructive measures to evaluate the concrete crack repairs, and compare the results of the different evaluation techniques.
5. The development of an experimental setup to initiate non-structural cracks in concrete naturally and consistently.
6. Once the concrete crack repairs have deteriorated, apply new repairs, and examine the effectiveness of the second repairs.
7. Examine the possibility of replacing traditional crack repair methods with emerging self-healing concrete. Compare the long term effectiveness of the two types of repairs to determine whether the self-healing properties would reduce inspection and maintenance costs of concrete structures.

REFERENCES

ACI Committe 503. (1992). *Guide for the Selection of Polymer Adhesives with Concrete.* Farmington Hills: American Concrete Institute.

ACI Committee 209. (2008). *ACI 209.2R-08: Modelling and Calculation of Shrinkage and Creep in Hardened Concrete.* Farmington Hills: American Concrete Institute.

ACI Committee 503. (2007). *Specification for Crack Repair by Epoxy Injection.* Farmington Hills: American Concrete Institute.

ACI Committee 546. (2006). *Guide for the Selection of Materials for the Repair of Concrete.* Farmington Hills: American Concrete Institute.

Acker, C., & Ehrlacher, A. (1995). Analyses and models of the autogenous shrinkage of hardening cement paste: I. Modelling at macroscopic scale. *Cement and Concrete Research*, 1457–1468.

Afridi, M., Ohama, Y., Iqba, M., & Demura, K. (1995). Water retention and adhesion of powdered and aqueous polymer-modified mortars. *Cement and Concrete Composites*, 113-118.

Aitcin, P., & Pigeon, M. (1986). Performance of condensed silica fume concrete used in pavements and sidewalks. *Durable Building Materials*, 353-368.

Aitcin, P., Neville, A., & Acker, P. (1997). Integrated View of Shrinkage Deformation. *Concrete International*, 35-41.

Akhavan, A., Shafaatian, S., & Rajabipour, F. (2012). Quantifying the effects of crackwidth, tortuosity, and roughness on water permeability of cracked mortars. *Cement and Concrete Research, 42*(2), 313-320.

Aldea, C., Shah, S., & Karr, A. (1999). Effect of Cracking on Water and Chloride Permeability of Concrete. *Journal of Materials in Civil Engineering, 11*(3), 181-187.

Alexander, M., Ballim, Y., & Stanish, K. (2008). A framework for use of durability indexes in performance based design and specification for reinforced concrete structures. *Materials and Structures, 41*, 921-936.

Ali, Y., & Ambalavanan, R. (1999). Flexural behaviour of reinforced concrete beams repaired with styrene—butadiene rubber latex, silica fume and methylcellulose repair formulations. *Magazine of Concrete Research*, 113-120.

Al-Mandil, M., Khalil, H., Baluch, M., & Azad, A. (1990). Performance of Epoxy-Repaired Concrete under Thermal Cycling. *Cement and Concrete Composites, 12*(1), 47-52.

Asad, M., M.H., B., & Al-Gadhib, A. (1997). Drying shrinkage stresses in concrete patch repair systems. *Magazine of Concrete Research*, 283-242.

ASTM C597. (2009). *Standard Test Method for Pulse velocity Through Concrete.* West Conshohocken: American Society for Testing and Materials.

Bang, S., Galinat, J., & Ramakrishnan, V. (2001). Calcite precipitation induced by polyurethane-immobilized Bacillus pasteurii. *Enzyme and Microbial Technology, 28*(4-5), 404-409.

Banthia, N., & Gupta, R. (2009). Plastic shrinkage cracking in cementitious repairs. *Materials and Structures*, 567-579.

BASF. (2010). *Glenium 7700: Product Data.* BASF Corporation.

BASF. (2010). *Micro Air: Product Data.* BASF Corporation.

Basheer. (1991). *'Clam' permeability tests for assessing the durability of concrete, PhD Thesis.* Belfast: The Queen's University of Belfast.

Basheer, L., Kropp, J., & Cleland, D. (2001). Assessment of the durability of concrete from its permeation properties: a review. *Construction and Building Materials, 15*(2), 93-103.

Bazant, Z. (1988). Material Models for Structural Creep Analysis. In Z. Bazant, *Mathematical Modeling of Creep and Shrinkage of Concrete* (pp. 99-177). New York: John Wiley and Sons.

Bazant, Z., & Baweja, S. (2000). Creep and Shrinkage Prediction Model for Analysis and Design of. *American Concrete Institute Special Publication,*, 1-84.

Beaushausen, H., & Alexander, M. (2006). Failure mechanisms and tensile relaxation of bonded concrete overlays subjected to differential shrinkage. *Cement and Concrete Research*, 1908-1914.

Bjegovic, D., Skazlic, M., & Jambresic, M. (2005). Crack repair assessment by ultrasonic method. *The 8th International Conference of the Slovenian Society for Non-Destructive Testing* (pp. 81-89). Portoroz: Slovenian Society for Nondestructive Testing.

Bordeleau, D., Pigeon, M., & Banthia, N. (1992). Comparative Study of Latex-Modified Concretes and Normal Concretes Subjected to Freezing and Thawing in the Presence of a Deicer Salt Solution. *ACI Materials Journal*, 547-553.

Bowers, R., & Zisman, W. (1964). Surface Properties. In E. Baer, *Engineering Design for Plastics* (pp. 689-741). New York: Reinhold Publishing Corporation.

Brien, J., & Mahboub, K. (2013). Influence of polymer type on adhesion performance of a blended cement mortar. *Internation Jounmral of Adhesion and Adhesives*, 7-13.

Brown, E., Kessler, M., & White, S. (2003). In situ poly(urea-formaldehyde) microencapsulation of dicyclopentadadiene. *Journal of Microencapsulation*, 719-730.

Cai, W., Dong, A., & Zhang, X. (2012). Crack Width Detection of the Concrete Surfaced Based on Images. *Advances in Computer, Communication, Control, and Automation, 121*, 625-632.

CAN/CSA A23.3-04. (2010). *Design of Concrete Structures.* Mississauga: Canadian Standards Association.

Cement Association of Canada. (2011). *Design and Control of Concrete Mixtures.* Ottawa: Cement Association of Canada.

Colak, A., Cosgun, T., & Bakirci, A. (2009). Effects of environmental factors on the adhesion and durability characteristics of epoxy-bonded concrete prisms. *Construction and Building Materials, 23*(2), 758-767.

Comité Euro-International du Béton. (1993). *CEB-FIP Model Code 1990.* London: Thomas Telford.

Conover, W. (1999). *Practical Nonparametruc Statistics.* New York: John Wiley and Sons.

CSA A23.1. (2009). *Concrete Materials and Methods of Concrete Construction/Methods of Test for Concrete.* Mississauga: Canadian Standards Association.

CSA Test Method A 23.2-9C. (2009). *Compressive Strength of Cylindrical Concrete Specimens: Concrete Materials and Methods of Concrete Construction/Methods of Tests for Concrete.* Mississauga: Canadian Standards Association.

CSA Test Method A23.2-10A. (2009). *Density of Aggregate: Concrete Materials and Methods of Concrete Construction/Methods of Tests for Concrete.* Mississauga: Canadian Standards Association.

CSA Test Method A23.2-12A. (2009). *Relative Density and Absorption of Coarse Aggregate: Concrete Materials and Methods of Concrete Construction/Methods of Tests for Concrete.* Mississauga: Canadian Standards Association.

CSA Test Method A23.2-2A. (2009). *Sieve Analysis of Fine and Coarse Aggregate: Concrete Materials and Methods of Concrete Construction/Methods of Tests for Concrete.* Mississauga: Canadian Standards Association.

CSA Test Method A23.2-3C. (2009). *Making and curing concrete compression and flexural test specimens: Concrete Materials and Methods of Concrete Construction/Methods of Tests for Concrete.* Mississauga: Canadian Standards Association.

CSA Test Method A23.2-4C. (2009). *Air Content of Plastic Concrete by the Pressure Method: Concrete Materials and Methods of Concrete Construction/Methods of Tests for Concrete.* Mississauga: Canadian Standards Association.

CSA Test Method A23.2-5C. (2009). *Slump of Concrete: Concrete Materials and Methods of Concrete Construction/Methods of Tests for Concrete.* Mississauga: Canadian Standards Association.

CSA Test Method A23.2-6A. (2009). *Relative Density and Absorption of Fine Aggregate: Concrete Materials and Methods of Concrete Construction/Methods of Tests for Concrete.* Mississauga: Canadian Standards Association.

Danish Standards Association. (2004). *Repair of Concrete Structures to EN 1054.* Burlington: Elsevier.

Delatte, N., Fowler, D., McCullough, B., & Grater, S. (1998). Investigating performance of bonded concrete overlays. *Journal of Performance of Constructed Facilities*, 62-70.

Djerbi, A., Bonnet, S., Khelidj, A., & Baroghel-bouny, V. (2008). Influence of transerving crack on chloride diffusion into concrete. *Cement and Concrete Research*, 877-883.

Dry, C. (1994). Matrix cracking repair and filling using active and passive modes for amrt time release of chemicals from fibers into matrices. *Smart Materials and Structures*, 118-123.

Dry, C., & McMillan, W. (1996). Three-part methylmethacrylate adhesive syste, as an internal delivery system for smart responsive concrete. *Smart Materials and Structures*, 297-300.

Dry, C., Corsaw, M., & Bayer, E. (2003). A comparison of internal self-repair with resin injection in repair of concrete. *Journal Adhesion Science Technology*, 79-89.

Dunn, K. (2011, March). Process Improvement Using Data. Hamilton, ON, Canada: Statistics for Engineers, Class Notes.

Eash, R., & Shafer, H. (1975). Concrete, Reactions of Polymer Latexes with Portland Cement. *Transportation Research Record*, 1-8.

Edvardsen, C. (1999). Water Permeability and Autogenous Healing of Cracks in Concrete. *ACI Materials Journal*(96), 448-455.

Ehlers, G. (1964). Thermal Stability. In E. Baer, *Engineering design for plastics.* New York: Reinhold Publishiong Corporation.

Ekenel, M., & Myers, J. (2007). Durability performance of RC beams strengthened with epoxy injection and CFRP fabrics. *Construction and Building Materials, 21*(6), 1182-1190.

El-Hawary, M., Al-Khaiat, H., & Fereig, S. (1998). Effect of Sea Water on Epoxy-repaired Concrete. *Cement and Concrete Composite*, 41-52.

Emberson, N., & Mays, G. (1996). Significance of property mismatch in the patch repair of structural concrete. *Magazine of Concrete Research*, 45-57.

Emborg, M., & Bernander, S. (1994). Assessment of risk of thermal cracking in hardening concrete. *Journal of Structural Engineering, 120*(10), 2893-2912.

Emmons, P., & Sordyl, D. (2006, July/August). The state of the concrete repair industry, and a vision for its future. *Concrete Repair Bulletin*, pp. 7-14.

Feldman, R., & Sereda, P. (1970). A New Model for Hydrated Portland Cement and its Practical Implications. *Engineering Journal*, 53-59.

Ge, S., Wan, F., Lu, J., & Yu, J. (2011). Molecular self-assembled microcapsules prepared by in situ polymerization technology for self-healing cement materials. *Journal of Inorganic Organometallic Polymers*, 1-5.

Gerard, B., & Marchand, J. (2000). Influence of cracking on the diffusion properties of cement-based materials: Part I: Influence of continuous cracks on the steady-state regime. *Cement and Concrete Research*, 37-43.

Gettu, R., Bazant, Z., & Karr, M. (1990). Fracture Properties and Brittleness of High Strength Concrete. *ACI Materials Journal, 87*(6), 608-618.

Ghosh, S. (2009). *Self-Healing Materials: Fundamentals, Design Strategies, and Applications.* Weinheim: Wiley-VCH.

Gowripalana, N., Sirivivatnanonb, V., & Lim, C. (2000). Chloride diffusivity of concrete cracked in flexure. *Cement and Concrete Research*, 725-730.

Granju, J. (2001). Debonding of Thin Sement-Based Overlays. *Journal of Materials in Civil Engineering*, 114-120.

Gupta, A., Mani, P., & Krishnamoorthy, S. (1983). Interfacial adhesion is polyester resin concrete. *nternational Journal of Adhesion and Adhesives*, 149–154.

Henkel Corporation. (2011). *The Adhesive Sourcebook.* Rockey Hill: Henkel Corporation.

Hickey, J., Burke, N., & Stover, H. (2011). Layer-by-layer deposition of clay and a polycation to control diffusive release from polyurea microcapsules. *Journal of Membrane Science*, 68-76.

Hilsdorf, H., Schonlin, K., & Burieke, F. (1992). *Dauerhaftigkeit von Betonen.* Universtat Karlsruhe: Institute for Massivbau and Baustofftechnologie.

Holt, E. (2001). *Early Age Autogenous Shrinkage of Concrete.* Finland: VTT Publications.

Hoseini, M., Bindiganavile, V., & Banthia, N. (2009). The effect of mechanical stress on permeability of concrete: a review. *Cement and Concrete Composites*, 213-220.

Huang, M., & Yang, J. (2011). facile microencapsulation of HDI for self-healing anticorrosion coatings. *Journal of Material Chemistry*, 1-8.

ICRI Technical Committee. (2006). *Guide for the Selection of Grouts to Control Leakage in Concrete Structures.* Des Plaines: International Concrete Repair Institute.

Iman, R., Quade, D., & Alexander, D. (1975). Exact probability levels for the Kruskal-Wallis test. In H. Harter, & D. Owen, *Selected Tables in Mathematical Statistics* (Vol. 3, pp. 329-384). New York: American Mathematical Society.

Issa, C., & Debs, P. (2007). Experimental study of epoxy repairing of cracks in concrete. *Construction and Building Materials, 21*(1), 157-163.

Jang, S., Kim, B., & Oh, B. (2011). Effect of crack width on chloride diffusion coefficients of concrete by steady-state. *Cement and Concrete Research, 41*(1), 9-19.

Jensen, O., & Hensen, P. (2001). Autogenous deformation and RH-change in perspective. *Cement and Concrete Research*, 1859-1865.

Jonkers, H., & Schlangen, E. (2007). Crack repair by concrete-immobilized bacteria. In A. Schmets, & S. van der Zwaag (Ed.), *Proceedings of the First International Conference on Self Healing Materials* (pp. 1-7). Noordwijk aan Zee, The Netherlands: Springer.

Jonkers, H., & Schlangen, E. (2009). A two component bacteria-based self-healing concrete. *Concrete Repair, Rehabilitation and Retrofitting II* (pp. 215-220). Cape Town: CRC Press.

Jonkers, H., A., T., Copuroglu, O., & Schlangen, E. (2010). Application of bacteria as self-healing agent for the development. *Ecological Engineering, 36*(2), 230-235.

Joseph, C., Gardner, D., Jefferson, T., Isaacs, B., & Lark, B. (2011). Self-healing cementitious materials: a review of recent work. *Construction Materials*, 29-41.

Joseph, C., Jefferson, A., & Cantoni, M. (2007). Issues relating to the autonomic healing of cementitious materials. *Proceedings of the First International Conference on Self-Healing Materials* (pp. 1-8). The Netherlands: Springer.

Kaltzakorta, I., & Erkizila, E. (2010). Study of the effect of sol-gel parameters on the size and morphology of silica microcapsules containing different organic components. *Physica Status Solidi*, 2697-2700.

Khairallah, R. (2009). *Analysis of Autogenous and Drying Shrinkage of Concrete.* Hamilton: McMaster University.

Klisińska-Kopacz, A., Tišlova, R., Adamski, G., & Kozłowski, R. (2010). Pore structure of historic and repair Roman cement mortars to establish their compatibility. *Journal of Cultural Heritage, 11*(4), 404-410.

Kwon, S., Na, U., Park, S., & Jung, S. (2009). Service life prediction of concrete wharves with early-aged crack: Probabilistic approach for chloride diffusion. *Structural Safety*, 75-83.

Lafarge Cement. (2011). *Cement Mill Test Report.* Bath: Lafarge.

Langlois, M., Beaupre, D., Pigeon, M., & Foy, C. (1989). Influence of Curing on the Salt Scaling Resistance of Concrete With and Without Silica Fume. *ACI Special Publication, 114*, 971-990.

Larsen Building Products. (2012). *Product Listing.* Dublin: Larsen Building Products.

Lawler, J., Zampini, D., & Shah, S. (2002). Permeability of Cracked Hybrid Fiber-Reinforced Mortar. *ACI Materials Journal, 99*(4), 379–385.

Lee, H., Cody, R., Cody, A., & Spry, P. (2000). Effects of Various Deicing Chemicals on Pavement Concrete Deterioration. *Mid-Continent Transportation Symposium, Center for Transportation Research and Education,* (pp. 151-155). Iowa: Iowa State University.

Lee, H., Wong, H., & Buenfeld, N. (2010). Potential of superabsorbent polymerfor seld-sealing cracks in concrete. *Advances in Applied Ceramics, 109*(5), 296-302.

Letsch, R. (1986). Resin injection of cracks with changing width. In H. Sasse (Ed.), *Adhesion between polymers and concrete* (pp. 432-437). Paris: Chapman and Hall.

Li, J., Hitchcock, A., Stover, H., & Shirley, I. (2009). A New Approach to Studying Microcapsule Wall Growth Mechanisms. *Macrocolecules*, 2428-2432.

Litorowicz, A. (2006). Identification and quantification of cracks in concrete by optical fluorescent microscopy. *Cement and Concrete Research, 36*, 1508-1515.

Lura, P., Jensen, O., & van Breugel, K. (2003). Autogenous shrinkage in high-performance cement paste: An evaluation of basic mechanisms. *Cement and Concrete Research*, 223-232.

Lv, Z., Chen, H., & Yuan, H. (2011). Quantitative solution on dosage of repair-agent for healing of 3D simplified cracks in materials: short capsule model. *Materials and Structures*, 987-995.

Marsavina, L., Audenaert, K., De Schutter, G., Faur, N., & Marsavina, D. (2009). Experimental and numerical determination of the chloride penetration in cracked concrete. *Construction and Building Materials*, 264-274.

McIlroy, D., Blaiszik, B., Caruso, M., White, S., Moore, J., & Sottos, N. (2010). Microencapsulation of a Reactive Liquid-Phase Amine for Self-Healing Epoxy Composites. *Macromolecules*, 1855-1859.

Mehta, P., & Monteiro, P. (2006). *Concrete: Microstructure, properties and materials.* New York: McGraw Hill.

Milosevski, M., Bossert, J., Milosevski, D., & Gruevska, N. (1999). Preparation and properties of dense and porous calcium phosphate. *Ceramics International*, 693-696.

Momayez, A., Ehsani, M., Ramezanianpoura, A., & Rajaiea, H. (2005). Comparison of methods for evaluating bond strength between concrete substrate and repair materials. *Cement and Concrete Research*, 748-757.

Montgomery, D., & Runger, G. (1994). *Applied Statistics and Probability for Engineers.* New York: John Wiley and Sons.

Moradllo, M., Shekarchi, M., & Hoseini, M. (2012). Time-dependent performance of concrete surface coatings in tidal zone of marine environment. *Construction and Building Materials, 30*, 198-205.

MTO Test Method LS-412 Rev. No 17. (1997). *Method of test for scaling resistance of concrete surfaces exposed to de-icing chemicals.* Ministry of Transportation Ontario.

Naderi, M. (2008). Adhesion of Different Concrete Repair Systems Exposed to Different Environments. *The Journal of Adhesion, 84*, 78-104.

Naderi, M. (2008). Effects of Cyclic Loading, Freeze-Thaw and Temperature Changes on Shear Bond Strengths of Different Concrete Repair Systems. *Journal of Adhesion, 84*, 743-763.

Naik, T., & Malhotra, V. (2004). The Ultrasonic Pulse Velocity Method. In V. Malhotra, & N. Carino, *Handbook on Nondestructive Testing of Concrete* (pp. 1-14). West Conshohocken: CRC Press.

Nedhi, M., Mindess, S., & Aitcin, P. (1998). Rheology of High-Performance Concrete: Effect of Ultrafine Particles. *Cement and Concrete Research, 28*(5), 687-697.

Noble, K. (1997). Waterborne polyurethanes. *Progress in Organic Coatings, 32*(1-4), 131-136.

O'Connor, D., & Saiidi, M. (1993). Compatibility of Polyester-styrene Polymer Concrete Overlays with Portland Cement Concrete Bridge Decks. *ACI Materials Journal*, 59-68.

Ohama, Y. (1998). Polymer-based Admixtures. *Cement and Concrete Composites, 20*(2-3), 189-212.

Pailliere, A., Buil, M., & Serrano, J. (1987). Durabilite du beton a tres hautes performances. In J. Maso, *Materials Science to Construction Material Engineering* (pp. 990-997). London: Chapman & Hall.

Pelletier, M., Brown, R., Shukla, A., & Bose, A. (2011). *Self-Healing Concrete with a Microencapsulated Healing Agent.* Kingston: University of Rhode Island.

Picandet, V., Khelidj, A., & Bellegou, H. (2009). Crack effects on gas and water permeability of concretes. *Cement and Concrete Research, 39*(6), 537-547.

Pinto, R., & Kenneth, C. (2001). *Frost and Scaling Resistance of High-Strength Concrete.* Skokie: Portland Cement Association.

Powers, T. (1958). *The Physical Structure and Engineering Properties of Concrete.* Skokie: Portland Cement Association.

Powers, T. (1968). *The Properties of Fresh Concrete.* New York: John Wiley & Sons.

Powers, T., & Brownyard, T. (1948). Studies of the physical properties of hardened Portland cement paste. *American Concrete Institute*.

Promboon, Y., Olson, L., & Lund, J. (2002). Nondestructive evaluation methods for qualityn assurance of epoxy injection crack repairs. *Concrete Repair Bulletin*, 12-16.

Qasrawi, H., & Marie, I. (2003). The use of USPV to anticipate failure in concrete under compression. *Cement and Concrete Research, 33*, 2017-2021.

Ramakrishnan, S., Panchalan, R., & Bang, S. (2001). Improvement of concrete durability. *11th International conference on Fracture.* Turin, Italy.

Reinhardt, H., & Jooss, M. (2003). Permeability and self-healing of cracked concrete as a function of temperature and crackwidth. *Cement and Concrete Research, 33*(7), 981-985.

RILEM TC 162-TDF. (2002). Test and design methods for steel fibre reinforced concrete: Bending test. *Materials and Structures, 35*, 579-582.

Romer, M., & Leeman, A. (2005). Sensitivity of a non-destructive vacuum test method to characterize concrete permeability. *International conference on concrete repair, rehabilitation and retrofitting* (pp. 467-473). Cape Town: Taylor & Francis.

Santos, P., Julio, E., & Silva, V. (2007). Correlation between concrete-to-concrete bond strength and the roughness of the substrate surface. *Construction and Building Materials*, 1688–1695.

Schlegel, H. (1993). *General Microbiology* (7th Edition ed.). Cambridge University Press.

Shashoua, Y. (1992). *Evaluation of Polyester Filling Materials for use in Ceramics Conservation.* London: British Museum.

Sika. (2012). *Sikadur 55 SLV: Product Data Sheet.* Mississauga: Sika Canada.

Sika. (2012). *Sikadur 55 SLV: Product Data Sheet.* Mississauga: Sika Canada.

Sika. (2012). *SikaFix PU: Product Data Sheet.* Mississauga: Sika Canada.

Sika. (2012). *SikaTop Seal 107: Product Data Sheet.* Mississauga: Sika Canada Inc.

Slowik, V., Hubner, T., Schmidt, M., & Villmann, B. (2009). Simulation of capillary shrinkage cracking in cement-like materials. *Cement and Concrete Composites*, 461-469.

Sorenson, E. (1983). Freezing and thawing resistance of condensed silica fume (microsilica) concrete exposed to deicing chemicals. (V. malhotra, Ed.) *ACI Special Publications*, 709-719.

Spragg, R., Castro, J., Li, W., Pour-Ghaz, M., Huang, P., & Weiss, J. (2011). Wetting and drying of concrete using aqueous solutions containing deicing salts. *Cemeny and Concrete Composites*, 535-542.

Swiss Standard SIA 505 262/1 - Annex E. (2003). *Air Permeability on the Structure: Concrete Construction - Complementary Specifications.* Zurich: Swiss Society for Engineers and Architects.

Tanzawa, E. (1999). *Autogenous Shrinkage of Concrete.* London: E&FN Spon.

Tayeh, B., Bakar, B., Johari, M., & Voo, Y. (2012). Mechanical and permeability properties of the interface between normal concrete substrate and ultra high performance fiber concrete overlay. *Construction and Building Materials*, 538-548.

Thanoon, W., Jaafar, M., Kadir, M., & Noorzaei, J. (2005). Repair and structural performance of initially cracked reinforced concrete slabs. *Construction and Building Materials, 19*(8), 595-603.

Thao, T., Johnson, T., Tong, Q., & Dai, P. (2009). Implementation of self-healing concrete - Proof of Concept. *The IES Journal Part A: Civil and Structural Engineering, 2*(2), 116-125.

Thaulow, N., & Sahu, S. (2004). Mechanism of concrete deterioration due to salt crystallization. *Materials Characterization*, 123-127.

Torrent, R. (1992). A two-chamber vacuum cell for measuring the coefficient of permeability to air of the concrete cover on site. *Materials and Structures, 25*, 358-365.

Torrent, R. (2007). Performance-based specification and conformity control of durability. *International RILEM Workshop on Performance Based Evaluation and Indicators for Concrete Curability* (pp. 41-50). Paris: RILEM Publications.

Torrent, R., & Ebensperger, L. (1993). *VSS Rapport 506.* Bern, Suisse: Office Federal des Routes.

Torrent, R., & Frenzer, G. (1995). *VSS Rapport 516.* Bern, Suisse: Office Federal des Routes.

Torrent, R., Denarie, E., Jacobs, F., Leeman, A., & Teruzzi, T. (2012). Specification and site control of the permeability of cover concrete: The Swiss approach. *Materials and Corrosion, 63*, 1-7.

Trejo, D., & Pillai, R. (2003). Accelerated Chloride Threshold Testing: Part I - ASTM A 615 and A 706 Reinforcement. *ACI Materials Journal, 100*(6), 519-527.

Tsiatas, G., & Robinson, J. (2002). *Durability evaluation of concrete crack repair systems.* Transportation Research Record, Transportation Research Board.

Van Tittelboom, K., De Belie, N., De Muynck, W., & Verstraete, W. (2010). Use of bacteria to repair cracks in concrete. *Cement and Concrete Research, 40*(1), 157-166.

Van Tittelboom, K., De Belie, N., Van Loo, D., & Jacobs, P. (2011). Self-healing efficiency of cementitious materials containing tubular capsules filled with healing agent. *Cement and Concrete Composites, 33*(4), 497–505.

Vidal, T., Castel, A., & Francois, R. (2004). Analyzing crack width to predict corrosion in reinforced concrete. *Concrete and Cement Research, 34*, 165-174.

Vipulanandan, C., & Liu, J. (2005). Performace of polyurethane-coated concrete in sewer environment. *Cement and Concrete Research, 35*(9), 1754-1763.

Wang, K., Jansen, D., & Shah, S. (1997). Permeability study of cracked concrete. *Cement and Concrete Research, 27*(3), 381-393.

Weyers, R., Conway, J., & Cady, P. (1982). Photoelastic Analysis of Rigid Inclusions in Fresh Concrete. *Cement and Concrete Research*, 475-484.

Weyers, R., Prowell, B., Sprinkel, M., & Vortser, M. (1993). *Concrete bridge protection, repair, and rehabilitation relative to reinforcement corrosion methods application manual.* Strategic Highway Research Council. Washington: National Research Council.

Whiting, D., & Mohmad, N. (1998). *Manual on Control of Air Content in Concrete.* Skokie: Portland Cement Association.

Whittman, F. (1976). On the Action of Capillary Pressure in Fresh Concrete. *Cement and Concrete Research*, 49-56.

Whittmann, F. (1982). Creep and Shrinkage Mechanisms. In Z. Bazant, & F. Whittmann, *Creep and Shrinkage in Concrete Structures* (pp. 129-161). New York: John Wiley & Sons.

Yakabe, Y., Hendersen, K., Thompson, W., Pemberton, D., Tury, B., & Bailey, R. (1999). Fate of Methylenedipehnyl Diisocyanate and Toluene Diisocyanate in Aquatic Environment. *Environmental Science Technology*, 2579-2583.

Yaman, I., Inci, G., Yesiller, N., & Aktan, H. (2001). Ultrasonic pulse velocity in concrete using direct and indirect transmission. *ACI Materials Journal, 98*(6), 450-457.

Yan, C., Mai, Y., & Ye, L. (2001). Effect of Bond Thickness on Fracture Behaviour in Adhesive Joints. *The Journal of Adhesion*, 27-44.

Yang, J., Keller, M., Moore, J., White, S., & Sottos, N. (2008). Microencapsulation od Isocyanates for Self-Healing Polymers. *Macromolecules*, 9650-9655.

Yang, Z., Hollar, J., He, X., & Shi, X. (2011). A self-healing cementitious composite using oil core/silica gel shell microcapsule. *Cement and Concrete Composites, 33*, 506-512.

Ye, H., Jin, N., Jin, X., & Fu, C. (2012). Model of chloride penetration into cracked concrete subject to drying–wetting cycles. *Construction and Building Materials*, 259-269.

Ying, J., Xiao, J., & Tam, V. (2013). On the variability of chloride diffusion in modelled recycled aggregate concrete. *Construction and Building Materials*, 732-741.

Yow, H., & Routh, A. (2006). Formation of liquid core-polymer shell microcapsules. *Soft Matter*, 940-949.

Yuan, Y., & Marosszeky, M. (1991). Major factor influence the performance of structural repair. Evaluation and rehabilitation of concrete structures and innovations in design. *Proceedings of ACI international conference* (pp. 128-150). Hong Kong: American Concrete Institute.

Zemskov, S., Jonkers, H., & Vermolen, F. (2011). Two analytical models for the probability characteristics of a crack hitting encapsulated particles: Application to self-healing materials. *Computational Materials Science*, 3123-3333.

Zhang, J., & Lounis, Z. (2006). Sensitivity analysis of simplified diffusion-based corrosion initiation model of concrete structures exposed to chlorides. *Cement and Concrete Research*, 1312-1323.

Zhang, M., Tam, C., & Leow, M. (2003). Effect of water-to-cementitious materials ratio and silica fume on the autogenous shrinkage of concrete. *Cement and Concrete Research*, 1697-1694.

Zhong, W., & Yao, W. (2008). Influence of damage degree on seld-healing of concrete. *Construction and Building Materials, 22*, 1137-1142.

APPENDIX A: LIST OF ABBREVIATIONS

CON	Uncracked control specimens
E	Epoxy repair
FT	Freeze-thaw
FTL	Freeze-thaw and load regime
FTS	Freeze-thaw and salt regime
N	No environmental regime
OPC	Ordinary Portland cement
OV	Modified cementitious overlay repair
PU	Polyurethane repair
SF	Blended silica fume cement
SL	Service life
T	Temperature cycling regime
UPV	Ultrasonic pulse velocity

APPENDIX B: LIST OF EXPERIMENTAL TESTS

The tests used in the experimental program are listed below. Some of the tests have been modified to meet the objectives of the thesis and the modifications are addressed in the thesis manuscript. Those tests conducted by the material suppliers on the products used are not included.

ASTM C597	Standard Test Method for Pulse Velocity Through Concrete (2009)
CSA Test Method A23.2-9C	Strength of Cylindrical Concrete Specimens: Concrete Materials and Methods of Concrete Construction/Methods of Tests for Concrete (2009)
CSA Test Method A23.2-10A	Density of Aggregate: Concrete Materials and Methods of Concrete Construction/Methods of Tests for Concret (2009)
CSA Test Method A23.2-12A	Relative Density and Absorption of Coarse Aggregate: Concrete Materials and Methods of Concrete Construction/Methods of Tests for Concrete (2009)
CSA Test Method A23.2-2A	Sieve Analysis of Fine and Coarse Aggregate: Concrete Materials and Methods of Concrete Construction/Methods of Tests for Concrete (2009)
CSA Test Method A23.2-3C	Making and curing concrete compression and flexural test specimens: Concrete Materials and Methods of Concrete Construction/Methods of Tests for Concrete (2009)
CSA Test Method A23.2-4C	Air Content of Plastic Concrete by the Pressure Method: Concrete Materials and Methods of Concrete Construction/Methods of Tests for Concrete (2009)
CSA Test Method A23.2-5C	Slump of Concrete: Concrete Materials and Methods of Concrete Construction/Methods of Tests for Concrete (2009)
CSA Test Method A23.2-6A	Relative Density and Absorption of Fine Aggregate: Concrete Materials and Methods of Concrete Construction/Methods of Tests for Concrete (2009)
MTO LS-412	Method of Test For Scaling Resistance of Concrete Surfaces Exposed to Deicing Chemicals (1997)
RILEM TC 162-TDF	Test and design methods for steel fibre reinforced concrete: Bending test (2002)

APPENDIX C: SHRINKAGE-CRACK SETUP

C.1   Introduction

As part of the experimental program, an attempt was made to develop a test set-up which would induce cracks in concrete using early age mechanisms. Appendix A contains the experimental set-up created, the parameter of the trial test runs, the results of the trial tests, the modelled shrinkage strains, and future work required in order to complete the experimental program.

C.2   Experimental Set-Up

The goals of the test set-up were as follows:
- Develop natural shrinkage cracks in concrete;
- Create reproducible and consistent cracks;
- Make compact specimens for easy handling;
- Produce a single crack per specimen.

To meet all the criteria listed above, the set-up presented in Figure C.1 was developed. The set-up consists of a header block that is used to restrain a concrete slab that is cast against it. The set-up makes use of the shrinkages that develop in concrete at an early age and depending on the concrete mix design and environmental conditions may include the effects of: drying shrinkage, autogenous shrinkage, and/or thermal shrinkage.

In the set-up, the shrinkage that is of concern is in the lengthwise direction of the specimen. By restraining the concrete slab along one side of the length, stresses develop in the slab, generating the greatest stresses along the restrained edge. The greatest stress typically occurs at the ends of the slab, however due to slippage the actual greatest stress occurs at the centre of the restraint. When the stress exceeds the tensile strength of concrete a crack propagate through the section. This mechanism is illustrated in Figure C.2. This set-up was created with the intention of generating multiple cracks throughout the slab that could then be used as several specimens for testing.

The test set-up consisted of a header block, concrete slab, restraining steel, and a welded wire fabric mesh. The concrete slab acted as the actual test specimen, where early age shrinkage was used to induce cracking. It was cast against a concrete header block that is rigid and has fully developed its strength. In order to provide the restraint between the header block and the freshly poured concrete slab, steel rebar was used to connect the two elements. To ensure that the steel did not move and restrain the concrete slab, a washer was welded at the face of the header block, and a threaded rod was welded at the other end of the header block. The rebar was then bolted in place through the header block. The welded wire fabric was provided in order to keep the concrete slab in one piece after cracking and to distribute the stress post-cracking.
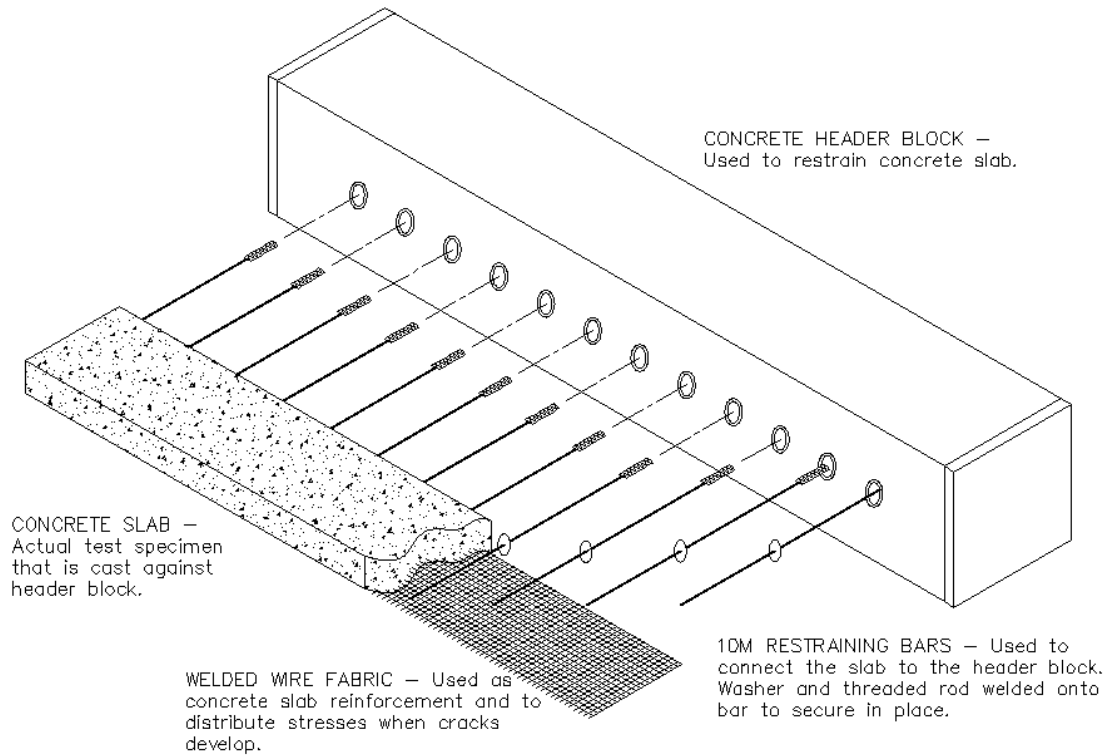
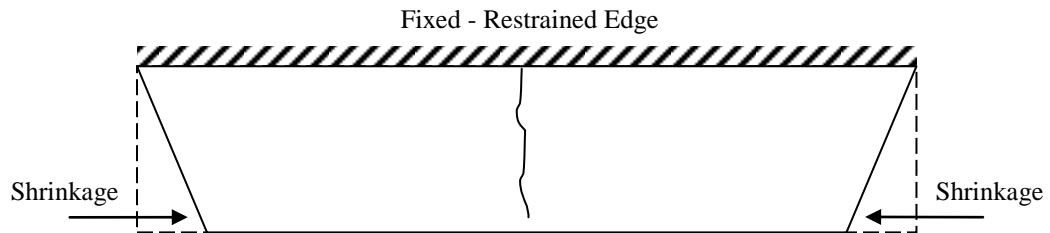**Figure C.1 Shrinkage crack set-up – General concept**

Figure C.2 Idealized shrinkage crack mechanism

C.3   Concrete Mixture Designs

The test set-up was developed to restrain the early age concrete shrinkage. However, it was the concrete mix design and the environmental conditions that dictated the amount of shrinkage. As such, the concrete mixes were designed in order to promote either drying shrinkage or autogenous shrinkage. After the first trial run, it was determined that the laboratory conditions were not sufficient to provide the necessary

drying shrinkage required to induce cracking. Furthermore, it was not possible to control the surrounding environment (temperature, relative humidity, etc.) therefore all subsequent trial runs were designed to utilize autogenous shrinkage to promote cracking. For each trial run the concrete mix was modified. Other parameters regarding the test set-up were also modified for the trial runs. All the test-set up parameters and concrete mix designs are presented in Table C.1.

Table C.1 Concrete mixture design and experiment parameters

Test Set-Up Parameters	Trial #1	Trial #2	Trial #3	Trial #4
Length (mm)	1200	1200	1200	2400
Width (mm)	200	200	100	200
Depth (mm)	60	60	60	60
Header Block	Concrete	Concrete	Concrete	Steel
Concrete Mix Design				
w/c Ratio	0.60	0.30	0.30	0.29
Water Content (kg/m^3)	217	186	246	210
OPC Content (kg/m^3)	351	540	690	714
Silica Fume (kg/m^3)	0	60	77	80
Coarse Aggregate (kg/m^3)	636	606	605	514
Fine Aggregate (kg/m^3)	990	926	659	764
Air Entrainer (mL per 100 kg cement)	78	78	78	78
Superplasticizer (mL per 100 kg cement)	0	975	975	975
Concrete Proportions				
Silica Fume (%)	0	10	10	10
% Aggregate Volume	60.7	57.9	48.1	47.3
Volume FA/CA	1.57	1.51	1.09	1.42

C.4   Trial Test Results

The tests were only monitored for the appearance of cracks in the concrete slab. The following observations were noted:

- Trial #1 failed to generate any cracks. This trial was designed so as to cause drying shrinkage with a high w/c ratio. A fan was placed to promote evaporation, however, due to the poorly controlled laboratory conditions, it was not possible to regulate the temperature and relative humidity to increase the amount of shrinkage. In addition, thin steel dividers were used to section the concrete slab into separate specimens. It was assumed that the dividers would not inhibit shrinkage of the concrete slab as a whole. Regardless of whether this assumption

116

was true, all subsequent trials eliminated the use of dividers. Trial #1 is shown in Figure C.3 Trial #1.

- Trial #2 used a concrete mix with a low w/c ratio, and cement blended with 10% silica fume. A crack developed in the middle of the concrete slab as shown in Figure C.4. The concrete slab was left for several days, however no further cracks were generated. The crack width was approximately 0.15 mm.

- Trial #3 used a similar concrete mix design as Trial #2, with the exception of lowering the aggregate volume. This was done in an attempt to increase the amount of shrinkage by increasing the cement content – the portion of the concrete experiencing the actual shrinkage. The width of the concrete slab was also decreased with the intention of increasing the stresses generated within the slab. A crack was formed at approximately 1/3 the length from the edge as seen in Figure C.4. This was the only crack that formed.

- Trial #4 once again slightly modified the concrete mix design. Similar to Trial #3, the dimensions of the concrete slab were altered. The length was doubled from the initial 1200 mm to 2400 mm while keeping the width and depth constant. The concrete header blocks that were cast were not sufficiently long to accommodate the increased dimensions, subsequently a steel beam was used as the header block as seen in Figure C.5. The restraining steel bar was spaced at the same intervals and was secured in place using the same method. The set-up was also placed outside rather than in the laboratory, where the average temperature during the day was 17˚C. The concrete slab was protected from the elements. No cracks were observed in the concrete slab.
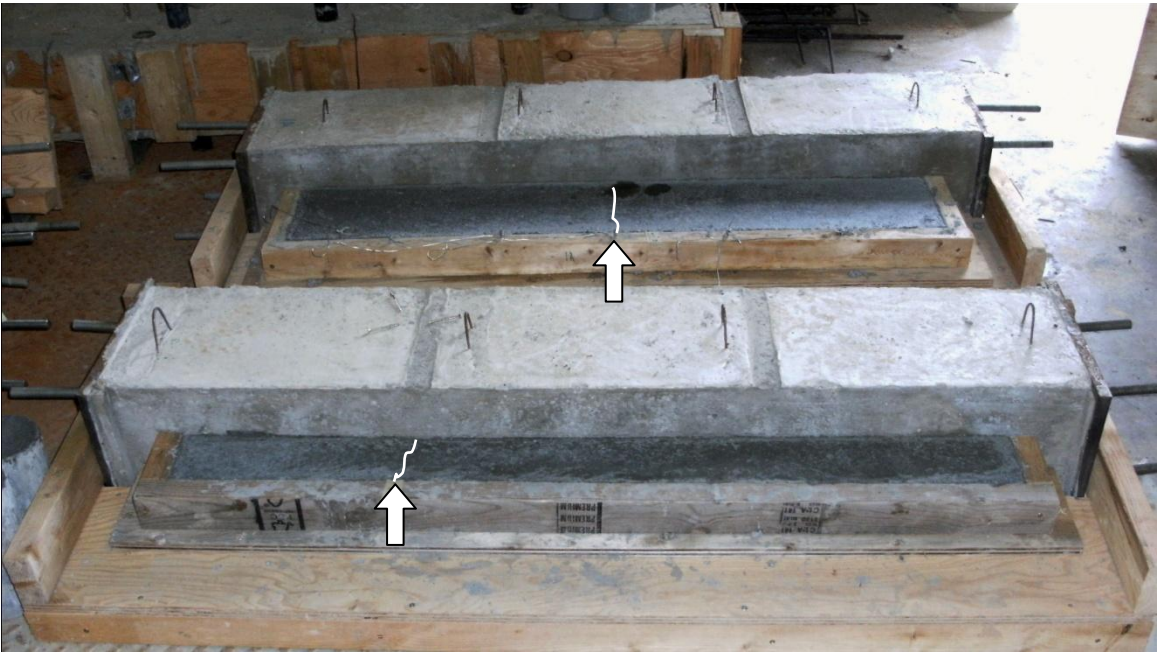
Figure C.3 Trial #1 – Immediately after pouring

Figure C.4 Trial #2 and Trial #3

Figure C.5 Trial #4

C.5   Shrinkage and Cracking Models

In order to better comprehend the mechanisms working in the shrinkage cracking set-up, several models were used to predict the shrinkage in the concrete. Furthermore, the failure of the set-up to generate multiple cracks is discussed using a mechanistic model.

The shrinkage developed in the concrete test trial set-up was predicted using three different shrinkage models as specified by the following: ACI-209R (ACI Committee 209, 2008), B3 – BP Model and BP-KX Model (Bazant & Baweja, 2000), and CEB-FIP 1990 (Comité Euro-International du Béton, 1993). It was assumed that all the trials were subjected to the same temperature and relative humidity – a temperature of 20˚C and relative humidity of 45%. The shrinkage is calculated at 7 days. The results are presented in Table C.2

Table C.2 Predicted concrete shrinkage

Shrinkage Model	Shrinkage at 7 Days (μm/m)			
	Trial #1	Trial #2	Trial #3	Trial#4
ACI – 209 R	150	142	154	159
B3	56.2	43.3	63.4	50.6
CEB-FIP 1990	84.1	59.4	59.4	59.4
Average Shrinkage	96.9	81.6	92.4	89.6

From the table, it is evident that the greatest shrinkage, theoretically, is in Trial #1. It is clear by the variation of results that emphasis is placed on different factors in each model. In a comparison of the models presented, it was found that the predictability of autogenous shrinkage of the assessed model, ranked from best to worst, are as follows: B3, ACI – 209, CEB- FEP 1990 (Khairallah, 2009). To confirm the models, and to get better results, it is also possible to experimentally monitor the shrinkage as proposed by various authors in the literature (Tanzawa, 1999) (Holt, 2001).

To better understand the development of shrinkage and stresses a mechanistic model is presented. The stresses developed in the concrete slab were modelled using SAP 2000, a finite element software. The development of shrinkage and strength of concrete with time was based on general relationship presented by Mehta and Monteiro (2006). Upon concrete setting, shrinkage initiates causing stresses to develop in the concrete slab. In Figure C.6, the development of these shrinkage, stress, and tensile strength is presented. When the stresses generated in the slab exceed the concrete's tensile strength a crack will propagate as indicated at time t_1.
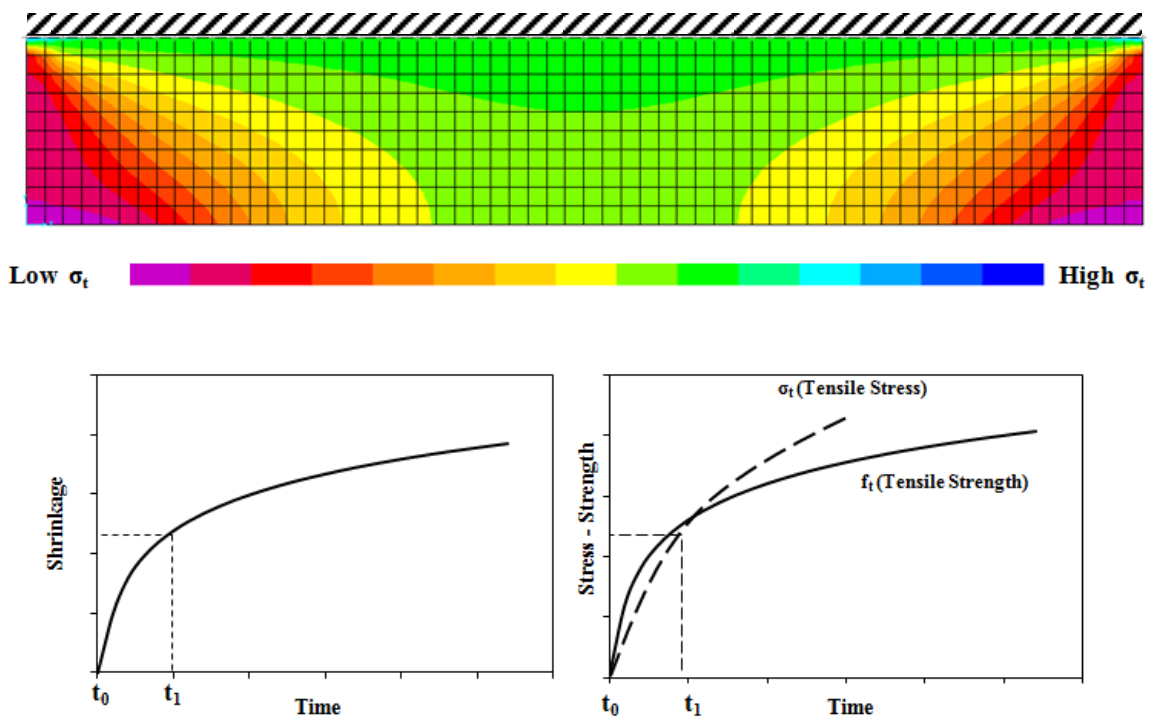

Figure C.6 Concrete slab shrinkage and stresses before first crack

Once the concrete has cracked, assuming no steel reinforcement for simplicity, the concrete can now be modelled as two separate slabs. The effects are twofold, first, the aspect ratio of the concrete slab is smaller, generating lower stresses. Furthermore, at time t_1, due to the cracking, the shrinkage now can be assumed to be zero as illustrated in

Figure C.7. Similarly, it is assumed that all the stress has dissipated, and begins to redevelop with the further shrinkage of concrete. Based on the various parameters, such as the shrinkage of concrete, and the tensile strength development, it may be possible that a great enough stress does not develop in order to produce additional cracking.
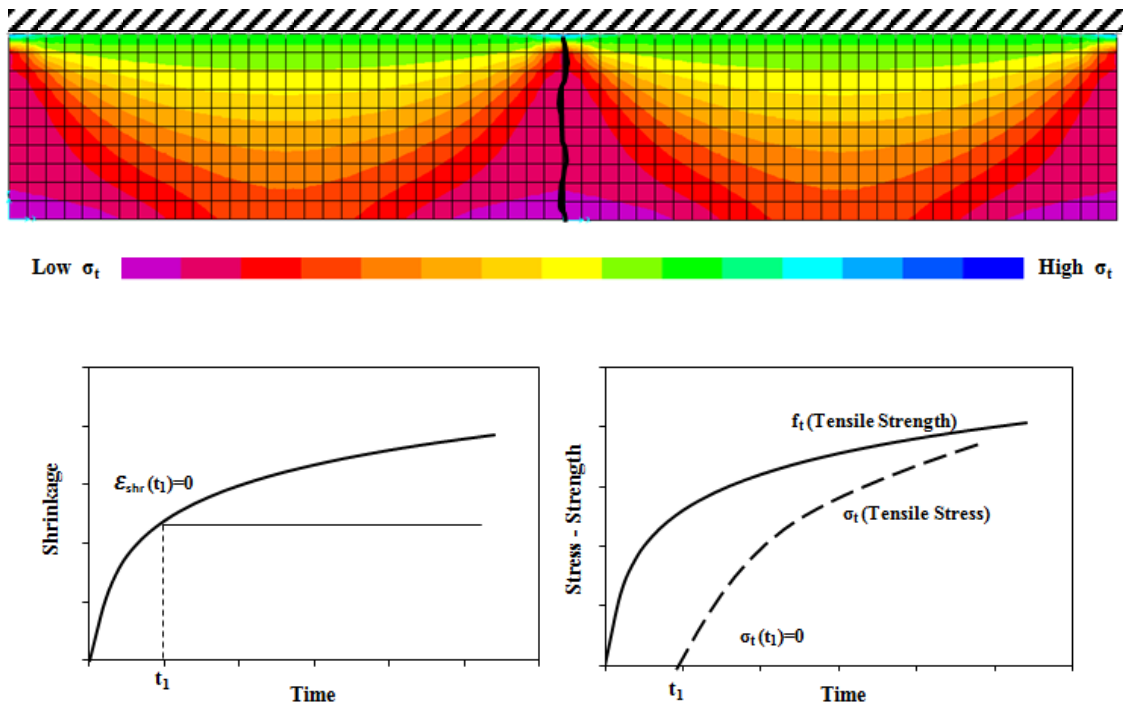

Figure C.7 Concrete slab shrinkage and stresses post cracking

C.6   Future Work

To properly develop the experimental set-up, further experimental and analytical work is required. Before conducting any further experiments, an analytical model would be beneficial in optimizing the experiment to determine the optimal concrete mix design and corresponding concrete slab dimensions. Recommendations for future work include:

1. Model the concrete shrinkage with respect to time using other models and confirm results using experimental tests. Parameters should include concrete mix proportions.
2. Predict the development of concrete properties (compressive strength, tensile strength, and elastic modulus) using available models using the same concrete mix design as for the concrete shrinkage model. The 28 day concrete compressive strength may be estimated or tested experimentally.
3. Use two dimensional Finite Element Models to model the stress generation in the concrete slab due to shrinkage. Iterative time-stepping would be required to compare the shrinkage-stress development to the concrete tensile strength.

4. Use the model to optimize the experimental set-up and modify the following variables to achieve desirable cracks: concrete slab aspect ratio, concrete mix design, and controllable environmental conditions.

APPENDIX D: SELF-HEALING PROTOTYPE

D.1   Introduction

In an attempt to include a self-healing repair in this thesis, the use of microcapsules in concrete was examined. This work was done in collaboration with the Department of Chemistry at McMaster University. The microcapsule manufacturing and investigations were completed with the aid of Dr. Harald Stover, Dr. Jian (Jeffrey) Li, and Dr. Nicholas Burke.

This appendix examines several aspects of using microcapsules in concrete as a self-healing technique. First, the self-healing mechanism for a one-component microcapsule is briefly presented. Secondly, the experimental work conducted to create and integrate microcapsules in concrete is summarized. Finally, the challenges that have yet to be addressed, both as part of this work as well as current literature, are examined.

D.2   Proposed Microcapsules

The use of microcapsules in concrete is a developing research field. Several attempts have been made for the use of self-healing as reviewed in Section 2.4.3 of this thesis. In most cases, the use of a two-component system is proposed, where two different microcapsules are integrated in the cement matrix. Upon cracking, ideally, the crack would propagate through both microcapsules, rupturing the capsules and mixing the two reactants to form a product that would fill and seal the crack. The probability that both types of capsules will be ruptured and provide the ratio volumes required for the reaction is low. Several statistical analyses have been conducted to develop models that estimate the probability that a crack will propagate through the capsules (Lv, Chen, & Yuan, 2011) (Zemskov, Jonkers, & Vermolen, 2011). It was found that the probability is highly dependent on the crack length, capsule size, and mean intercapsule distance.

A one component system eliminates the uncertain reaction of the two components. An event or the presence of some sort of material is required to cause the healing material to successfully solidify within the crack – this is typically moisture. The moisture, either from the concrete, the environment, or the atmosphere, can be utilized to trigger the encapsulated material.

The one-component material can also act in one of two ways: it can be used as an adhesive to bind the interface of the cracking concrete, or it can act as a plug, filling the crack and preventing the ingression of aggressive agents. Two issues present themselves with the adhesive microcapsule healing system. First, the adhesive may prevent cracking at one location, however the stress in the concrete will be redistributed and cracking will be initiated in a different location without microcapsules. Secondly, such adhesives, like cyanoacrylate, are difficult to encapsulate. Because most typical encapsulation methods use an oil in water emulsion technique, encapsulation of cyanoacrylate poses a challenge due to its high reactivity with water.

The proposed one-component microcapsule for this prototype is encapsulated isocyantes. This type of microcapsule is primarily used for the development of self-healing polymers. Using an oil-in-water emulsion, the microcapsules are formed though interfacial polymerization of isocyanates and amines at the oil-water boundary. The polyurea or polyurea hybrid capsule shell is formed and excess isocyanates remaining in the oil core are encapsulated. Isocyanates provide a one-part catalyst free self-healing system triggered in moist environments. The reaction products of isocyanate and water result in a solid insoluble polyurea product, which is unreactive under environmental conditions (Yakabe, et al., 1999). This self-healing mechanism acts as a non-structural repair, by filling the concrete crack and preventing the ingression of harmful agents.

D.3   Experimental Work

The first test conducted was used to determine whether microcapsule would be able to withstand the concrete mixing process. A sample of polyurea double walled microcapsules dissolved in an aqueous solution was obtained. The weight of microcapsules was estimated to be 5 grams. The microcapsule solution was dissolved in 2 kg of water. In a concrete pan mixer, 6 kg of sand and 6 kg of 10 mm coarse aggregate was placed. While mixing the aggregate, the 2 kg of water containing the microcapsules was slowly added. The water-aggregate mixture was mixed for 10 minutes. After mixing, the water was carefully drained into a separate container from the aggregate. Due to the oil core, any intact microcapsules surface to the top. To determine whether any of the microcapsules remained intact, samples of the water were analyzed using a microscope. It was determined that the microcapsules were capable of withstanding the mixing process as shown in Figure D.1. However, fractured segments were also found to have settled to the bottom of the slide, suggesting that not all microcapsules survive.
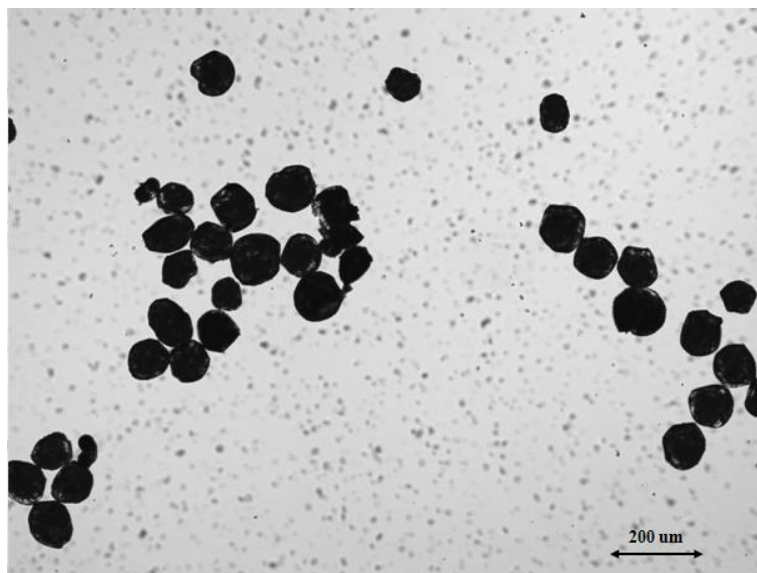

Figure D.1 Mixing surface water with microcapsules intact

In another series of experiments polyurea (PU) and poly(urea-formaldehyde) (PUF) microcapsules were synthesized in the laboratory in an attempt to investigate whether they could be successfully integrated into the cement matrix. The microcapsules were synthesized using interfacial polymerization as described in Section D.4. The PU microcapsules were manufactured based on protocols created in the Department of Chemistry at McMaster University, developed as part of another research study by Li et al. (2009). The PUF capsules were synthesized following the procedure as dictated by Brown et al. (2003) with some modifications. The procedures are summarized in Section D.5. Using these two procedures, it is clear the microcapsules had a wide range in size as is shown in Figure D.2.

After the microcapsules were synthesized, filtered, and diluted in water, they were mixed in cement paste samples. Cement paste samples with a w/c ratio of 0.4 and 0.6 were mixed using ordinary Portland cement. The cement paste was formed into small discs approximately 25mm in radius and 5mm in thickness. The microcapsules were added at 10% weight of cement. Cement paste samples with no microcapsules were also created as controls. When mixing the cement paste with the 10% microcapsules, the samples were significantly less workable than the controls. The cement paste samples were left to cure for 14 days.

The cement matrix was investigated using a microscope with up to 20X magnification. The surface of the cement paste showed no signs of the microcapsules. To better examine the integration of the microcapsule, the discs were completely ruptured, and the fractured surface was examined. Upon fracturing, the PUF cement paste samples released an odour, suggesting that upon cracking the microcapsules ruptured, releasing the core contents, however this was not proven as part of the experimentation. In both the PU and PUF cement paste samples, evidence of successful integration with the cement matrix was found as shown in Figure D.3. Note that the visible microcapsules are only partially exposed, which may be one reason as to why they did not ruptured.
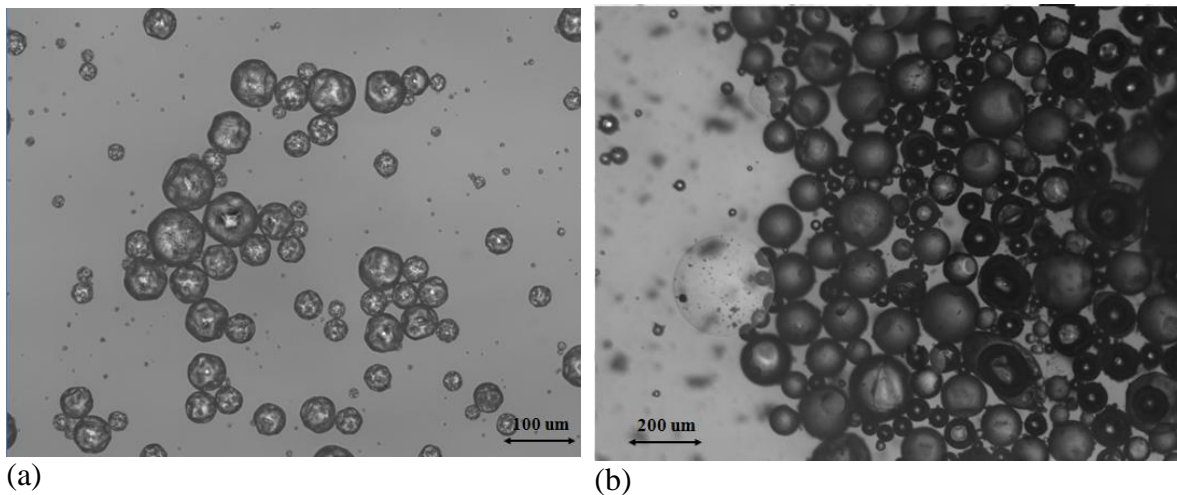

(a)   (b)

Figure D.2 Microcapsule suspended in water: (a) Polyurea Capsules and (b) Poly(Urea-Formaldehyde)

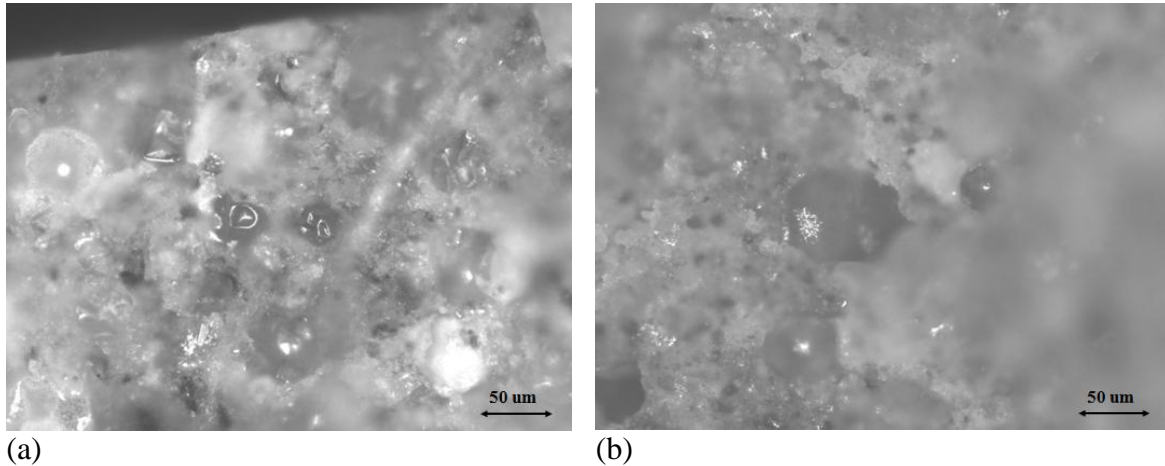(a)   (b)

Figure D.3 Microcapsules in w/c=0.6 cement paste (a) Polyurea Capsules and (b) Poly(Urea-Formaldehyde)

D.4   Microcapsule Synthesis Procedures

The procedure to manufacture the polyurea microcapsules is as follows:

1. A 1 wt% Poly (Vinyl Alcohol) (PVA) stock solution was prepared, stirring the solution for 24 hours using a magnetic stirrer.
1. 20g of Poly [(phenyl isocyanate)-co-formaldehyde] (PMPPI) was dissolved in 200 mL of Xylene, freshly preparing the solution.
2. 700mL of the PVA solution was poured into a 1L covered reactor.
3. The solution was stirred at approximately 850 rpm after which the PMPPI-Xylene solution was slowly poured in.
4. The mixture was emulsified for 15 minutes.
5. The stirring rate was reduced to approximately 550 rpm and 10g of Diethylenetriamine (DETA) was added.
6. The temperature was raised to 70°C for 6 hours.
7. After the reaction was cooled, the microcapsules were filtrated and washed with water until a near neutral pH of 7.0 was achieved. The filtration procedure was repeated approximately 3-4 times.

The procedure to synthesize the poly(urea-formaldehyde) microcapsules is as follows:

2. A 5 wt% poly(methyl vinyl ether-co-maleic anhydride) (PMVEM) solution in water was prepared, stirring the solution for 24 hours using a magnetic stirrer.
3. 675mL of water was mixed with 75mL of the PMVEM solution, followed by the addition of 15g urea, 1.5g of resorcinol and 1.5g of ammonium chloride (NH_4Cl).
4. The solution was stirred at 1200 rpm.
5. After solid dissolution, the solution pH was adjusted to approximately 3.5 by slowly adding 10wt% sodium hydroxide (NaOH) solution.

6. 200 mL of paraffin oil was added to the solution.
7. The stirring rate was increased to 1800 rpm.
8. 38.01g of solid formaldehyde was added to the solution. The stirring rate was increased to 1700 rpm. The temperature was raised to 55°C and kept for 4hrs.
9. After cooling the reaction, the microcapsules were washed with water until near neutral pH.

D.5   Future Work

The results of the experimental work included in this appendix are the preliminary findings from an attempt to address some of the issues of including microcapsules in concrete as a self-healing repair. It was found that microcapsules are capable of withstanding the mixing procedure and that PU and PUF microcapsules can be integrated into the cement matrix without rupturing due to the developing pore pressure or CSH crystal growth. Several other challenges and issues exist with the proposed self-healing mechanism. Recommendations and points that need to be addressed for future work include:

1. The ability of the microcapsules to rupture upon concrete cracking needs to be confirmed. The strength of the microcapsule and the bond strength between the microcapsule and cement matrix should be quantified. If the microcapsule strength is greater than the bond strength the microcapsule will not rupture.
2. Modifications to the microcapsule synthesis procedure may be necessary to decrease the microcapsule strength. However, sufficient strength must be maintained to avoid premature rupturing during the mixing and concrete setting stages. One possible solution could include grafting additional layers on the shell of the microcapsule to increase the bond strength, in particular, the deposition of clay particles (Hickey, Burke, & Stover, 2011).
3. The amount of core material released needs to be determined analytically and experimentally. Existing statistical models can theoretically render the amount of core material available on fracturing. During initial stages, experimental work should be performed to confirm the area exposed to the core healing agent. This can be accomplished by dissolving dye within the oil core of the microcapsule, and examining the concrete fractured surface.
4. The efficiency of the healing core material needs to be assessed. This will be dependent on the quantity of remaining isocyanates in the core as well as the reactivity of the isocyanates with water. Preliminary tests can be conducted on the reactivity of the specified isocyanate used in the oil core. Furthermore, the proposed self-healing method with the PU and PUF microcapsules is a non-structural repair; subsequently, the concrete's water permeability can be used as a measure of the repair's effectiveness.